

AD-A031 774

MINNESOTA UNIV MINNEAPOLIS DEPT OF AERONAUTICS AND --ETC F/G 11/2
DAMPING IN PORCELAIN ENAMEL COATINGS.(U)
JUL 76 P I SRIDHARAN

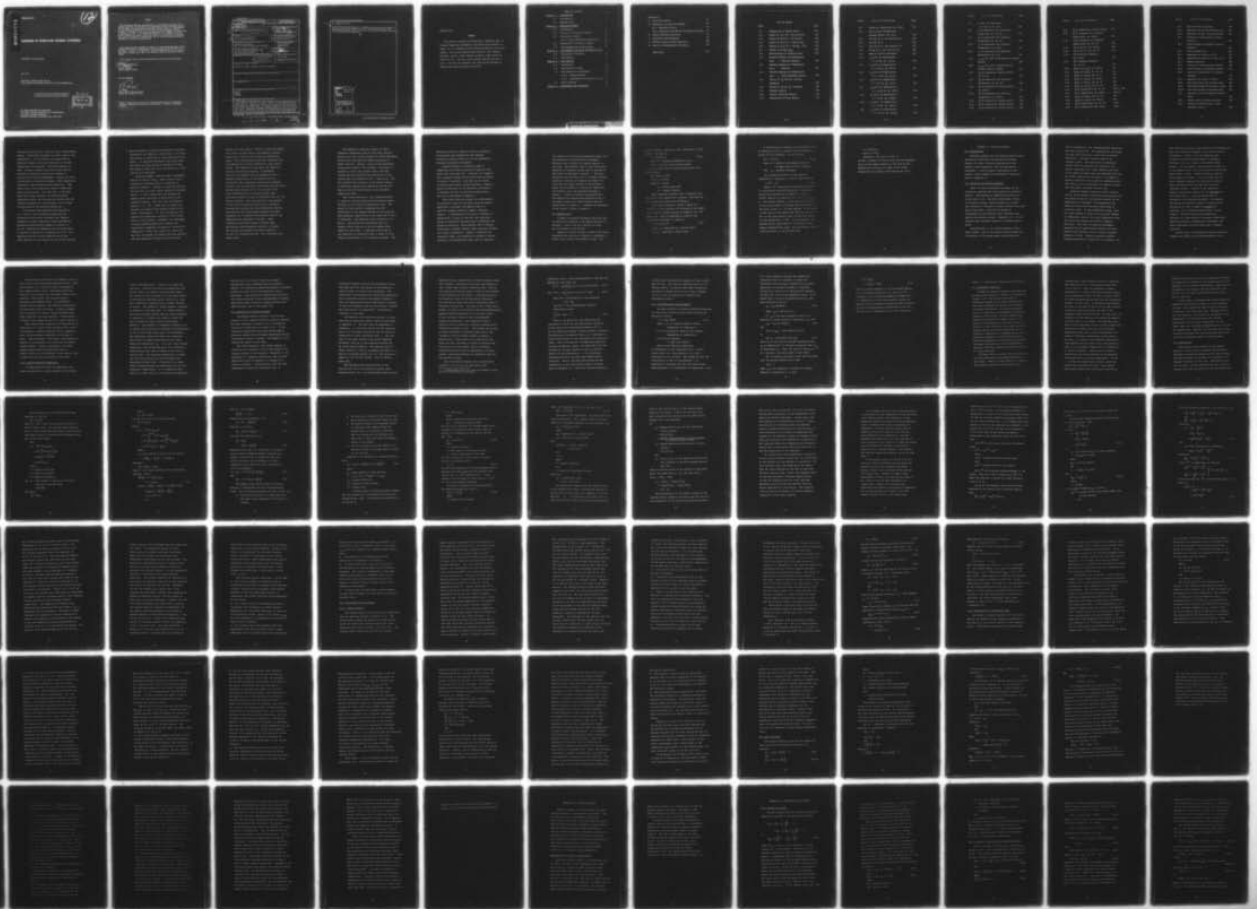
F33615-72-C-1315

UNCLASSIFIED

AFML-TR-74-191

NL

1 of 3
ADA031774



ADA031774

AFML-TR-74-191

12

DAMPING IN PORCELAIN ENAMEL COATINGS

UNIVERSITY OF MINNESOTA

JULY 1976

TECHNICAL REPORT AFML-TR-74-191
FINAL REPORT FOR PERIOD AUGUST 1971 TO SEPTEMBER 1974

Approved for public release; distribution unlimited

DDC
RECEIVED
NOV 9 1976
B

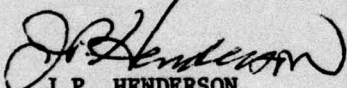
AIR FORCE MATERIALS LABORATORY
AIR FORCE WRIGHT AERONAUTICAL LABORATORIES
AIR FORCE SYSTEMS COMMAND
WRIGHT-PATTERSON AIR FORCE BASE, OHIO 45433

NOTICE

When Government drawings, specifications, or other data are used for any purpose other than in connection with a definitely related Government procurement operation, the United States Government thereby incurs no responsibility nor any obligation whatsoever; and the fact that the government may have formulated, furnished, or in any way supplied the said drawings, specifications, or other data, is not to be regarded by implication or otherwise as in any manner licensing the holder or any other person or corporation, or conveying any rights or permission to manufacture, use, or sell any patented invention that may in any way be related thereto.

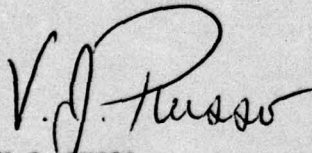
This report has been reviewed and cleared for open publication and/or public release by the Office of Information (OI) in accordance with AFR 190-17 and DOD 5230.9. There is no objection to unlimited distribution of this report to the public at large, or by DDC to the National Technical Information Service (NTIS).

This technical report has been reviewed and is approved for publication.



J.P. HENDERSON
Project Engineer
Metals Behavior Branch

FOR THE COMMANDER



V.J. RUSSO
Chief, Metals Behavior Branch
Metals and Ceramics Division

Copies of this report should not be returned unless return is required by security considerations, contractual obligations, or notice on a specific document.

UNCLASSIFIED

SECURITY CLASSIFICATION OF THIS PAGE (When Data Entered)

REPORT DOCUMENTATION PAGE		READ INSTRUCTIONS BEFORE COMPLETING FORM
1. REPORT NUMBER AFML-TR-74-191	2. GOVT ACCESSION NO.	3. RECIPIENT'S CATALOG NUMBER
4. TITLE (and Subtitle) DAMPING IN PORCELAIN ENAMEL COATINGS	5. TYPE OF REPORT & PERIOD COVERED FINAL REPORT Aug 71 - Sep 74	6. PERFORMING ORG. REPORT NUMBER
7. AUTHOR(s) Prabha Iyengar/Sridharan	8. CONTRACT OR GRANT NUMBER(s) F33615-72-C-1315 <i>new</i>	
9. PERFORMING ORGANIZATION NAME AND ADDRESS University of Minnesota Dept. of Aerospace Engineering & Mechanics	10. PROGRAM ELEMENT, PROJECT, TASK AREA & WORK UNIT NUMBERS Project: 7351 Task: 73510603	
11. CONTROLLING OFFICE NAME AND ADDRESS Air Force Materials Laboratory (LLN) Air Force Systems Command Wright-Patterson Air Force Base, Ohio 45433	12. REPORT DATE Jul 1976	13. NUMBER OF PAGES 211
14. MONITORING AGENCY NAME & ADDRESS (if different from Controlling Office) <i>12 224 P.</i>	15. SECURITY CLASS. (of this report) Unclassified	15a. DECLASSIFICATION/DOWNGRADING SCHEDULE
16. DISTRIBUTION STATEMENT (of this Report) Approved for public release; distribution unlimited.		
17. DISTRIBUTION STATEMENT (of the abstract entered in Block 20, if different from Report)		
18. SUPPLEMENTARY NOTES		
19. KEY WORDS (Continue on reverse side if necessary and identify by block number) Enamels Damping Coatings		
20. ABSTRACT (Continue on reverse side if necessary and identify by block number) Equipment was developed and tested which was used for measuring the complex elastic moduli of thin porcelain enamel coatings at temperatures where they became very soft. Previous work has been done in glasses, almost exclusively at relatively low temperatures, to measure the effects of ionic diffusion or other chemical activation changes or at high temperatures where one is dealing with a melt. Measurements from 10^3 to 10^{12} Poise have been conducted mainly for production control and have relied on standard tests. The present work shows how the storage and loss portions of the shear and Young's modulus can		

DD FORM 1473 1 JAN 73 EDITION OF 1 NOV 65 IS OBSOLETE

SECURITY CLASSIFICATION OF THIS PAGE (When Data Entered)

TEN TO THE 2ND POWER

TEN TO THE 12TH POWER 233 510

over
[Signature]

20. Abstract (Con't)

be measured directly as functions of temperature and frequency and proposes a general relation which depends only on the room temperature modulus, the activation energy, the critical temperature and one other parameter which gives the relaxation spectrum bandwidth.

ACCESSION for	
NTIS	White Section <input checked="" type="checkbox"/>
DDC	Buff Section <input type="checkbox"/>
UNANNOUNCED	<input type="checkbox"/>
JUSTIFICATION	
BY	
DISTRIBUTION/AVAILABILITY CODES	
Dist.	AVAIL. and/or SPECIAL
A	

AFML-TR-74-191

FOREWORD

This report was prepared by the University of Minnesota, Dept. of Aerospace Engineering and Mechanics, with Prabha Iyengar Sridharan as author. Dr. J.P. Henderson, Air Force Materials Laboratory, was project engineer. The work was conducted under Project No. 7351, "Metallic Materials", Task No. 735106, "Behavior of Metals", under Contract No. F33615-72-C-1315. The report covers research conducted from Aug 71 - Sep 74. The report was released by the author and the University of Minnesota for general publication in May 1975.

TABLE OF CONTENTS

	Page
<u>Chapter 1. INTRODUCTION</u>	
1.1 Introduction	1
1.2 Damping Units	7
<u>Chapter 2. PORCELAIN ENAMELS</u>	
2.1 Introduction	11
2.2 Structure of Porcelain Enamels	11
2.3 Structure of Glass	15
2.3.1. Glass Transition Temperature	16
2.4 Relaxation in Porcelain Enamels	18
2.5 Time-Temperature Relationships	22
<u>Chapter 3. EXPERIMENTAL TECHNIQUE AND CALCULATIONS</u>	
3.1 Experimental Technique	25
3.2 Calculations	27
<u>Chapter 4. TEST RESULTS</u>	
4.1 Introduction	43
4.2 Presentation of Data	43
4.3 Data Reduction and Analysis	47
4.3.1. Complex Modulus	47
4.3.2. Distribution of Relaxation Times	53
4.4 Error Analysis	65
<u>Chapter 5. CONCLUSIONS AND DISCUSSION</u>	70

Appendices

1. Porcelain Enamels	77
2. Relaxation in Porcelain Enamels	79
A2.1 Mechanical Models	79
A2.2 Lognormal Distribution of Relaxation Times	81
3. Torsion Pendulum Apparatus	85
4. Cantilever Beam Apparatus	90
5. Hollow Torsion Cylinder Apparatus	101
6. Details of Experimental Procedures	110

References	132
------------	-----

LIST OF TABLES

TABLE		Page
2.1	Composition of Enamel Frits	117
2.2	Values of $F(x', \beta) = M''(x')/M''(0)$	118
2.3	Values of $2f(0, \beta) = 2M''(0)/\delta M$	119
2.4	Values of $2f(x', \beta) = 2M''(x')/M_U$	120
2.5	Values of $f_1(x', \beta) = (M'/M_U - 0.5)$	121
3.1	Values of R and η_A/η_B	122
4.1	Manufacturers of Coating Frits	123
4.2	Maximum Damping and Temperature Data - Torsion Pendulum	124
4.3	Maximum Damping and Temperature Data - Bending	125
4.4	Maximum Damping and Temperature Data - High Frequency Torsion	126
4.5	Values of G_2' and G_2'' - Torsion Pendulum	127
4.6	Values of E_2' and E_2'' - Bending	128
4.7	Bending Results	129
4.8	Torsion Pendulum Results	130
4.9	Composition of Base Metals	131

Figure	List of Illustrations	Page
2.1	Volume Vs Temperature for Glass	137
2.2	E_2' and E_2'' Vs Temperature; Coating S9919D, Sp. #5,B	138
2.3	$F(x',\beta)$ Vs x' for Various β 's	139
2.4	$2f(0,\beta)$ Vs β	140
2.5	$f(x',\beta)$ Vs x' for Various β 's	141
2.6	M'/M_U Vs x' for various β 's	142
3.1	Beam of Uniform Thickness	143
3.2	η_s and f Vs Temperature; $f = 47$ Hz, Sp. #16,B	144
3.3	η_s and f Vs Temperature; $f = 170$ Hz, Sp. #16,B	145
4.1	η_s and f Vs Temperature; $f = 1.2$ Hz, Sp. #2,TP	146
4.2	η_s and f Vs Temperature; $f = 8.4$ Hz, Sp. #2,TP	147
4.3	η_s and f Vs Temperature; $f = 14.25$ Hz, Sp. #2,TP	148
4.4	η_s and f Vs Temperature; $f = 11$ Hz, Sp. #16A,B	149
4.5	η_s and f Vs Temperature; $f = 47$ Hz, Sp. #16A,B	150
4.6	η_s and f Vs Temperature; $f = 170$ Hz, Sp. #16A,B	151

Figure	List of Illustrations	Page
4.7	η_c and f Vs Temperature; f = 165 Hz, Sp. #1,T	152
4.8	η_c Vs Temperature for Different Frequencies; Sp. #1, TP	153
4.9	η_c Vs Temperature for Different Frequencies; Sp. #2, TP	154
4.10	η_c Vs Temperature for Different Frequencies; Sp. #16A,B	155
4.11	η_c Vs Temperature for Different Frequencies; Sp. #1,T	156
4.12	η_c max Per Inch Vs Thickness of Coating, Bending	157
4.13	η_c max Per Inch Vs Temperature of Maximum Damping, Bending	157
4.14	G_2' Vs Temperature; Coating #12325, Sp. #2, TP	158
4.15	G_2'' Vs Temperature for Different Frequencies; Sp. #2, TP	159
4.16	E_2' Vs Temperature; Coating #12325, Sp. #16A,B	160
4.17	E_2'' Vs Temperature for Different Frequencies; Sp. #16A,B	161
4.18	G_2' Vs Temperature; Coating #12325	162
4.19	G_2'' Vs Temperature; Coating #12325	163
4.20	E_2' Vs Temperature; Coating #12325	164

Figure	List of Illustrations	Page
4.21	E_2'' Vs Temperature; Coating #12325	165
4.22	E_2'' Vs Frequency for Different Temperatures; Sp. #16A,B	166
4.23	G_2'' Vs Frequency for Different Temperatures; Sp. #2, TP	167
4.24	Log α_T Vs T^{-1} ; Sp. #16A,B	168
4.25	Log α_T Vs T^{-1} ; Sp. #2, TP	169
4.26	E_2'' Vs Reduced Frequency; Sp. #16A,B	170
4.27	G_2'' Vs Reduced Frequency; Sp. #2, TP	171
4.28	E_2''/E_U Vs $f\alpha_T/f_m$; Sp. #16A,B	172
4.29	G_2''/G_U Vs $f\alpha_T/f_m$; Sp. #2, TP	173
4.30	E_2''/E_U Vs $f\alpha_T/f_m$; Sp. #7, B	174
4.31	E_2''/E_U Vs $f\alpha_T/f_m$; Sp. #15A,B	175
4.32	G_2''/G_U Vs $f\alpha_T/f_m$; Sp. #1, TP	176
4.33	G_2''/G_U Vs $f\alpha_T/f_m$; Sp. #3, TP	177
4.34	G_2'' Vs Temperature; Sp. #2, TP	178,9 & 180
4.35	E_2'' Vs Temperature; Sp. #16A,B	181,2,3
4.36	G_2'/G_U Vs $f\alpha_T/f_m$; Sp. #2, TP	184
4.37	E_2'/E_U Vs $f\alpha_T/f_m$; Sp. #16A,B	185
4.38	G_2' Vs Temperature; Sp. #2, TP	186,7
4.39	E_2' Vs Temperature; Sp. #16A,B	188,9

Figure	List of Illustrations	Page
A3.1	Torsion Pendulum Specimen	190
A3.2	Apparatus for Torsion Pendulum Tests	191
A3.3	Additional Weight; Torsion Pendulum	192
A3.4	Position of Thermocouples; Torsion Pendulum	193
A3.5	Block Diagram of Equipment; Torsion Pendulum	194
A3.6	Level Recorder Plot	195
A4.1	Apparatus for Tests at 32 Hz	196
A4.2	Apparatus for Tests at 47 and 11 Hz	197
A4.3	Bending Specimen	198
A4.4	Position of Thermocouples; Bending	199
A4.5	Block Diagram of Equipment; Bending	200
A4.6	Strain Vs Displacement for Bending Specimen	201
A4.7	Apparatus for Tests at 170 Hz	202
A4.8	Cantilever Beam with Extended Mass	203
A4.9	Free Body Diagram of Cantilever Beam	203
A4.10	Free Body Diagram of Extended Mass	203
A5.1	Apparatus for High Frequency Torsion Tests	204
A5.2	Hollow Torsion Cylinder Specimen	205
A5.3	Position of Thermocouples; High Frequency Torsion	206

Figure	List of Illustrations	Page
A5.4	Shear Strain Vs Angular Displacement; High Frequency Torsion Specimen	207
A5.5	Steel Disc	208
A5.6	Loss Coefficient Vs Amplitude; High Frequency Torsion, 165 Hz	209
A5.7	Applied Moment Vs Angular Displacement	210
A5.8	Angular Displacement Vs Frequency, Holzer	211
A5.9	Mode Shape at 4050 Rad./Sec.	211

Chapter 1. Introduction

1.1 Introduction

This thesis reports the results of an investigation of the damping properties of porcelain enamel coatings. The aim of the investigation was to determine the material parameters which govern the damping behavior of porcelain enamel coatings.

Damping is the term used in vibration and shock analysis to describe any mechanism that dissipates energy. Damping in a material keeps the amplitude of vibration of a system of which the material is a part, under control, thus decreasing the possibility of failure due to fatigue or wear.

Damping measurements have been used as an investigatory tool to aid in understanding the fundamental atomic behavior of materials. Material damping and the development of methods of damping measurement and analysis have been dealt with by Lazan [1]. A review of system damping and an extensive bibliography is given by Plunkett [2]. Plunkett [3], Entwistle [4] and Bradfield [5], review the methods of damping measurement that have been developed and their limitations.

If there is not enough inherent damping in a material, the system damping may be increased by

coating some parts with a material with a high damping energy. Viscoelastic polymers are often used at room temperatures. In this thesis, the properties of porcelain enamels as coating materials at elevated temperatures are examined. Porcelain enamels are hard, inorganic, glassy materials, widely used as protective coatings on metal parts exposed to corrosive and erosive atmospheres. Andrews [6] gives a description of porcelain enamels, their composition, properties, uses and application techniques. They soften over a wide temperature range in which they behave anelastically. For some time, it has been known that enamel coatings, in their softening temperature range, may increase the fatigue life and vibratory damping of a coated member, but no study has been made of the governing parameters.

A cantilever beam apparatus was designed by B. J. Lazan to test porcelain enamels, and the preliminary tests which confirmed their damping capability at high temperatures were performed at Airesearch Manufacturing Company of Arizona [7]. Lee [8] modified the apparatus and conducted tests on porcelain enamels at a frequency of 32 Hz. Lee's apparatus has been further modified during the study reported in this thesis and two torsion devices

were developed to increase the frequency range and investigate the effects of stress state; all three apparatuses are described in later sections of this thesis. An important constraint which controlled the design of these pieces of equipment was that the material under test had to be applied as a thin coating on a base metal.

Porcelain enamels have an atomic arrangement similar to that of glass. There is very little information available about the structure of porcelain enamels. However, a great deal of work has been done on glass, and an extensive literature exists. In 1932, Zachariasen [9] proposed the random network structure of glass which is now commonly accepted. This was later confirmed by Warren et al [10]. Morey [11] and Jones [12] describe the physical and chemical properties of glass. Fitzgerald et al [13] and Spinner [14] studied the temperature variation of the elastic moduli of some glasses. McCormick [15] developed a torsion pendulum apparatus to measure the viscoelastic properties of glass as a function of temperature. Forry [16], Kirby [17], Moore and Day [18], and Copley and Oakley [19] have analyzed the low temperature internal friction peak in

various silicate glasses. However, except for Kadota et al [20], no work reports the damping or modulus properties of glass in the softening temperature range. Most investigations have been concerned with the damping due to ionic diffusion at lower temperatures. This damping is very small and cannot be used for engineering purposes. An Arrhenius relation [21] between time and temperature and a Gaussian distribution in the logarithm of the relaxation times (lognormal distribution) proposed by Yager [22] for dielectric relaxation has been found by most investigators to fit all or part of the ionic diffusion peak in several glasses, with activation energies around 30 kcal/mole [16, 18, 19]. Nowick and Berry [23] have worked out the analysis of continuous relaxation spectra with a Gaussian distribution function and have numerically obtained and tabulated the relationships between the three parameters of a lognormal distribution function and experimentally measurable functions. Other relaxation mechanisms causing a damping peak, particularly grain boundary viscosity, in metals and crystalline ceramics have been studied by Ke [24, 25], Wachtman and Lam [26], and Chang [27], among others.

The damping in porcelain enamels in their softening temperature range is very high, and has hitherto not been studied except for crude experiments which merely confirmed the damping potential of enamel coatings. However, various other properties of porcelain enamels, like strength, resistance to corrosion, erosion and thermal shock, have been studied and the techniques for application of the coating have been perfected [28]. Cowan et al [29] also reported the variation of the Young's modulus of porcelain enamels with temperature but did not make any detailed observations in the softening temperature range.

This thesis describes a test program designed to study the damping properties of porcelain enamel coatings in the softening temperature range. The design of three pieces of apparatus for the measurement of the complex modulus of thin coatings with softening temperatures in the range 400 to 750 C is discussed. The frequency range covered is 1 to 600 Hz. The methods for determining both the complex Young's modulus E^* and the complex shear modulus G^* are shown. A Gaussian distribution in the logarithm of relaxation times is shown to be an adequate description of the relaxation process. The

softening process is shown to follow an Arrhenius relationship with anomalously high apparent activation energies which can only be explained by extensive cooperative processes.

Polymers exhibit a transition range of temperature and stress relaxation studies in this region have been made [30]. Bartenev [31] suggests that inorganic glasses can be looked upon as having a polymeric structure; that they can be viewed as highly cross-linked, spatial polymers. However, certain differences in the structure and behavior of polymers and that of porcelain enamels exist and will be discussed in Chapter 2.

This thesis uses the concept of a distribution of relaxation times and the data reduction methods applicable to polymers and applies them to a specific inorganic material, namely, porcelain enamels. It demonstrates that such a treatment is appropriate, in spite of the fact that porcelain enamel is chemically and structurally different from polymeric materials. These methods lead to several conclusions, hitherto unknown, about porcelain enamels as a class of materials. Chapter 2 describes the porcelain enamel, its composition, method of coating, structure, the mathematical model used to represent

its response in the softening temperature range, and the calculation of experimentally measurable functions from the model--the complex modulus, in this case. The equipment used to study the material properties of porcelain enamels used as coatings on base metals is described in Chapter 3. The basic observation was the decay rate of a freely vibrating system as a function of frequency and temperature, from which the complex modulus of the porcelain enamel was determined as a function of temperature and frequency using the equations developed in Chapter 3. Chapter 4 presents the measured data and compares the experimentally observed values of the complex moduli with those predicted from the assumed model of Chapter 2. A summary and discussion of the results is given in Chapter 5.

1.2 Damping Units

A number of different parameters have been used as quantitative measures of the damping capacity of materials. Some of the more important of these will be defined in this section.

Damping is usually defined in terms of the energy dissipated per cycle when a material is subjected to cyclic strain varying sinusoidally in time. The

specific damping capacity or loss coefficient or loss factor η is given by

$$\eta = (\Delta U)/(2\pi U) \quad (1.1)$$

where ΔU = energy dissipated per cycle

and U = maximum strain energy stored.

If the sinusoidal strain results solely from a uniaxial stress,

$$\Delta U = \oint \sigma d\epsilon = \oint \sigma \dot{\epsilon} dt$$

$$\text{and } U = (1/2)E\epsilon_0^2$$

$$\text{where } \dot{\epsilon} = d\epsilon/dt$$

ϵ_0 = strain amplitude

E = Young's modulus

and \oint indicates integral over a complete cycle.

If ΔU and U are computed for a system, then equation (1.1) gives the system loss coefficient.

The energy dissipation causes a decay or a reduction in the amplitude of vibration of the system which leads to another measure of damping, viz, the decay rate. This is expressed in terms of the logarithmic decrement, δ , given by

$$\delta = \ln(x_0/x_n)/n \quad (1.2)$$

where x_0 = amplitude at a certain cycle

and x_n = amplitude n cycles later.

A third measure of damping is the quality factor Q , determined from the resonant curve of amplitude versus forcing frequency; it is given by

$$Q^{-1} = (\Delta f)/f_r \quad (1.3)$$

where Δf = width of the response curve at
an amplitude of $1/\sqrt{2}$ of maximum
and f_r = resonant frequency

For systems with small, linear damping, independent of amplitude, it can be shown that [1]

$$\eta = Q^{-1} = \delta/\pi \quad (1.4)$$

Oberst [29] characterized the damping behavior of viscoelastic materials subjected to sinusoidal strain-time deformation by means of a complex elastic modulus E^* , where $E^* = E' + iE'' = E'(1+i\eta)$. E' , the storage modulus, is the ratio of that part of the stress which is in phase with the strain, to the total strain; E'' , the loss modulus, is the ratio of that part of the stress that leads the strain by 90° , to the total strain; and η is the loss factor or loss coefficient = E''/E' . E' is related to the maximum stored energy while E'' is related to the energy dissipated per cycle. For the uniaxial stress condition above, it can be shown that

$$U = (1/2)E'\epsilon_0^2$$

$$\text{and } \Delta U = \pi E''\epsilon_0^2$$

$$\text{therefore, } (\Delta U)/(2\pi U) = E''/E' = \eta$$

so that η defined in terms of the real and imaginary parts of the complex modulus is the same as the η defined for a material in terms of the energy dissipation and maximum stored energy per cycle.

Chapter 2. Porcelain Enamels

2.1 Introduction

Porcelain enamels are thin coatings used on metal surfaces for decorative and protective purposes. Andrews [6] gives a detailed description of the enamels, their properties, uses and application techniques. A brief physical description of the enamels, their composition and method of coating is given in Appendix (1).

2.2 Structure of Porcelain Enamels

There is little information available in the literature regarding the microstructure of porcelain enamels. They possess an amorphous structure with little order in it. The major constituent, silica, of porcelain enamels, usually present up to about 30%, possesses a vitreous or glassy structure with only short range order. Even this is broken up considerably by the numerous other substances that make up the porcelain enamel (Appendix (1)). In its simplest form, porcelain enamel is a highly complex glass.

Qualitatively, it is a multi-component, multi-phase system; some of the various oxides present are in solution in the glassy matrix while others are

held in suspension. The suspended phases themselves are often crystalline. The components of the enamel are very inert and do not react with one another chemically. The matrix usually consists of vitreous silica. The oxides held in suspension include those of titanium, tin, antimony, zinc, sodium, potassium, etc. Other chemicals are used in the enamel to ensure that the suspended particles are evenly dispersed in the matrix. An important property imparted to the enamel by suspended oxides like those of tin and titanium, is opacity, and has been the object of chosen scrutiny [32].

Porcelain enamels, because of their vitreous nature, do not possess a definite melting point, but are characterized by a decreasing viscosity as the temperature is increased. The temperature band width over which this softening takes place is relatively wide. In this temperature range, there are large changes in moduli for very small changes in temperature, and it is in this temperature range that porcelain enamels are useful as damping materials. This kind of transition phenomena, characterized by rapid modulus changes, has been observed and studied in several organic polymeric materials [33,34]. However, porcelain enamels, although exhibiting a transition like polymers, are

very different materials, both chemically and physically. They are inorganic as opposed to the organic nature of polymers. Bartenev [31] has suggested that inorganic glasses do indeed possess a polymeric structure--that of a highly cross-linked spatial polymer. In its simplest form, porcelain enamel is a very complex glass, with only as much as 30% of the glass former, silica. Enamels cannot be viewed as multi-component glasses. It is true that they are multi-component systems, but they are also multi-phase systems which is not the case for multi-component glasses. Several of the components present in porcelain enamels are not dissolved in the glassy matrix; they are merely held in suspension, but dispersed uniformly. For example, the opacity of porcelain enamels is caused by the scattering of light incident on crystals of titanium, tin or antimony oxides present in the enamels. Porcelain enamels are homogeneous mixtures of a large number of inorganic oxides with varying structures, crystalline or amorphous; the major constituent is silica which has a vitreous structure.

Another point of dissimilarity between porcelain enamels and organic cross-linked polymers is the

behavior at temperatures greater than the transition temperature. Cross-linked polymers, in general, show a rubbery region, the transition being from a 'glassy' state to a 'rubbery' state [35]. Porcelain enamels, on the other hand, transit from a 'glassy' state to a liquid state; they behave as highly viscous Newtonian liquids at temperatures greater than the transition temperature. This behavior is like that of un-cross linked polymers, which also exhibit a transition from a 'glassy' to a liquid state. It is quite apparent from their other properties, however, that structurally, porcelain enamels cannot be viewed as un-cross linked polymers.

The effect of the numerous oxides suspended in the vitreous silica is to decrease the softening temperature band considerably. Pure vitreous silica softens in the range 1200 to 1500 C. The porcelain enamels used in the study reported in this thesis had softening temperatures between 400 and 800 C. Table 2.1 shows the composition of two enamel frits used in the tests. The difference in composition between the two frits is small - a 6% lower silica content in frit #16845 is made up by slight increases in the percentages of zinc oxide, magnesium oxide, antimony oxide and molybdenum oxide. However, the

softening temperature bands for these two coatings differed widely. They were centered around 465 C for frit #16845 and around 600 C for frit #12325. As one would expect, the softening temperature is higher for the frit with the greater silica content.

Most porcelain enamels have specific gravities varying between 2.35 and 3.00. Table (2.1) shows that frit #16845 contains more of the heavier elements, zinc, antimony and molybdenum, than does frit #12325, and the specific gravities, as reported by the manufacturer [36], are 2.94 for frit #16845 and 2.84 for frit #12325. In this thesis, it will be shown that most porcelain enamels have the same value for elastic moduli below their softening temperatures.

2.3 Structure of Glass

As was mentioned in the last section, the major component of porcelain enamels has a glass-like structure and it is this component which is responsible for the high damping capacity of porcelain enamels at elevated temperatures. Hence, a brief review of the structure of glass in general, and the effect of temperature on a glass, is in order.

Glass basically consists of tetrahedral units of silica, but is far from being crystalline [12]. Each unit consists of an atom of silicon surrounded by four oxygen atoms to form a tetrahedron with the silicon at the centroid and the oxygen atoms at the vertices. Each oxygen atom is shared by two neighboring tetrahedral units. In crystalline silicon dioxide (quartz), the relative orientations of these basic units are fixed. In glass, however, this orientation is random; glass possesses short range order but long range disorder. The structure of glass can be viewed as that of a liquid "frozen in."

Some authors have suggested that glass should be looked upon as a fourth state of matter [37], not as a transparent, fragile substance, but as a separate state in which several substances can be made to exist. Some substances, like silica, lend themselves readily to the formation of a glass and are called "glass formers." Others, like metals, if cooled rapidly enough from the liquid state and if crystallization can be prevented, can be made to form a glass, but are not very stable in this form.

2.3.1 Glass Transition Temperature

To understand the effect of temperature on a glass, consider how a typical property, like volume,

varies with temperature. Figure (2.1) shows this variation. Starting from the high temperature end of the figure, on cooling a glass forming liquid, the volume at first decreases like any other liquid. At the melting (freezing) point, shown by T_f , most pure crystalline substances show a sudden decrease in volume. The volume of a glass, however, continues to decrease at the same rate. On further cooling, the slope decreases rapidly and the volume continues to decrease at a slower rate, which is often the rate at which the solid crystal volume would decrease. This behavior is sometimes referred to as a "second order transition", because the discontinuity is not in the volume itself but in its derivative. The temperature range over which this transition takes place is roughly identified by the "Glass Transition temperature" T_g . It is not a well defined temperature like the melting point of a crystalline solid and has been found to depend on the rate of cooling [38]. The transition temperature is lowest for very slow cooling rates and increases with increasing cooling rates. In practice, the large times involved prohibit the measurement of very low transition temperatures. It is conjectured that there is a lower limit for the transition temperature

and that it is 10 to 100 C below the average experimental value, depending upon the material. However, the transition temperature appears to increase without any limit as the characteristic time is decreased. Glass transition temperatures well above the average measured T_g have been measured in dynamic experiments using ultrasonic frequencies where the characteristic time is very small [39].

2.4 Relaxation in Porcelain Enamels

The storage Young's modulus E' and the loss modulus E'' for a typical porcelain enamel as observed by tests described in Chapter (3.1), are shown as functions of temperature in figure (2.2). In the transition temperature range the storage modulus decreases rapidly with increasing temperature and the loss modulus attains a maximum. The damping in this temperature region is very high.

The rapid decrease in the storage modulus is caused by the relaxation of the atomic bonds in the vitreous network of the material. Relaxation is the adjustment of a material system with time to a new equilibrium state in response to a change in an external variable. A characteristic time for this adjustment is termed the relaxation time. A

definition commonly used for the relaxation time is the time taken for the modulus of the material to relax through $1/e$ of the total relaxation. The relaxation time decreases with increasing temperature and a transition occurs in the material behavior when its temperature has been sufficiently increased so that the relaxation time of the material "crosses" the time scale of the experiment - the period of vibration in this case.

The behavior of an anelastic material is often described by mechanical models, which are discussed in Appendix (2). We start with the dependence on frequency, ω , of the real part M' and the imaginary part M'' of the complex modulus M^* for the case of a system with a single relaxation time, τ . The real part M' decreases from M_U to M_R as the frequency decreases, where M_U is the unrelaxed modulus and M_R is the relaxed modulus. The imaginary part M'' shows a peak at a value of frequency such that $\omega\tau = 1$. When M'' is plotted against $\log(\omega\tau)$, the curve has a width of 1.144 at half maximum. This is called a Debye peak.

The experimentally observed peaks in the functions E'' and G'' for porcelain enamels, when plotted against $\log \omega$, are much broader than the peak

appropriate for a system with a single relaxation time. This suggests a spectrum of more than one relaxation time, rather than a single relaxation time. This is also reasonable from the point of view of the disorder in the structure of the enamel. A discrete spectrum of relaxation times can be obtained by choosing a multi-parameter (more than three) mechanical model to represent the material. But this is not a very useful method, as there is no indication from the experimentally observed modulus functions as to the exact values of the relaxation times or their corresponding relaxation magnitudes. The functions E'' and G'' could be used to determine a discrete spectrum using Tobolsky's procedure X [30]. This method can be used to obtain meaningful relaxation times only if the relaxation times are widely spaced, at least a decade apart. Since there is no evidence of such being the case, and there is reason to believe from the structure of the enamel, that a continuous relaxation spectrum would be appropriate, we shall assume a continuous spectrum of relaxation times for the porcelain enamel.

For an anelastic material with a distribution function $\phi(\ln \tau)$ [†] for the logarithm of the

[†] A logarithmic scale for time and frequency turns out to be particularly convenient.

relaxation times τ , the storage modulus M' and the loss modulus M'' , from [40], are

$$M'(\omega) = M_R + \delta M \int_{-\infty}^{\infty} (\phi(\ln \tau) \omega^2 \tau^2) / (1 + \omega^2 \tau^2) d \ln \tau \quad (2.1)$$

$$\text{and } M''(\omega) = \delta M \int_{-\infty}^{\infty} (\phi(\ln \tau) \omega \tau) / (1 + \omega^2 \tau^2) d \ln \tau \quad (2.2)$$

where δM = the magnitude of the relaxation

$$= M_U - M_R$$

and $\phi(\ln \tau)$ is a distribution function

normalized so that

$$\int_{-\infty}^{\infty} \phi(\ln \tau) d \ln \tau = 1 \quad (2.3)$$

Nowick and Berry [40] have shown that the functions M' and M'' are not particularly sensitive to the form of the distribution function $\phi(\ln \tau)$. For the porcelain enamels, we shall assume a lognormal distribution of relaxation times, i.e. a Gaussian or normal distribution in the logarithm of the relaxation times. Such a distribution is completely specified by three parameters, namely, the magnitude δM of the relaxation, the mean relaxation time τ_m , and the width β of the distribution. It is a realistic distribution and at the same time mathematically tractable. Nowick and Berry have worked out the mathematics of this distribution which is briefly shown in Appendix (2). Since the relaxed modulus M_R

is very small for porcelain enamels, we have assumed that $\delta M = M_U$. The real and imaginary parts of the complex modulus, calculated from these assumptions are shown in Tables (2.2) to (2.5) and in figures (2.3) to (2.6) as functions of frequency and distribution width β .

2.5 Time-Temperature Relationships

For many thermally activated relaxation processes, the relaxation times have been found to follow the Arrhenius relation

$$\tau = \tau_* \exp (Q/RT) \quad (2.4)$$

where τ_* is an inverse frequency factor,
independent of temperature.

Q is the activation energy of the process,
independent of temperature.

R is the gas constant
 $= 1.986 \text{ cal./mole/}^\circ\text{K}$

and T is the absolute temperature.

A distribution in the relaxation times τ can be caused either by a distribution in τ_* or by a distribution in Q , or both. The assumption that the distribution is only in the parameter τ_* is equivalent to assuming that the distribution peak width parameter β is independent of temperature. This

is a valid assumption because the temperature differences that are required to change the relaxation time by several decades are very small. Typically, for porcelain enamels, a frequency increase by a factor of 10 shifts the M" function by about 30F (17C) on the temperature axis. If we assume that Q is not a distributed function, the mean relaxation time is:

$$\tau_m = \tau_{*m} \exp(Q/RT) \quad (2.5)$$

where τ_{*m} is the mean of τ_* .

If τ_{m0} is the mean relaxation time at an arbitrarily chosen reference temperature T_0 , then:

$$\tau_{m0} = \tau_{*m} \exp(Q/RT_0) \quad (2.6)$$

and,

$$\log(\tau_m/\tau_{m0}) = (Q/2.303R)(1/T - 1/T_0)$$

or

$$\log \alpha_T = (Q/2.303R)(1/T - 1/T_0) \quad (2.7)$$

where α_T is the ratio of the mean relaxation time τ_m at temperature T to the mean relaxation time τ_{m0} at temperature T_0 . Thus, the curve of $\log \alpha_T$ vs. T^{-1} is a straight line whose slope is $(Q/2.303R)$.

For an anelastic material, Zener [41] has shown that the maximum damping occurs when

$$\omega_m \tau_m = 1$$

Then ω_m is the frequency in rad/sec for maximum damping at temperature T, so that

$$\begin{aligned}\alpha_T &= \tau_m / \tau_{m0} \\ &= \omega_0 / \omega_m = f_0 / f_m\end{aligned}\quad (2.8)$$

where f_0 is the frequency in Hz for maximum damping at the reference temperature T_0 , and f_m is the frequency in Hz for maximum damping at temperature T . Equations (2.7) and (2.8) provide a means for determining the activation energy Q of the relaxation process from experimentally observed M' or M'' data as functions of temperature at various frequencies.

Chapter 3. Experimental Technique and Calculations

3.1 Experimental Technique

A number of different parameters have been used as quantitative measures of damping, as indicated in Chapter (1.2). The one most often used for engineering purposes is the energy dissipated per cycle when a material is subjected to sinusoidal strain-time deformation. The energy dissipation leads to a reduction in the amplitude or decay of vibration of the system. The most commonly used method for determining the damping capacity of a system is the measurement of the rate at which the amplitude of free vibration of the system decreases. Damping capacity can also be determined from the increase in amplitude of a vibrating system as the excitation frequency is varied through resonance holding the amplitude of the exciting force constant. The energy dissipation can also be determined by measuring the power necessary to maintain vibration at a given amplitude.

The decay rate of a freely vibrating system was the basic observation in the method described in this thesis. Since it is very difficult to obtain a wide frequency range from any one simple test

configuration, three different pieces of apparatus were designed to cover the frequency range from 1 Hz to 600 Hz. They were designed to operate satisfactorily, without undergoing permanent damage, in the temperature range 70F (20C) to 2000F (1100C). A torsion pendulum specimen was used for frequencies between 1 Hz and 15 Hz. A cantilever beam specimen was used in the range 10 Hz to 170 Hz, and a hollow cylindrical torsion specimen was used in the frequency range 165 Hz to 600 Hz. In each case, the frequency of free vibration was changed by changing the total mass of the system. The specimens were made of high temperature alloys and were coated with the porcelain enamel over part of the surface. Measurements were made on each configuration at a number of different temperatures in the range of interest. All parts of the apparatus subjected to high temperatures were made of the same material in order to avoid geometry changes due to differences in thermal expansion. Heating was by electric furnaces and the coated sections of the specimens were maintained at a uniform temperature. In the worst case, the temperature variation across the coating was less than 20F (11C). Since system measurements depend upon integrated properties of

the whole volume being tested, the apparent dependence on temperature is reduced if the various parts of the specimen are at different temperatures. The effective bandwidth in the present tests was about 100F (55C), and 20F (11C) is about the maximum variation that can be tolerated.

In each case, a transducer was used to sense the mechanical vibration and convert it to an analogous voltage. This voltage was used to drive a recorder to determine the decay rate, and a frequency counter for the frequency. The details of the design of the apparatuses, the instrumentation used and the calculation of the natural frequencies, for the three cases are discussed in Appendices (3), (4) and (5) respectively. Appendix (6) describes the various procedural problems that were encountered during the tests and the measures taken to overcome them.

3.2 Calculations

The complex elastic modulus of the coating material is found from the measured system damping, frequency and specimen geometry in all three systems. The general method is the same, but the details are somewhat different in each case. Subscripts b and c will be used to denote system quantities; b for the system with a bare specimen and c for the system with

a coated specimen. Subscripts 1 and 2 will be used to denote the materials; 1 for the base material and 2 for the coating material.

The complex Young's modulus E_2^* of the coating material is determined from the bending test measurements following the methods used by Van Oort [42] and Nashif [43]. The following assumptions are made in deriving the formulae for determining E_2^* .

- 1) The beam is of uniform thickness as shown in figure (3.1).
- 2) Anticlastic curvature is completely constrained so that $\epsilon_{zz} = 0$.
- 3) Since the coating is very thin, and the normal stress on the surface is zero, σ_{yy} is assumed to be zero in the coating.
- 4) The base metal damping is zero, so that the Young's modulus E_1 of the base metal is real.
- 5) The kinetic energy of the mass at the free end is far greater than the kinetic energy of the beam itself. The mass of the coating itself is so small that it does not appreciably change the kinetic energy of the system.
- 6) All strain energy stored is in the beam itself and none in any other part of the system.

Following the same development as Lee [8], the complex bending moment M_C^* of the system from which the system loss coefficient can be determined is

$$\begin{aligned} M_C^* &= M_C' + iM_C'' \\ &= (2/3\rho) [E_1 d_1^3 + E_2' (3d_1^2 d_2 + 3d_1 d_2^2 + d_2^3)] \\ &\quad + i\eta_E E_2' (2/3\rho) (3d_1^2 d_2 + 3d_1 d_2^2 + d_2^3) \end{aligned}$$

where

ρ = radius of curvature of the beam

d_1 = half thickness of the specimen

d_2 = thickness of the coating

E_1 = Young's modulus of base metal

E_2' = Real part of Young's modulus E_2^* of the coating material

η_E = loss tangent of the coating material
 $= E_2''/E_2'$

E_2'' = Imaginary part of Young's modulus E_2^* of the coating material.

The loss coefficient for uniform bending in this system is

$$\begin{aligned} \eta &= M_C''/M_C' \\ &= \eta_E ac/(1+ac) \end{aligned} \tag{3.1}$$

where

a = modulus ratio E_2'/E_1

c = $3t + 3t^2 + t^3$

t = thickness ratio d_2/d_1

The frequency f_b of the system with a bare specimen is given by

$$f_b^2 = U_b / (KE)$$

where U_b = the strain energy stored and (KE) is a kinetic energy term. For the cantilever specimen with a large rigidly connected mass at the free end, the kinetic energy of the mass is much greater than that of the beam itself.

Now,

$$\begin{aligned} U_b &= \int_v (1/2) \sigma_{xx} \epsilon_{xx} dv \\ &= 2Lw \int_0^d (1/2) E_1 \epsilon_{xx}^2 dy \\ &= (LwE_1/\rho^2) \int_0^d y^2 dy \\ &= (L/2\rho^2) E_1 I_1 \end{aligned}$$

where

L = length of the beam

w = width of the beam

ρ = radius of curvature

and I_1 = area moment of inertia of the cross section of the bare beam

$$= (2/3) d_1^3 w$$

Therefore,

$$f_b^2 = KE_1 I_1$$

where

$$K = L/(2\rho^2 (KE))$$

For the system with the coated specimen,

$$f_c^2 = U_c/(KE)$$

Again,

$$\begin{aligned} U_c &= \int_v (1/2) \sigma_{xx} \epsilon_{xx} dv \\ &= 2Lw \int_0^{d_1+d_2} (1/2) \sigma_{xx} \epsilon_{xx} dy \\ &= Lw \int_0^{d_1} E_1 \epsilon_{xx}^2 dy + Lw \int_{d_1}^{d_1+d_2} E_2' \epsilon_{xx}^2 dy \\ &= (L/2\rho^2) (E_1 I_1 + E_2' I_2) \end{aligned}$$

where

I_2 = area moment of inertia of the coating

$$= (2d_1^2 d_2 + 2d_1 d_2^2 + (2/3)d_2^3)w.$$

Therefore,

$$f_c^2 = K(E_1 I_1 + E_2' I_2)$$

where K is the same constant as for the uncoated specimen. Hence,

$$\begin{aligned} f_c^2/f_b^2 &= 1 + E_2' I_2 / (E_1 I_1) \\ &= 1 + a I_2 / I_1 \quad (3.2) \\ I_2 / I_1 &= (2d_1^2 d_2 + 2d_1 d_2^2 + (2/3)d_2^3) / (2/3)d_1^3 \\ &= 3d_2/d_1 + 3d_2^2/d_1^2 + d_2^3/d_1^3 \\ &= 3t + 3t^2 + t^3 \\ &= c \end{aligned}$$

Equation (3.2) becomes

$$f_c^2/f_b^2 = 1 + ac \quad (3.3)$$

Substituting into equation (3.1)

$$\eta_E = \eta(1 - f_b^2/f_c^2)^{-1} \quad (3.4)$$

Equation (3.2) gives

$$E_2' = (E_1/c) (f_c^2/f_b^2 - 1) \quad (3.5)$$

and from the definition of η_E

$$\begin{aligned} E_2'' &= E_2' \eta_E \\ &= (E_1/c) \eta f_c^2/f_b^2 \end{aligned} \quad (3.6)$$

Equations (3.5) and (3.6) are valid for uniaxial stress conditions but our bending specimen has a length to width ratio of almost one; the anti-clastic curvature can be assumed to be fully constrained and a Poisson's ratio correction of $(1-\nu^2)$ is necessary.

$$\text{i.e. } E_2' = (1-\nu^2) (E_1/c) (f_c^2/f_b^2 - 1) \quad (3.7)$$

and

$$E_2'' = (1-\nu^2) (E_1/c) \eta f_c^2/f_b^2 \quad (3.8)$$

The complex shear modulus G_2^* of the coating material is determined from the torsion pendulum tests. The following assumptions are made in this case.

- 1) The coating material is in pure shear and the shear strain amplitude in the coating is uniform.

- 2) The base metal damping is zero so that the shear modulus G_1 of the base metal is real.
- 3) The kinetic energy of the specimen itself is negligible when compared with the kinetic energy of the mass at the free end, and the mass of the coating is so small that it does not change the kinetic energy of the system.
- 4) All strain energy is in the length of the specimen between the support and the weight at the free end.

Equation (3.5) modified by a length correction gives

$$G_2' = (G_1/c) (1 - f_b^2/f_c^2) / (b - (1 - f_b^2/f_c^2)) \quad (3.9)$$

where

G_1 = shear modulus of base material

$c = 3t + 3t^2 + t^3$ where $t = r_2/r_1$

r_2 = coating thickness

r_1 = radius of bare specimen

b = length ratio

= (coated length of specimen)/(total length).

The loss modulus G_2'' is determined from the energy dissipated per cycle. The system loss coefficient η is defined as

$$\eta = (\Delta U)_s / (2\pi U_s)$$

where

$(\Delta U)_s$ = energy dissipated per cycle and

U_s = the maximum energy stored.

For the torsion specimens, the maximum energy stored is equal to the maximum kinetic energy, which is assumed to be completely in the mass at the free end. Thus

$$U_s = (1/2)\omega^2 J\theta^2 \quad (3.10)$$

where

ω = circular frequency

J = mass moment of inertia of the mass

θ = angular displacement of the mass

The strain amplitude in the coating is uniform through its thickness and is

$$\gamma_0 = k\theta \quad (3.11)$$

The strain was measured in the high frequency torsion specimen with strain gages and the constant k was found to be 3.0×10^{-2} (figure (A5.4)). k was assumed to be the radius to length ratio 3.3×10^{-3} for the torsion pendulum specimen.

If there is no damping in the base material, the energy dissipated per cycle is,

$$(\Delta U)_s = \pi G_2'' v \gamma_0^2 \quad (3.12)$$

where

v = volume of the coating.

Thus, from equations (3.10), (3.11) and (3.12)

$$G_2'' = (\eta J \omega^2) / V k^2 \quad (3.13)$$

The system loss coefficient was determined from decay measurements. For a linear system, with low, amplitude independent damping, in free vibration [1],

$$\eta_s = (\ln(x_0/x_n)) / (\pi n)$$

where

x_0 = amplitude at a certain cycle

x_n = amplitude n cycles later.

Now,

$$\begin{aligned} \ln(x_0/x_n) &= (\ln 10) A(\text{dB})/20 \\ &= 2.303 A/20 \end{aligned}$$

and

$$n = ft$$

where

f = natural frequency

and

t = time for a decrease of A dB.

Therefore,

$$\begin{aligned} \eta_s &= (2.303/(20\pi)) A/ft \\ &= 3.66 \times 10^{-2} A/ft \end{aligned}$$

In deriving the formulas for the complex moduli, it was assumed that energy is dissipated entirely in the coating and that there is no damping in the base material. i.e. η in equations (3.8) and (3.13) is $(\Delta U)_c / (2\pi U_s)$ where $(\Delta U)_c$ is the energy dissipated per

cycle in the coating and U_s is the maximum energy stored in the system. This is not strictly true and a correction must be made for the actual system damping with a bare specimen.

Let

$$\begin{aligned}\eta_b &= \text{damping coefficient for the system with} \\ &\quad \text{a bare specimen} \\ &= (\Delta U)_b / (2\pi U_b) \\ &= \frac{\text{energy dissipated/cycle in bare specimen}}{2\pi (\text{maximum energy stored})}\end{aligned}$$

$$\begin{aligned}\eta_s &= \text{system damping coefficient with a coated} \\ &\quad \text{specimen} \\ &= (\Delta U)_s / (2\pi U_s)\end{aligned}$$

and

$$\eta_c = (\Delta U)_c / (2\pi U_s) \text{ is the damping that would have been observed if the bare specimen damping were zero.}$$

Since the energy stored in the coating is negligibly small, we assume that $U_b = U_s$, and that $(\Delta U)_c = (\Delta U)_s - (\Delta U)_b$. Then,

$$\begin{aligned}\eta_c &= ((\Delta U)_s - (\Delta U)_b) / (2\pi U_s) \\ &= (\Delta U)_s / (2\pi U_s) - (\Delta U)_b / (2\pi U_b) \\ &= \eta_s - \eta_b\end{aligned}$$

The determination of the complex modulus of the coating material depends critically upon the ratio of the frequencies of the coated and uncoated specimens.

This can be seen in equations (3.7) and (3.9) which use the small differences in the frequencies of the coated and uncoated specimens. In some cases, the bare specimen was tested before coating it. Since there was little difference among the measured values of damping coefficients, an average curve of loss coefficient as a function of temperature was assumed for all specimens, except for support effects which were assumed to be independent of temperature. The frequency change with temperature was assumed to depend only on the modulus change and thus to be in the same proportion for all specimens.

At a sufficiently high temperature the modulus of the coating decreases enough that its contribution to the stiffness of the specimen is negligible. For thin coatings, then, the frequency of the system with the coated specimen is the same as that with the bare specimen alone. Hence, the frequency curve of the bare specimen is adjusted proportionally so that the frequency with the coated specimen approaches that with the bare specimen near the firing temperature of the coating. This adjusted curve is used as an estimate of the bare specimen frequencies of the given specimen.

It is assumed that there is no energy dissipation in the coating at room temperature and that any change in the measured system loss coefficient at room temperature between the coated and uncoated specimens is due to support effects and is independent of temperature. The bare specimen damping curve is adjusted vertically to match the curve for the coated specimen at room temperature. The bare specimen loss coefficient for a given specimen is found from this curve. Figure (3.2) shows the system loss coefficient and frequency as functions of temperature for a typical specimen. The adjusted bare specimen damping and frequency curves are also shown.

In the bending tests at 11 Hz and 47 Hz, the heavy arm rigidly attached to the free end of the specimen justifies the assumption that strain energy is stored only in the beam itself and none in the heavy mass. However, in order to make measurements at 170 Hz, the heavy arm was replaced by a light rod and the above assumption is no longer valid. Figure (3.3) shows the loss coefficient and frequency as functions of temperature for the same specimen as in figure (3.2), when decaying freely at 170 Hz. The maximum loss

coefficient is 6.0×10^{-3} at 170 Hz as compared with 11.5×10^{-3} at 47 Hz. The percentage decrease in frequency as a result of the softening of the coating is less for the high frequency measurement than it is for the lower frequency one. If we assume that strain energy is stored in the specimen and elsewhere in the system also at 170 Hz, but only in the specimen at 11 or 47 Hz, then we may correct the damping coefficient to get comparable values for the 170 Hz case.

Let $U^{(1)}$ be the energy stored in the specimen alone

$$U^{(1)} = U_1^{(1)} + U_2^{(1)}$$

where

$U_1^{(1)}$ = energy stored in the base metal

and

$U_2^{(1)}$ = energy stored in the coating.

Let $U^{(2)}$ be the energy stored elsewhere in the system. Then for a lower frequency f_A , $U_A^{(2)} = 0$, where the subscript A refers to a lower frequency, 11 Hz or 47 Hz.

Let f_A be the frequency that would have been observed if the coating had not softened rapidly.

Then

$$f_A^2 = (U_{1A}^{(1)} + U_{2A}^{(1)}) / KE(\epsilon_0)$$

where $KE(\epsilon_0)$ is a function of the strain amplitude ϵ_0 only.

Let \tilde{f}_A be the frequency actually measured when the coating softens. Then

$$\tilde{f}_A^2 = U_{1A}^{(1)} / KE(\epsilon_0)$$

Therefore,

$$\begin{aligned} r_A &\approx (f_A^2 - \tilde{f}_A^2) / \tilde{f}_A^2 \\ &\approx 2(f_A - \tilde{f}_A) / f_A \\ &= U_{2A}^{(1)} / U_{1A}^{(1)} \end{aligned} \quad (3.14)$$

Now,

$$\begin{aligned} \eta_A &= \text{loss coefficient at a lower frequency} \\ &= (\pi E_{2A}'' \epsilon_0^2 V) / (2\pi U_{1A}^{(1)}) \end{aligned}$$

where

E_{2A}'' = the loss modulus

and

V = volume of coating

Then

$$E_{2A}'' = k U_{1A}^{(1)} \eta_A \quad (3.15)$$

where

$$k = 2 / (\epsilon_0^2 V)$$

At the higher frequency $f_B = 170$ Hz,

$U_B^{(2)}$ = energy stored in the system other than
in the specimen

$\neq 0$

Defining f_B and \tilde{f}_B similarly to f_A and \tilde{f}_A , we have

$$f_B^2 = (U_{1B}^{(1)} + U_{2B}^{(1)} + U_B^{(2)})/KE(\epsilon_0)$$

and

$$\tilde{f}_B^2 = (U_{1B}^{(1)} + U_B^{(2)})/KE(\epsilon_0)$$

Therefore,

$$\begin{aligned} r_B &\hat{=} (f_B^2 - \tilde{f}_B^2)/\tilde{f}_B^2 \\ &\approx 2(f_B - \tilde{f}_B)/\tilde{f}_B \\ &= U_{2B}^{(1)}/(U_{1B}^{(1)} + U_B^{(2)}) \end{aligned} \quad (3.16)$$

and

$$\begin{aligned} \eta_B &= \text{loss coefficient at frequency } f_B \\ &= E_{2B}'' / k(U_{1B}^{(1)} + U_B^{(2)}) \end{aligned}$$

Therefore,

$$E_{2B}'' = k(U_{1B}^{(1)} + U_B^{(2)})\eta_B \quad (3.17)$$

Since $U^{(1)}$ is independent of frequency

$$\left. \begin{aligned} U_{1A}^{(1)} &= U_{1B}^{(1)} = U_1^{(1)} \\ U_{2A}^{(1)} &= U_{2B}^{(1)} = U_2^{(1)} \end{aligned} \right\} \text{for the same } \epsilon_0$$

and writing $U_B^{(2)}$ as $U^{(2)}$, we have from equations (3.1)

and (3.3)

$$\begin{aligned} r_A/r_B &= R \\ &= (U_1^{(1)} + U^{(2)})/U_1^{(1)} \\ &= 1 + U^{(2)}/U_1^{(1)} \end{aligned} \quad (3.18)$$

The quantities r_A and r_B can be determined from the frequency curves at 47 and 170 Hz. Again,

$$\begin{aligned} E_{2B}'' / E_{2A}'' &= (U_1^{(1)} + U^{(2)}) / U_1^{(1)} \cdot \eta_B / \eta_A \\ &= (1 + U^{(2)} / U_1^{(1)}) \cdot \eta_B / \eta_A \\ &= R \cdot \eta_B / \eta_A \end{aligned} \quad (3.19)$$

The ratio η_B / η_A can be determined from the measured values of the loss coefficient.

Table (3.1) lists the frequencies, frequency changes, loss coefficients and the ratios R and η_A / η_B for several specimens coated with porcelain enamels of various types. Since the ratios R and η_A / η_B are both approximately 1.8 for all specimens, equation (3.19) shows that the loss modulus E_2'' of the coating material does not depend appreciably upon frequency. Therefore, the lower value of the loss coefficient measured at the higher frequency is not due to an increase in frequency but to the change in the test conditions. Hence, the loss coefficient measured at 170 Hz should be multiplied by 1.8 to obtain the loss coefficient that would have been observed had all of the strain energy been in the specimen alone and none in the rest of the system.

Chapter 4. Test Results

4.1 Introduction

The data from the damping experiments conducted on porcelain enamel coatings using the method and equipment described in Chapter 3, and its analysis will be presented in this chapter. The system loss coefficient in the torsion pendulum and bending tests was independent of stress level. The torsion pendulum tests were conducted at a shear stress amplitude of 5,000 psi, and the bending tests at an amplitude of 10,000 psi. For the high frequency torsion specimen as indicated in Appendix (5), the system loss coefficient was amplitude dependent. The results of tests on this apparatus correspond to a shear stress level of 50 psi. However, the loss coefficient in the coating alone did not depend on the stress level. The various coatings tested, their firing temperatures and manufacturers are listed in Table (4.1). Only one coated high frequency torsion specimen was tested, using a frit of C.V. #12325.

4.2 Presentation of Data

Figures (4.1) to (4.3) show the measured loss coefficient and frequency as functions of temperature

for a torsion pendulum specimen (#2) at three nominal frequencies of 1.2 Hz, 8.4 Hz and 14.25 Hz. The same functions are shown in figures (4.4) to (4.6) for a bending specimen (#16A) at frequencies of 11 Hz, 47 Hz and 170 Hz. The bare specimen damping and frequency curves are also shown in each case. Figure (4.7) shows the damping η_c due to the coating alone and frequency as functions of temperature for the high frequency torsion specimen at a frequency of 165 Hz. The bare specimen damping measured in this case was very high, greater than 0.002 at room temperature. This was a result of improper fit in the expansion joints between the test section and the end grips of the specimen. Tables (4.2), (4.3) and (4.4) list the maximum loss coefficient and corresponding temperatures for specimens tested in low frequency torsion, bending and high frequency torsion respectively. The temperature of maximum loss coefficient was determined from the graphs of η_c vs temperature for all specimens. The peaks in these functions were symmetrical and the temperature of maximum loss coefficient was obtained as the average of the two temperature readings corresponding to the same value of η_c a little below the maximum. The tests at 33 Hz were performed by Lee [8] and the

results shown at that frequency have been taken from his thesis. The temperature points in Lee's thesis around the damping peak were very widely spaced and the maximum loss coefficient and temperature values shown are not very reliable. The coating for specimens #16A and 22, bending, used a frit with the same number (#12325) as that for specimens #16 and 18A, bending; but was prepared and applied at a different place under different conditions. This perhaps explains the difference in the results for specimens #16A and 22, when compared with those for specimens #16 and 18A. Specimens #15 and 15A, bending, were coated with a frit carrying the same number (#16845) also, prepared and applied at different places; but the results in this case are not much different. Figures (4.8) and (4.9) show the system loss coefficient, η_c due to the coating alone as a function of temperature for two torsion pendulum specimens in the region of maximum damping at three nominal frequencies 1.2 Hz, 8.4 Hz and 14.25 Hz. Figure (4.10) shows the same curves for a bending specimen (#16A) at frequencies 11 Hz, 47 Hz and 170 Hz. The loss coefficient measured at 170 Hz has been multiplied by 1.8, as indicated earlier, to obtain the loss coefficient

that would have been measured had all of the strain energy been in the bending specimen. Figure (4.11) shows η_c vs temperature for the high frequency torsion specimen at frequencies 165 Hz, 340 Hz, 430 Hz and 600 Hz. Where measurements were made at sufficiently high temperatures that the damping peak could be completed, the peak width at half maximum loss coefficient is also shown in Tables (4.2) to (4.4).

The following general observation can be made:

- a) All coatings exhibit a transition range of temperature during which the system loss coefficient reaches a maximum and the frequency drops sharply. The peak in the loss coefficient occurs at a temperature 100 to 200C below the firing temperature of the coating.
- b) For a given coating, the maximum magnitude of the system loss coefficient is almost directly proportional to the coating thickness, at least for the thicknesses tested. Figure (4.12) shows η_c max per unit thickness vs thickness of the coating for those tested in bending.
- c) For coatings made from different frits with approximately the same thickness, there is some indication that the maximum system loss coefficient

increases with the maximum damping temperature. For the coatings tested in bending, figure (4.13) shows $\eta_{c \text{ max}}$ per unit thickness vs. maximum damping temperature.

d) The magnitude of the maximum system loss coefficient is independent of frequency.

e) In almost every case, there is an increase in the temperature of maximum damping with increasing frequency. This shift in temperature is very small, typically about 20C for a frequency factor of 10; and in some cases this temperature shift is not apparent, probably because of small errors in the temperature measurement.

f) In most cases, the peak width at half maximum is about 60C in bending and about 50C in the torsion pendulum tests.

4.3 Data Reduction and Analysis

4.3.1 Complex Modulus

The complex modulus of the coating was determined from the equations derived in Chapter (3.2). The storage shear modulus G_2' and the loss shear modulus G_2'' of the coating were calculated from the torsion pendulum tests using equations (3.9) and (3.13). The storage Young's modulus E_2' and the loss Young's

modulus E_2'' were calculated from the bending tests using equations (3.5) and (3.6). The results from the hollow torsion cylinder apparatus were not satisfactory. The loss shear modulus G_2'' was calculated for coating #12325 from the data shown in figure (4.11) obtained using the hollow torsion cylinder apparatus. The value obtained for G_2'' , however, was inconsistent with the loss modulus values from the bending and torsion pendulum tests for the same coating. Figures (4.14) and (4.15) show G_2' and G_2'' of coating #12325 as functions of temperature calculated from tests on torsion pendulum specimen #2. Figures (4.16) and (4.17) show E_2' and E_2'' for the same coating as functions of temperature calculated from tests on bending specimen #16A. The storage modulus shows a sharp drop with increasing temperature in the transition region and the loss modulus reaches a maximum. Tables (4.5) and (4.6) list the room temperature values of the storage modulus and the maximum loss modulus values for the various coatings. For torsion pendulum specimen #3, the coating was so thin that the system frequency difference between the coated and uncoated specimens was very small. Hence, reliable G_2' values for coating #16845 could not be obtained. Except for results from specimen

#16, the Young's storage modulus for all coatings is about $10-11 \times 10^6$ psi at room temperature. The maximum value of E_2'' is about 1.45×10^6 psi for coatings #12325 and #16845, and as high as 2.0×10^6 psi for coating S9919D. For coating #12325, the storage modulus and the loss modulus, obtained from tests on sp. #16, are both about 30% higher than the moduli obtained from tests on sps. #16A or 22. The coatings on the three specimens carried the same frit number, but the frit used for sp. #16 belonged to a different batch and the coating on sp. #16 was applied at a different place. However, it is doubtful that this is the cause of the high modulus. The storage modulus of other porcelain enamels tested agree with the values obtained from sps. #16A and 22. The high values obtained for sp. #16 are probably due to an error in measurement. Equations (3.5) and (3.6) show that only an error in the measurement of the coating thickness could cause both the storage modulus and the loss modulus to increase or decrease in the same proportion. The thickness of the coating on sp. #16 is only 0.00185 inch, and more likely to be in error than the thicknesses of other thicker coatings. The coating thicknesses were obtained as the difference in thickness between the coated and

uncoated specimens. Unfortunately, once a specimen is coated, the uncoated specimen thickness measurement cannot be repeated to check the value obtained for the coating thickness. It is believed that the high modulus values measured for the coating on sp. #16 is due to a 30% error in the measurement of the coating thickness. Some general observations can be made about the modulus values.

- a) The maximum value of the loss modulus does not depend on frequency.
- b) The width of the loss modulus peak at half maximum is about 60C for coatings tested in bending and 50C for those tested in torsion--the same as observed for the η_c peak in the two cases.
- c) There is an increase in the temperature of maximum loss modulus with increasing frequency. This shift in temperature with frequency is not very apparent in the storage modulus plots because the system frequency difference between the coated and uncoated specimens is very small near the transition region and the modulus values calculated from equations (3.5) and (3.9) are prone to large errors--as much as 50% as will be shown in a later section.
- d) The measured modulus values for the same coating using different specimens and different

thicknesses show good agreement. Figures (4.18) and (4.19) show G_2' and G_2'' for coating #12325 as functions of temperature at two different frequencies calculated from two torsion pendulum specimens with different coating thicknesses. Figures (4.20) and (4.21) show E_2' and E_2'' for the same coating as functions of temperature at two different frequencies calculated from two different bending specimens with different coating thicknesses. The scatter is greater for the storage modulus data because of the small frequency differences used in its computation. This is discussed further in a later section. The consistency with which the low temperature values for the storage modulus for a given specimen at a specific frequency lie above or below the trend line is because smoothed curve values were used for the frequency rather than individual points.

From figures (4.19) and (4.21) it can be seen that the maximum values of G_2'' and E_2'' for coating #12325 are 0.74×10^6 psi and 1.34×10^6 psi respectively.

For a material with stress strain relation $\sigma = M^* \epsilon$, where $M^* = M' + iM''$ is a complex modulus, subjected to sinusoidal deformation $\epsilon = \epsilon_0 \cos \omega t$, it can be shown that the energy dissipated per cycle is given by [1]

$$\Delta U = \pi M'' \epsilon_0^2 \quad (4.1)$$

For the bending specimen configuration with anti-clastic curvature completely constrained, the effective Young's modulus is given by $E^*/(1-\nu^2)$ i.e.

$$\sigma_x = (E^*/(1-\nu^2)) \epsilon_x \quad (4.2)$$

so that the energy dissipated is given by

$$\Delta U = \pi E'' \epsilon_0^2 / (1-\nu^2) \quad (4.3)$$

where ϵ_0 is now the amplitude of the strain in the x direction (figure 3.1). From Hooke's Law:

$$\epsilon_x = (1/E) (\sigma_x - \nu \sigma_y - \nu \sigma_z)$$

$$\epsilon_y = (1/E) (\sigma_y - \nu \sigma_x - \nu \sigma_z)$$

and

$$\epsilon_z = (1/E) (\sigma_z - \nu \sigma_x - \nu \sigma_y)$$

With no anticlastic curvature, $\epsilon_z = 0$ and assuming $\sigma_y = 0$, we get,

$$\epsilon_y = -(\nu/(1-\nu)) \epsilon_x \quad (4.4)$$

From a Mohr strain diagram, it can be seen that the amplitude of maximum shear stress γ_{\max} is:

$$\gamma_{\max} = (1/(1-\nu)) \epsilon_0 \quad (4.5)$$

Assuming that energy dissipation is due to shear deformation alone, we get

$$\begin{aligned} \Delta U &= \pi G'' \gamma_{\max}^2 \\ &= \pi G'' \epsilon_0^2 / (1-\nu)^2 \end{aligned} \quad (4.6)$$

From equations (4.3) and (4.6), we get

$$E'' = ((1+\nu)/(1-\nu)) \cdot G'' \quad (4.7)$$

Substituting for E'' and G'' from figures (4.19) and (4.21), we get

$$1.34 = ((1+\nu)/(1-\nu)) 0.74$$

or

$$(1+\nu)/(1-\nu) = 1.81$$

which corresponds to a value of $\nu = 0.29$. The value of ν for coating #16845 at the critical temperature with $E''_{\max} = 1.30 \times 10^6$ psi and $G''_{\max} = 0.53 \times 10^6$ psi is 0.40. Room temperature values for the Poisson's ratio for glass lie between 0.2 and 0.25. As the temperature increases, the value of ν also increases [14]. At the firing temperature of the coating, one would expect ν to have reached its maximum value of 0.5; the peak in the loss modulus occurs at about 100 to 200C below the firing temperature, and a value between 0.3 and 0.4 for ν at this temperature is a reasonable one.

4.3.2 Distribution of Relaxation Times

The method of reduced variables [35] was used to analyze the temperature and frequency dependence of the modulus of the coating material in the transition region. This method transforms the temperature and

frequency scales so that the observed modulus values can be brought on to a single curve covering a very wide range of temperature and frequency. It is particularly useful if the available frequency range is limited, which is usually true for simple testing apparatus. If the tests can be made at various temperatures, it is possible by this method to predict the effect of a much wider range of frequencies than that available experimentally.

The procedure was as follows. First, from the graph of E_2'' vs temperature at 3 different frequencies (figure (4.17)), the variation of E_2'' with the logarithm of frequency, using temperature as a parameter, was obtained. This is shown in figure (4.22). Figure (4.23) shows this variation for G_2'' . A reference temperature T_0 within the range of experiments was chosen, usually about the middle of the transition region. At each temperature, the average frequency factor by which the corresponding curve (figure (4.22)) had to be shifted to match the curve corresponding to T_0 was determined. The logarithm of the frequency shift factor α_T is shown as a function of T^{-1} in figures (4.24) and (4.25), for the bending and torsion pendulum cases respectively. From equation (2.7), this curve should

be a straight line for constant activation energy. The points fall reasonably close to a straight line; so the best straight line was drawn through the points by inspection. The activation energy, Q , of the relaxation process was determined from the slope of this line using the formula

$$Q = 2.303 Rs \quad (4.8)$$

where

R = the gas constant

$$= 1.987 \text{ cal/mole/}^\circ\text{C}$$

and

s = slope of the line.

The E_2'' and G_2'' data at all temperatures was shifted to the reference temperature by using the frequency shift parameter α_T . $E_2'' (G_2'')$ was found from measurements at a given temperature T and frequency f ; the frequency f was multiplied by that α_T corresponding to T to obtain $f\alpha_T = f_0$ which is the frequency which would give the same value of $E_2'' (G_2'')$ at the reference temperature T_0 . Figures (4.26) and (4.27) show E_2'' and G_2'' as functions of frequency for coating #12325 obtained from tests on specimens #16A (Bending) and #2 (Torsion Pendulum). Some observations on the dependence of $E_2'' (G_2'')$ on frequency:

a) The points in figures (4.26) and (4.27) fall reasonably close to a curve that peaks symmetrically at a certain frequency. The curves shown have been drawn by inspection.

b) The width of the peak indicates a distribution of relaxation times rather than a single relaxation time. As indicated in Chapter (2.4), the width at half maximum for a single relaxation time would be equal to that for a Debye peak, i.e. 1.144 when E_2'' (G_2'') is plotted against the common logarithm of frequency.

The mean relaxation time τ_m , at temperature T_0 was determined as the reciprocal of the reduced circular frequency, ω_m , at which E_2'' (G_2'') attains a maximum. The loss modulus was normalized with respect to the unrelaxed modulus, E_U or G_U , and the frequency with respect to the frequency f_m at the peak (corresponding to the mean relaxation time τ_m). The unrelaxed modulus, E_U or G_U , was chosen as the value of the storage modulus, E' or G' , at approximately 150C below the temperature for maximum loss modulus. This is approximately the temperature at which the loss modulus begins to increase, indicating the beginning of the relaxation process. The points in figures (4.26) and (4.27) were then

replotted on the curves shown in figure (2.5) obtained from a lognormal assumption for the distribution of relaxation times. The points so plotted are shown in figures (4.28) and (4.29). By inspection of the peak height, the value of the width parameter, β , was obtained as 6 for the bending specimen #16A, and 4.0 for the torsion pendulum specimen #2. For bending specimen #16A, the points closely follow the curve for $\beta = 6$. For torsion specimen #2, the points do not follow the curve for $\beta = 4.0$ closely. There is more scatter in the torsion pendulum data. Figures (4.30) and (4.31) show the same data for two other bending specimens and figures (4.32) and (4.33) show the data for two other torsion pendulum specimens. The bending data, in general, show less scatter than the torsion pendulum data. For bending specimens #7 and 15A, β can be read off as 3 and 5 respectively, and the points in each case follow the corresponding curve closely. For torsion pendulum specimens #1 and 2, both with the same coating, #12325, $\beta = 4$ is satisfactory. The points are distributed with reasonable scatter around the curve for $\beta = 4$. The most scatter is seen in the low frequency or high temperature end. For torsion pendulum specimen #3, the peak height corresponds to

$\beta = 5$, but the points follow a curve approximately parallel to the one for $\beta = 4$. From the evidence of the behavior of the other porcelain enamels, one can disregard the possibility that the enamel (#16845) on specimen #3 does not obey a lognormal relaxation law. The discrepancy observed can then be ascribed to errors in measurement. The loss modulus can be obtained quite accurately, and as shown in the previous section, the peak value of the shear loss modulus, obtained from the torsion pendulum experiments compared well with the peak value of the Young's loss modulus obtained from the bending experiments for the same coating, with a value of 0.40 for ν at the transition temperature. The difficulty is in getting an accurate value for the unrelaxed modulus G_U . As mentioned earlier, (Chapter 4.3.1), the storage modulus G' was not calculated for the coating on specimen #3 because the coating was so thin that the difference in the system frequency with the coated and uncoated specimens was extremely small. G_U was assumed to be $1/(2(1+\nu))$ times E_U , where E_U was obtained from a bending test on the same coating (specimen #15A). ν was assumed to be 0.25. A change in the choice of ν from 0.25 to 0.35 will raise each point in figure (4.33) by as much as 8%. The points need be raised

about 20% to match with the curves for $\beta = 4$. There is no reason to believe that the enamel on specimen #3 behaves differently from other enamels. It is believed that errors in measurements caused the difference observed in the case of specimen #3, and that $\beta = 4$ is the appropriate value for that coating. One can conclude from figures (4.28) to (4.33) that the bending measurements are more accurate than those in torsion.

Tables (4.7) and (4.8) list the values of E_2'' max (G_2'' max), E_U (G_U), f_m at T_0 , T_0 , β and Q for the various coatings tested in bending and torsion. For each coating, the temperature corresponding to a peak frequency f_m of 50 Hz was determined using the graph of $\log \alpha_T$ vs T^{-1} for that coating. The following comments can be made about the values shown in Tables (4.7) and (4.8).

a) For a given coating, prepared and applied under identical conditions, there is very good agreement in the values of the loss modulus, the temperature T_0 , the width parameter β , and the activation energy Q regardless of coating thickness. See for instance coating S9919D in the bending specimens and coating #12325 in the torsion specimens.

b) For the same coating applied under different conditions and subjected to the same deformation, for instance, specimens #16 and 16A, and specimens #15 and 15A in bending, values shown in the Table do not agree. The coating used for each pair of specimens had the same frit number, but the frit was bought in different batches. Other differences were possibly in (1) the additions to the frit--normally referred to as mill additions--used to impart certain qualities like opacity, ease of firing, etc., and (2) the firing process, in which several factors such as surface preparation, rate of heating, duration of hold of the firing temperature, and rate of cooling could have been different. The coatings applied at the University of Minnesota, on specimens #15A and 16A, tend to have a higher temperature T_0 , for the same peak frequency f_m . As has been discussed earlier, it is suspected that the high value for the modulus observed for the coating on specimen #16 is due to an error in the measurement of the coating thickness.

c) For coatings prepared and applied at the same place but subjected to different states of stress (bending specimen #16A and torsion pendulum specimens #1 or 2), there is a difference in the value of the

width parameter β measured. From figures (4.28) and (4.29) it can be seen that $\beta = 6$ is appropriate for the bending case while $\beta = 4$ fits the torsion case. However, the values of $E_2''_{\max}$, $G_2''_{\max}$ and the temperature T_0 for the same peak frequency agree very well. The width of the peak for the loss coefficient vs. temperature curve was also narrower for the torsion case (Tables (4.2) and (4.3)). Since system measurements depend on integrated properties through the whole volume being tested, the apparent dependence on temperature is reduced if different parts of the specimen are at different temperatures. Since the temperature distribution in the torsion specimen is less uniform than that in the bending specimen, any errors in the temperature measurement should cause a wider peak in the torsion case than in bending. Hence, we can safely say that the difference in β between the two cases does not arise from erroneous temperature measurements. The lower β in torsion is accompanied by a lower measured activation energy Q . The difference in β between torsion and bending cases is also apparent for the coating #16845.

There appear to be two possible reasons for the difference in β . 1) The state of stress to which the

coating is subjected, sinusoidal shear in one case (superimposed upon a very small static tension due to the weight of the pendulum) and constrained uniaxial tension in the other. 2) The composition of the base metal in the two cases. The torsion pendulum specimens were made of multimet alloy due to lack of immediate availability of Hastelloy X stock of the required size.

In order to investigate this, a bending specimen (#M1) was made of Multimet alloy and coated with frit #12325. Tests on this specimen gave the following results.

$$E_U \approx 9 \times 10^6 \text{ psi}$$

$$E''_{2 \text{ max}} \approx 1.7 \times 10^6 \text{ psi}$$

$$T_0 \text{ (for } f_m = 50 \text{ Hz)} = 589\text{C}$$

$$Q = 220 \text{ kcal/mole}$$

and

$$\beta = 4.5$$

The modulus values agree well with the previous measurements on this coating. The temperatures measured for this specimen were in general about 15C lower than those for specimen #16A or for the torsion specimens. However, what is interesting is that the values for activation energy Q and the width parameter β agree better with the values obtained

from the torsion specimen with the multimet alloy base, than with those from the bending specimen made of Hastelloy X, both coated with the same coating #12325. This means that 1) the state of stress does not affect the value of β . Most of the energy dissipation is due to shear deformation [44], and it has been so assumed in earlier calculations in this thesis. If there is only one mechanism that causes energy dissipation, it is indeed doubtful that the state of stress to which the coating is subjected can influence the value of β so significantly.

2) The composition of the base metal does affect β . The compositions of the two alloys used as bases in the two cases are shown in Table (4.9). The multimet alloy contains a significantly higher percentage of Cobalt and Iron, while the Hastelloy X is high in Nickel and Molybdenum. It is possible that during the firing process, some of the metallic elements diffuse into the coating. Since the coatings are very thin, this is sufficient to significantly change the composition of the coating from that of the uncoated frit. Hence, the difference in measured β between the Hastelloy X and multimet alloy specimens coated with the same material. This change in the final composition of the coating might also account for the lower temperatures measured in

the case of specimen M1.

d) The value of β does not have any observable relation with the firing temperature of the coating.

e) An increase in β is associated with an increase in Q , i.e. the wider the distribution, the greater the activation energy.

f) The activation energies measured are very high. The activation energy for a diffusion mechanism is typically 30 kcal/mole. The activation energy for coating S9919D and #16845 are within the range of activation energies for viscous flow in glass forming silicon dioxide [12]. But the activation energy of about 300 kcal/mole for coating #12325 is considerably higher.

Figures (4.34) and (4.35) show the values of G_2'' and E_2'' calculated from the actual measured data for specimen #2 in torsion and specimen #16A in bending compared with the curve calculated from the lognormal distribution assumption using the parameters determined as shown above. The agreement is well within experimental error, particularly in the temperature region where the loss modulus peaks. (An error analysis is made in the next section.)

In determining the frequency shift factor α_T as a function of temperature, the loss modulus rather than the storage modulus was used because the error

involved in the calculation of the loss modulus is smaller and there is less scatter in the data. This can be seen in figures (4.18), (4.19), (4.20) and (4.21). Once α_T is known as a function of temperature, it can be used to shift the storage modulus data also to a reference temperature. The points taken from a smoothed curve of E_2' vs. temperature and G_2' vs. temperature were reduced to temperature T_0 and normalized and are shown in figures (4.36) and (4.37) plotted with the normalized curves of figure (2.6) obtained from a lognormal assumption for the distribution of relaxation times. Figures (4.38) and (4.39) show the actual measured values of G_2' and E_2' compared with the curve of G_2' or E_2' vs. temperature calculated from the lognormal assumption using the parameters determined above. It can be seen that the agreement is again within experimental error.

4.4 Error Analysis

The storage modulus E_2' and the loss modulus E_2'' were calculated from measured data using the equations

$$E_2' = (E_1/c) (f_c^2/f_b^2 - 1) \quad (4.9)$$

and

$$E_2'' = (E_1/c) \eta f_c^2/f_b^2 \quad (4.10)$$

where

E_1 - Young's modulus of base metal

$$c = 3t + 3t^2 + t^3$$

t = thickness ratio d_2/d_1

f_c = system frequency with coated specimen

f_b = system frequency with bare specimen

and

η = system loss coefficient due to the coating alone.

This method of calculation introduces large errors in the value of E_2' even for small errors in the measured frequency values. It can be seen that the calculation of the storage modulus depends critically upon the small differences in the system frequency with the coated and uncoated specimens.

Let $\Delta()$ represent the relative error in the quantity in parentheses. Assuming

$$\Delta(f) = \pm e_f$$

$$\Delta(f_c/f_b) = \pm 2e_f$$

and

$$\Delta(f_c^2/f_b^2) = \pm 4e_f$$

Therefore

$$\Delta(f_c^2/f_b^2 - 1) = (\pm 4e_f)/(f_c^2/f_b^2 - 1)$$

In the transition region, f_c/f_b is about 1.04.

therefore,

$$\Delta(f_c^2/f_b^2 - 1) = \pm 100e_f \quad (4.11)$$

The thickness of the coating cannot be controlled accurately while applying it. It has therefore to be measured after application. It was obtained as the difference in specimen thickness (diameters) before and after application of the coating. Let d_1^* be the coated specimen thickness

d_1 is the bare specimen thickness

and

$d_2 = d_1^* - d_1$ is the coating thickness.

Suppose the relative error in measuring d is e_d .

i.e. $\Delta(d) = \pm e_d$

Therefore,

$$\Delta(d_1) = \pm e_d$$

and

$$\Delta(d_1^*) = \pm e_d$$

Then,

$$\begin{aligned} \Delta(d_2) &= \Delta(d_1^* - d_1) = \pm 2e_d d_1/d_2 \\ &\approx \pm 40e_d \text{ with } d_1/d_2 \approx 20. \end{aligned}$$

Therefore,

$$\Delta(d_2/d_1) = \Delta(t) \approx \pm 40e_d.$$

Now, $c = 3t + 3t^2 + t^3$, and because t is very small compared to 1, we get

$$\Delta(c) = \pm 40e_d = \pm e_c \quad (4.12)$$

Now,

$$\begin{aligned} \Delta(E_2') &= \Delta(f_c^2/f_b^2 - 1) + \Delta(c) \\ &= \pm 100 e_f \pm 40 e_d \end{aligned} \quad (4.13)$$

It is estimated that in the worst case, the error in the frequency measurements can be controlled to 0.3% and the error in measuring the specimen thickness to 0.05% (Appendix (6)). A conservative estimate, which allows for other inaccuracies that might occur during the reduction process, as when matching bare specimen curves, is that the elastic modulus of the coating material can be determined from equation (4.9) using measured frequency and thickness values with an error of less than 50%. The least accurate values are at temperatures above the transition temperature region where the difference between the frequencies with the coated and uncoated specimens is very small and measurement errors are magnified considerably.

Now from equation (4.10),

$$\Delta(E_2'') = \pm 4e_f \pm 40e_d \pm \Delta(\eta).$$

The error in measuring η is relatively low. By subtracting out the system loss coefficient with the specimen uncoated, not only the base material damping,

but also other extraneous losses like air friction and support effects are eliminated. Also, the measured system loss coefficient with the bare specimen in the temperature range of interest is very low, about 10^{-3} , (except for the high frequency torsion specimen), while the loss coefficient with the coating in the transition region in most cases exceeds 10^{-2} . The loss modulus, therefore, can be calculated from measured data using equation (4.10) with a maximum error of $\pm 5\%$.

Chapter 5. Conclusions and Discussion

A test program designed to study the damping to be had from porcelain enamel coatings at temperatures where they soften was described in the preceding chapters. Three different pieces of apparatus were built; the first measured the vibration decay of a coated solid cylindrical specimen in torsion in the frequency range 1 Hz to 15 Hz. The second measured the decay of a coated flat plate specimen in bending in the frequency range 11 Hz to 170 Hz, and the third measured the decay of a coated hollow cylindrical specimen in torsion in the frequency range 165 Hz to 600 Hz. Several different enamel frits were used in the tests; the lowest effective damping temperature was 400C and the highest was 750C. The coating thicknesses ranged from 0.001 to 0.006 inches. From the test results presented in Chapter 4, the following broad conclusions can be drawn about the equipment used and about the porcelain enamels.

- 1) The torsion pendulum and the cantilever beam apparatus can be used satisfactorily to obtain the complex modulus of porcelain enamels as a function of temperature.

- 2) The hollow cylindrical torsion specimen apparatus is not a satisfactory piece of equipment because of the expansion joints in the specimen assembly which caused high, non-linear damping. The loss coefficient data obtained from this equipment in the frequency range 165 to 600 Hz was not used to calculate the complex modulus; but it does show the same general trend as the data at the lower frequencies.
- 3) The damping tests on some specimens were repeated. The results obtained were the same as for previous tests. This indicates that the testing procedure does not damage the coating, that the heating-cooling cycle does not change the mechanical properties of the enamel, and that the relaxation process is reversible.
- 4) The interface between the enamel and the metal is not important as there is very good agreement among tests using different enamel thicknesses.
- 5) The storage modulus for the various enamels is approximately the same. At room temperature, the storage Young's modulus is about 10×10^6 psi, and the shear modulus measured for one frit (#12325) is about 5×10^6 psi. These agree well with values for glass reported elsewhere.
- 6) The loss modulus shows a symmetric peak when plotted against either temperature or frequency.

The maximum value is 1.4×10^6 psi for the loss Young's modulus and 0.7×10^6 psi for the loss shear modulus.

7) The widths of the peaks in the loss modulus vs. temperature curves indicate multiple relaxations. A lognormal distribution of relaxation times was used to describe the relaxation process. The scatter in the experimental data is high, because the porcelain enamels can be tested only as thin coatings, and a lognormal distribution function for the relaxation process is an adequate one. Three parameters suffice to describe the behavior of the porcelain enamels, namely, $E''_{2 \max}$ or $G''_{2 \max}$, β and τ_m . Since the relaxed modulus, E_R or G_R , can be assumed to be zero, the unrelaxed modulus, E_U or G_U , β and τ_m can be used to completely describe the relaxation process.

8) The temperature bandwidth varies between 50C and 70C for all enamels.

9) The frequency bandwidth, β , is different for different enamels and has no observable relationship to the softening temperature of the porcelain enamel.

10) The composition of the enamel significantly affects the softening temperature and the width β , but not the modulus. The β 's measured for the same coating on different base metals are also

different. It is possible that during the initial firing process, there is some diffusion of ions between the enamel and the base metal. The coating being very thin, this would significantly alter its composition; that is, the composition of the coated enamel is different from that of the uncoated frit. The final composition of the coating would then depend on the composition of the base metal also. Such an interaction must be complete during the firing process, because later heating-cooling cycles do not change the measured properties of the enamel. Also, the interface between the enamel and the metal surface is not important.

11) The relaxation process follows an Arrhenius equation for several decades of frequency--at least 7 decades in bending (figure (4.24)), and at least 5 decades in torsion (figure (4.25)). This does not imply that the enamels are Arrhenius over a smaller frequency range when subjected to torsional strain. The measured range of Arrhenius behavior is smaller in torsion only because i) the torsion measurements were made over a smaller frequency range; they covered a factor of 11.6 compared with a factor of 15.5 in bending, and ii) the activation energy

measured in bending is greater than that in torsion. It has been pointed out earlier that this did not depend on the state of stress, but was due to the base metals in the two cases being different, thus altering the final composition of the coating.

12) The activation energies measured are very high, of the order of 200 kcals/mole. The typical activation energy for alkali ion diffusion in glass is 20 - 30 kcals/mole; that for viscous flow is known to be higher, about 100 kcals/mole. Even the energy of the silicon-oxygen bond is only 109 kcals/mole. Extremely high values for activation energy, between 120 and 190 kcals/mole, have also been measured for stress relaxation in sodium phosphate glasses in the transition temperature region [20]. Very high activation energies, up to 242 kcals/mole, have been reported for viscous flow in alkali borate glasses [45]. Polymers in the transition region also exhibit such high activation energies [46]. No satisfactory explanation is available for these high activation energies. A value of 200 kcals/mole cannot be associated with any known physical mechanism. One can speculate that the network structure of the enamel is such as to impose severe constraints on the atomic movements

which cause the relaxation in the material, thus increasing the activation energy of the relaxation process. One can also speculate that the atomic movement, when it does take place, cannot do so without disturbing other neighboring atoms, thus initiating a sequence of motions. It is apparent that such a cooperative process would be extremely complex and cannot be described in detail. It is also doubtful that one can assign a single activation energy to such a complicated process.

This is the first work that investigates the damping properties of porcelain enamels in detail. It has left unanswered some questions regarding 1) the effect of the coating composition and 2) the anomalously high activation energies, which provides interesting areas for future work. It has demonstrated convincingly that porcelain enamels can be used as efficient damping materials, and that there is a need for better and more accurate testing equipment. It would be worthwhile to develop porcelain enamels with lower softening temperatures. Porcelain enamels with softening temperatures up to about 1200C are being used; but there are hardly any with softening temperatures lower than 400C. It would be useful to extend the

temperature range over which porcelain enamels, as a class, can be used efficiently for damping purposes.

Appendix 1. Porcelain Enamels

Porcelain enamels are thin, glassy, inorganic coatings bonded to a metal surface by fusion. They are usually laid in thicknesses varying from 0.001 inch to 0.01 inch. They are primarily oxides and are highly resistant to oxidation and corrosion. They are smooth and hard and very resistant to thermal stresses and shock. Porcelain enamels are extensively used to provide protection for metal parts exposed to corrosive and erosive environments. They behave anelastically in their softening temperature range and hence are good candidate materials for damping at high temperatures.

Composition and Method of Coating [6]

Porcelain enamels consist of raw materials such as quartz, feldspar, clay, fluorspar, borax, soda ash, kryolite, nitrate of soda, zirconium oxide, titanium oxide, cobalt oxide, nickel oxide, and manganese oxide which are fused together to form the frit in granular form. The frit is finely powdered along with some additional chemicals to impart certain desirable properties to the enamel. The chemicals added include floating agents, opacifiers, coloring

agents and electrolytes to deflocculate the clay and properly suspend the enamel. The powder is then mixed thoroughly with water as the vehicle to form a slurry or slip, and is ready for application.

The metal surface to be coated is prepared by chemical methods (like acid pickling) or by mechanical methods (like sand blasting) to produce a roughened surface free from any metallic oxides or organic material. The slip is then applied to the clean surface by dipping, brushing or spraying, and dried in air. The dried coating is fired for two to fifteen minutes in an oxidizing atmosphere at the temperature required to re-fuse the glassy constituents, until the coating material bonds with the metal to form a homogeneous vitreous coating [36].

Appendix 2. Relaxation in Porcelain

A2.1 Mechanical Models

The most general form of a linear constitutive equation to describe an anelastic solid is [40]

$$\begin{aligned} & (a_0 + a_1 \frac{d}{dt} + a_2 \frac{d^2}{dt^2} + \dots) \sigma \\ & = (b_0 + b_1 \frac{d}{dt} + b_2 \frac{d^2}{dt^2} + \dots) \epsilon \end{aligned}$$

or

$$\left(\sum_{i=0} a_i \frac{d^i}{dt^i} \right) \sigma = \left(\sum_{i=0} b_i \frac{d^i}{dt^i} \right) \epsilon \quad (\text{A2.1})$$

where the a_i 's and b_i 's are constants, σ is the stress and ϵ is the strain. The behavior of an anelastic material is often described by mechanical models. A mechanical model is appropriate to a particular material if the relations between force, displacement and time for the model are the same as those for stress, strain and time in the material. There are two basic elements in any mechanical model--the ideal spring and the Newtonian dashpot. The ideal spring alone represents an elastic body for which only a_0 and b_0 in equation (A2.1) are different from zero. In the dashpot alone, the force

is proportional to the velocity, or, only a_0 and b_1 in equation (A2.1) are different from zero. An anelastic solid is represented by a combination of springs and dashpots--the springs providing the elasticity and the dashpots the internal friction.

The simplest models that can be constructed from the two basic elements are the Voight and the Maxwell models. The Voight model has a spring and dashpot connected in parallel while the Maxwell model has the elements connected in series. These two are rather too simple to represent any real material. The simplest model which is representative of a real material is what is called the standard three parameter model, consisting of a Voight unit in series with a spring. It can be shown [41] that for a sinusoidal deformation, the modulus $M^* = M' + iM''$, where M^* is the Young's modulus for longitudinal deformation or the shear modulus for shear deformation, is given by

$$M'(\omega) = M_R + \delta M (\omega^2 \tau_\epsilon^2) / (1 + \omega^2 \tau_\epsilon^2) \quad (A2.2)$$

and

$$M''(\omega) = \delta M \omega \tau_\epsilon / (1 + \omega^2 \tau_\epsilon^2) \quad (A2.3)$$

where

M_U = unrelaxed modulus

M_R = relaxed modulus

$\delta M = M_U - M_R =$ magnitude of the relaxation

$\omega =$ circular frequency

$\tau_\epsilon =$ relaxation time at constant strain

$$= \mu \cdot \delta M / M_U^2$$

and

$\mu =$ viscosity of the dashpot.

M' decreases from M_U to M_R as the frequency decreases.

The function M'' reaches its maximum value at a frequency such that $\omega\tau_\epsilon = 1$. When plotted against $\log(\omega\tau_\epsilon)$, the curve has a width at half maximum of 1.144. This is called a Debye peak.

A2.2 Lognormal Distribution of Relaxation Times

For an anelastic material with a distribution function $\phi(\ln \tau)$ for the logarithm of the relaxation times τ , the storage modulus M' and the loss modulus M'' are, as shown in equations (2.1) and (2.2)

$$M'(\omega) = M_R + \delta M \int_{-\infty}^{\infty} (\phi(\ln \tau) \omega^2 \tau^2) / (1 + \omega^2 \tau^2) d \ln \tau \quad (\text{A2.4})$$

and

$$M''(\omega) = \delta M \int_{-\infty}^{\infty} (\phi(\ln \tau) \omega \tau) / (1 + \omega^2 \tau^2) d \ln \tau \quad (\text{A2.5})$$

where

$$\int_{-\infty}^{\infty} \phi(\ln \tau) d \ln \tau = 1 \quad (\text{A2.6})$$

Assuming a normalized Gaussian distribution in $\ln \tau$, and introducing a new variable $z = \ln(\tau/\tau_m)$, where τ_m is the mean value of τ , we get

$$\phi(z) = (1/(\beta\sqrt{\pi})) \exp. (-z^2/\beta^2) \quad (\text{A2.7})$$

where β is the value of $|z|$ for which $\phi(z)$ falls to $1/e$ of its maximum at $z = 0$. Then,

$$M''(\omega) = \delta M \int_{-\infty}^{\infty} (\phi(z)\omega\tau)/(1 + \omega^2\tau^2) dz \quad (\text{A2.8})$$

Introducing the variable $x = \ln(\omega\tau_m)$,

$$\begin{aligned} M''(x)/\delta M &= (1/(2\sqrt{\pi})) \int_{-\infty}^{\infty} \exp(-u^2) \operatorname{sech}(x+\beta u) du \\ &= f(x, \beta) \end{aligned} \quad (\text{A2.9})$$

Thus,

$$M''(x)/M''(0) = f(x', \beta)/f(0, \beta) = F(x', \beta) \quad (\text{A2.10})$$

where $x' = \log(\omega\tau_m) = x/2.303$. Also,

$$M''(0)/\delta M = f(0, \beta) \quad (\text{A2.11})$$

Reference [40] tabulates the function F for different values of x' and β , and $2f(0, \beta)$ for different β 's. A portion of these tabulations are shown in Tables (2.2) and (2.3). Figure (2.3) shows plots of F vs x' for various values of β . The case $\beta = 0$ corresponds to the case of a material with a single relaxation time. For all β , the function $F(x', \beta)$ reaches its

maximum value of l at $\omega\tau_m = 1$ or $x' = 0$. Figure (2.4) shows $2f(0, \beta)$ as a function of β . The function $f(x', \beta)$ was obtained from $F(x', \beta)$ and $f(0, \beta)$ and is tabulated in Table (2.4). Figure (2.5) shows plots of $f(x', \beta)$ vs. x' for various β 's. It can be seen from figures (2.4) and (2.5) that the peak value of the loss modulus decreases with increasing β .

The storage modulus M' is given by equation (A2.4). For porcelain enamels, we shall assume that the relaxed modulus M_R is very small, and that $\delta M = M_U$. Therefore,

$$M'(\omega) = M_U \int_{-\infty}^{\infty} (\phi(\ln \tau) \omega^2 \tau^2) / (1 + \omega^2 \tau^2) d \ln \tau \quad (\text{A2.12})$$

with the distribution given by equation (A2.7), and for z , x , and x' defined as above, we get

$$(M'/M_U - 0.5) = f_1(x', \beta) \quad (\text{A2.13})$$

where

$$f_1(x', \beta) = (1/(2\sqrt{\pi})) \int_{-\infty}^{\infty} \exp(-u^2) \tanh(x + \beta u) du \quad (\text{A2.14})$$

It can be shown that for all β ,

$$f_1(0, \beta) = 0 \quad (\text{A2.15})$$

or

$$M'/M_U = 0.5 \text{ at } x = 0 \text{ or } \omega\tau_m = 1.$$

Table (2.5) shows $f_1(x', \beta)$ for different values of x' and β . The integral defined in equation (A2.14)

AD-A031 774

MINNESOTA UNIV MINNEAPOLIS DEPT OF AERONAUTICS AND --ETC F/G 11/2
DAMPING IN PORCELAIN ENAMEL COATINGS.(U)
JUL 76 P I SRIDHARAN

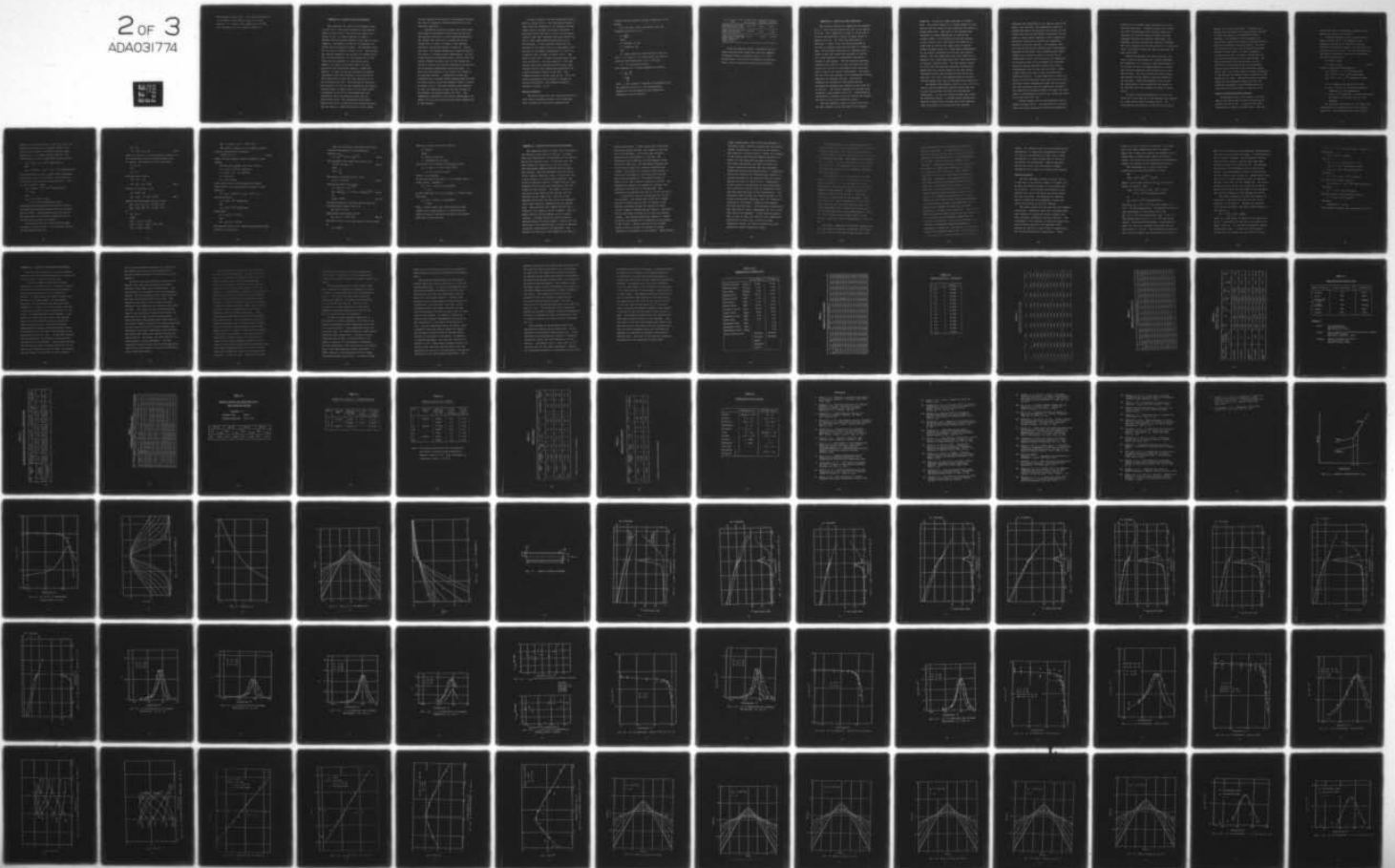
F33615-72-C-1315

UNCLASSIFIED

AFML-TR-74-191

NL

2 of 3
ADA031774



was evaluated numerically. Only positive values of x' are shown as the function $f_1(x', \beta)$ is odd about $x' = 0$. Figure (2.6) shows plots of M'/M_U as a function of x' for various values of β .

Appendix 3. Torsion Pendulum Apparatus

This apparatus was used in the frequency range 1 Hz. to 15 Hz. The solid cylindrical test specimen shown in figure (A3.1) was made of multimet alloy, (Table (4.9)), 15 inches long and 0.1 inch in diameter with flat plates welded to the ends to permit clamping. The middle 4 inches of the specimen was coated with the porcelain enamel. The apparatus used for the tests is shown in figure (A3.2). The specimen was rigidly clamped at the top end to a massive block. The 3/16 inch diameter, 1/2 inch projection at the lower end was fastened to a cylindrical steel adapter, the lower end of which had a 1/8 inch projection that was guided through a simple ball bearing. A steel driving arm carrying an aluminum capacitance plate was fastened to the lower plate. The system could be set into free vibration at 9.0 Hz by plucking the arm. The frequency of vibration was reduced to 1.3 Hz at room temperature by clamping the mass shown in figure (A3.3) to the lower plate. A frequency of 15.0 Hz at room temperature was obtained by using an aluminum driving arm and capacitance plate. The capacitance plate moved between two pairs of differentially connected plates, and the change in capacitance caused by the change

in area covered by the plate as the specimen vibrated was used to generate a voltage proportional to the vibration amplitude.

A cylindrical electric furnace with three zones with separate resistance controls was used to heat the specimen and hold it at the desired temperature. The furnace had a bore of 2.5 inches and was 12 inches long, so that 1.5 inches of the specimen projected outside the furnace at each end. During the tests, the furnace chamber was closed by insulating plates. A chromel-alumel thermocouple, its lead wires enclosed in refractory tubes, inserted into the furnace chamber through a hole in the furnace wall served to control the furnace temperature and was also the indicating thermocouple during the tests. It could be moved radially to be within 0.03 inches of the specimen surface. A temperature survey was conducted with 8 chromel-alumel thermocouples fastened at various points along the specimen length, as shown in figure (A3.4). The zone resistors were adjusted so that the temperature across the test section of the specimen was uniform within 20F (11C). The temperature indicated by the control thermocouple was found to be 20F (11C) less than the actual temperature of the specimen.

A block diagram of the instrumentation used is shown in figure (A3.5). The oscillatory change in capacitance was converted to an analogous voltage signal using a suitable electronic transducer. A band pass filter was used to filter out any stray signals--like high frequency electronic noise--and give a clean signal which was monitored on an oscilloscope. A level recorder which gave the envelope of the decay curve to a logarithmic scale was used at the higher frequencies of 9 and 15 Hz. A typical curve is shown in figure (A3.6). The slope of this curve is directly proportional to the loss coefficient. For tests made at 1.2 Hz, the voltage signal was recorded directly using a pen recorder and the loss coefficient determined from a semi-logarithmic replot of the data. The frequency counter could be used for a 1, 10 or 100 second measurement and by taking an average of several measurements the frequency could be obtained to within $\pm 0.1\%$.

Natural Frequency

The strain energy for data reduction was calculated from an assumed stiffness of the specimen. This stiffness was verified by comparing the

measured and the computed natural frequencies of the system.

For a uniform, solid, cylindrical rod, the torsional stiffness, K , is

$$K = \frac{\pi d^4}{32\ell} G$$

where

d = diameter of rod

ℓ = length of rod

and

G = shear modulus of the material of the rod.

For $d = 0.1$ inch, $\ell = 15$ inches and G for multimet alloy at room temperature = 11.6×10^6 psi,

$K = 7.6$ inch pounds/radian.

The frequency of a torsion pendulum is given by

$$f = \frac{1}{2\pi} \sqrt{\frac{K}{J}}$$
$$= \frac{0.44}{\sqrt{J}}$$

where J = mass moment of inertia of the pendulum bob.

The computed values of J , the corresponding frequencies and the measured room temperature frequencies were as follows.

with	J in lb. sec ²	f Hz computed	f Hz measured
Aluminum driving arm and capacitance plate	0.77×10^{-3}	15.8	15.5
Steel driving arm and capacitance plate	2.4×10^{-3}	9.0	8.99
Steel driving arm and capacitance plate and steel weight of figure (A3.3)	0.114	1.303	1.305

Since the measured natural frequencies for all three configurations agreed well with the computed frequencies using a stiffness value of 7.6 inch pounds/radian, this value of stiffness was used for strain energy calculations during data reduction.

Appendix 4. Cantilever Beam Apparatus

The original bending test apparatus was designed by B. J. Lazan and was modified by Lee [8] to operate at 32 Hz. Lee's apparatus is shown in figure (A4.1). It was later modified as shown in figure (A4.2) to operate at 47 Hz. The flat test beam made of Hastelloy X (Table (4.9)) was firmly fastened at one end to a support which was tied down to a massive base. An arm made of Hastelloy X, extending downwards outside the furnace was fastened to the free end of the specimen for measurement and control outside of the furnace. The arm could be displaced manually and a hook at its lower end held by a pawl carried at the end of a micrometer screw which was used to adjust the initial displacement. The system was set into free vibration at its fundamental natural frequency by releasing the arm. The natural frequency of vibration of the system could be decreased by clamping steel weights to the lower end of the arm. The lowest frequency so obtained using reasonably sized weights was 11 Hz. A piezoelectric accelerometer fastened to the arm outside the furnace was used to pick up the vibration signal.

The test specimen, shown in figure (A4.3) had the same geometry as the one used in the original

apparatus. It was 4.5 inches long and 1.5 inches wide. The middle length of 1.3 inches formed the test section and was coated on both sides with the porcelain enamel under test. Both ends of the specimen were thickened to reduce damping due to slip in the clamped joints. The thickness of the test section varied linearly from 0.095 inch at the base end to 0.088 inch at the arm end, which gives a uniform surface bending stress for a mode shape corresponding to the natural frequency of 32 Hz for the original system. The loss coefficient was later found not to depend on the stress amplitude; and it was unnecessary to maintain uniform stress. For the present system at 47 Hz with the same test specimen, calculations showed that the surface stress in the test section increased by less than 4% from the free end to the base end. At 11 Hz, the surface stress at the base end was smaller than that at the free end by about 11%.

An electric box furnace 5 1/2 in × 4 in × 8 1/2 in with an on-off temperature control console was used to heat the specimen and hold it at the desired temperature. In use, the furnace chamber was closed by insulating plates. A chromel-alumel thermocouple held in a groove under the base end of the specimen with its junction in contact with the specimen

indicated the temperature of the specimen during the tests. For each test, the temperature should be uniform throughout the specimen and constant in time. A soak time test was performed to determine the time taken to reach steady temperature and a temperature survey was conducted to measure the temperature variation along the specimen. The specimen used for this survey had two chromel-alumel thermocouples fastened to each face; other chromel-alumel thermocouples were located as shown in figure (A4.4). Thermocouple #7 was used to monitor the temperature at the point where the accelerometer was fastened. Since the maximum operating temperature of the accelerometer used in some tests was 350F (~180C), a small blower was used to keep its temperature within safe limits. It was found that it took 2 1/2 hours to reach temperature equilibrium for the first relatively large temperature change, and 45 minutes for each subsequent smaller temperature increment. The temperature variation between the upper and lower sides of the specimen and across its length was found to be less than 10F (~6C).

A block diagram of the instrumentation used is shown in figure (A4.5). The piezoelectric accelerometer and charge amplifier converted the mechanical

vibration to a voltage signal proportional to the vibration amplitude. Electronic noise was filtered out with the band-pass filter and the signal was displayed on an oscilloscope to monitor the wave shape and indicate the vibration amplitude. The frequency counter indicated the vibration frequency. The level recorder gave the decay curve to a logarithmic scale, the slope of which was used to determine the loss coefficient.

Before the damping tests were performed, the stress level on the surface of a typical specimen was determined as a function of the displacement at the trigger so that the stress amplitude at which each test was conducted could be monitored on the oscilloscope. For this calibration, strain gages were mounted on both sides of the test section of the specimen, a force was applied to the arm and the displacement at the trigger and the strain in the specimen were both recorded as shown in figure (A4.6).

In order to make measurements at 170 Hz, the rigid arm at the free end of the specimen was replaced by a light rod as shown in figure (A4.7). An accelerometer was fastened to the end of the rod to

measure the vibration amplitude. A magnetic coil excited by an oscillator and audio amplifier was used to drive the system at its fundamental natural frequency. The frequency of the excitation was varied until steady state resonant vibration, detected from the oscilloscope trace, was reached. The power to the driving coil was then cut off and the system allowed to decay freely. At lower frequencies, in reducing the data, it could be assumed that all of the strain energy was in the test specimen. For this configuration, the strain energy was not confined to the specimen alone, but some bending strain energy was stored in the relatively slender rod as well. For a given amount of energy dissipation in the specimen the measured loss coefficient for the system will be lower. Computations based on measured amplitudes and frequencies showed that the loss coefficient measured at this frequency had to be corrected by the factor shown in equation (3.18).

Natural Frequency and Stress Analysis

The maximum stress on the surface of the beam used in the bending tests can be calculated by the method given by Lee [8]. A sketch of the system configuration is shown in figure (A4.8). The mass

of the beam itself is negligible compared with the mass of the mass at the free end.

A free body diagram of the cantilever beam is shown in figure (A4.9). The deflection and rotation at the end of the cantilever beam are functions of the bending moment, the shear force and the axial force at the end. For small deformations, the effect of the axial force may be neglected and the static equations are

$$\begin{aligned}y &= \alpha_{11}V_0 + \alpha_{12}M_0 \\ \theta &= \alpha_{12}V_0 + \alpha_{22}M_0\end{aligned}\tag{A4.1}$$

where the influence coefficients are

$$\begin{aligned}\alpha_{11} &= L^3/3EI = 4.5 \times 10^{-4} \text{ inches/pound} \\ \alpha_{12} &= L^2/2EI = 4.74 \times 10^{-4} \text{ radians/pound} \\ \alpha_{22} &= L/EI = 6.31 \times 10^{-4} \text{ radians/inch pound.}\end{aligned}$$

$L = 1.5$ inches is the length of the beam

$E = 28.5 \times 10^6$ psi is the Young's modulus of Hastelloy X at room temperature

$I = 0.912 \times 10^{-4}$ (inches)⁴ is the mean area moment of inertia of the cross section of the specimen.

The influence coefficients for the tapered beam were measured for comparison with the calculated values [8]. The measurements were made first by

applying a vertical force V_0 at the free end of the cantilever beam (point A in figure (A4.8)); the vertical deflection, y , at point A and the axial displacement, x , at point B were recorded. The coefficients α_{11} and α_{12} were then calculated from

$$\alpha_{11} = y/V_0 = 6.2 \times 10^{-4} \text{ inches/pound}$$

and

$$\alpha_{12} = (x/l)/V_0 = \theta/V_0 = 5.5 \times 10^{-4} \text{ radians/pound.}$$

The coefficients α_{21} and α_{22} were found by applying a horizontal force F at the point B and measuring the vertical and horizontal displacements, y and x , at the same point. Then,

$$\alpha_{21} = y/(Fl) \approx 5.7 \times 10^{-4} \text{ radians/pound}$$

$$\approx \alpha_{12}$$

and

$$\begin{aligned} \alpha_{22} &= (x/l)/(Fl) = \theta/M_0 \\ &= 6.7 \times 10^{-4} \text{ radians/inch pound.} \end{aligned}$$

The measured coefficients were different from the calculated ones probably because the end conditions were not ideal. The measured values were used in the calculation of the natural frequency and the stress variation along the surface.

The free body diagram for the extended mass is shown in figure (A4.10). The equations of motion for the extended mass are:

$$\begin{aligned} m\ddot{x} &= -V_0 \\ J\ddot{\theta} &= -M_0 + aV_0 + bH \end{aligned} \quad (\text{A4.2})$$

where m is the mass, J the mass moment of inertia of the extended mass, and the constant weight force is ignored. The kinematics of the system give

$$x = y + a\theta$$

and

$$x_1 = b\theta$$

Equations (A4.2) become

$$\begin{aligned} m(\ddot{y} + a\ddot{\theta}) &= -V_0 \\ J\ddot{\theta} &= -M_0 + aV_0 - b^2m\ddot{\theta} \end{aligned} \quad (\text{A4.3})$$

Solving for V_0 and M_0 , we get

$$\begin{aligned} V_0 &= -m(\ddot{y} + a\ddot{\theta}) \\ M_0 &= -am\ddot{y} - (J + a^2m + b^2m)\ddot{\theta} \end{aligned} \quad (\text{A4.4})$$

Substituting into equation (A4.1) we have

$$\begin{bmatrix} M_{11} & M_{12} \\ M_{21} & M_{22} \end{bmatrix} \begin{bmatrix} \ddot{y} \\ \ddot{\theta} \end{bmatrix} + \begin{bmatrix} 1 & 0 \\ 0 & 1 \end{bmatrix} \begin{bmatrix} y \\ \theta \end{bmatrix} = \begin{bmatrix} 0 \\ 0 \end{bmatrix}$$

or

$$M\ddot{X} + KX = 0$$

where

$$M_{11} = -(\alpha_{11}m + \alpha_{12}am)$$

$$M_{12} = -\alpha_{11}am - \alpha_{12}(J + a^2m + b^2m)$$

$$M_{21} = -(\alpha_{12}m + \alpha_{22}am)$$

$$M_{22} = -\alpha_{12}am - \alpha_{22} (J + a^2m + b^2m)$$

The natural frequency of the system is found from the characteristic equation

$$|-\omega^2M + K| = 0 \quad (A4.5)$$

where ω is the circular natural frequency of the system.

For the test assembly at 47 Hz, we have

$$m = 1.435 \times 10^{-3} \text{ lb. sec}^2/\text{inch}$$

$$J = 8.365 \times 10^{-3} \text{ lb. sec}^2\text{inch}$$

$$a = 0.85 \text{ inch}$$

$$b = 1.805 \text{ inches}$$

Using these values and the measured influence coefficients, the characteristic equation of the system is

$$\omega^4 - (5.5 \times 10^6)\omega^2 + (4.72 \times 10^{11}) = 0$$

The solutions are

$$\omega_1 = 2.98 \times 10^2 \text{ radians/sec.}$$

and

$$\omega_2 = 2.36 \times 10^3 \text{ radians/sec.}$$

which gives

$$f_1 = \omega_1/(2\pi) = 47.6 \text{ Hz}$$

and

$$f_2 = \omega_2/(2\pi) = 376 \text{ Hz.}$$

The measured value of the lowest frequency was about 48-49 Hz for this mass.

Under free vibration, the deflection and the rotation corresponding to the fundamental frequency are

$$y = y_0 e^{i\omega_1 t} \quad \text{and} \quad \theta = \theta_0 e^{i\omega_1 t} \quad (\text{A4.6})$$

The fundamental mode shape can be found from

$$[-\omega^2 M + K] [X_0] = 0 \quad (\text{A4.7})$$

where

$$[X_0] = \begin{matrix} y_0 \\ \theta_0 \end{matrix}$$

The solution of equation (A4.7) gives

$$y_0/\theta_0 = 0.86 \text{ inch} \quad (\text{A4.8})$$

Substituting (A4.6) into (A4.4),

$$V_0 = m\omega_1^2 (y_0 + \theta_0) e^{i\omega_1 t}$$

$$M_0 = [am\omega_1^2 y_0 + (J + a^2m + b^2m)\omega_1^2 \theta_0] e^{i\omega_1 t} \quad (\text{A4.9})$$

or

$$V_0/M_0 = 0.162 \quad (\text{A4.10})$$

The bending moment at any cross section along the cantilever beam (figure (A4.9)) is

$$M_x = M_0 + V_0 (L-x)$$

Substituting from equation (A4.10)

$$M_x = M_0 (1 + 0.162 (L-x)) \quad (\text{A4.11})$$

The normal stress at any cross section along the beam is

$$\sigma_x = (M_x y)/I$$

where M_x is given by equation (A4.11)

$$I = wh^3/12$$

where

w = width of the beam

h = thickness of the beam

The stress on the surface of the beam is then

$$\begin{aligned}\sigma_x &= (6 M_0 (1 + 0.162 (L-x)))/(wh^2) \\ &= C (1 + 0.162 (L-x))/h^2\end{aligned}$$

where C is a constant.

At the free end of the beam, $x = 1.4$ inches, and $h = 0.088$ inches. Therefore,

$$\begin{aligned}\sigma_x &= C(1 + 0.162 \times 0.1)/(0.088)^2 \\ &= 131 C\end{aligned}$$

At the fixed end, at $x = 0.1$ inches, $h = 0.095$ inches. Therefore,

$$\begin{aligned}\sigma_x &= C(1 + 0.162 \times 1.4)/(0.095)^2 \\ &= 136 C\end{aligned}$$

Thus, a linear taper from 0.095 inches to 0.088 inches over a gage length of 1.3 inches gives a surface stress at the fixed end which is 4% greater than that at the free end.

Appendix 5. Hollow Torsion Cylinder Apparatus

This apparatus shown in figure (A5.1) was used in the frequency range 165 Hz to 600 Hz. To obtain these high frequencies, the stiffness of the specimen had to be relatively high. At the same time, the polar moment of inertia had to be low enough so that measureable damping could be obtained with a thin coating. The test specimen, shown in figure (A5.2), made of Hastelloy X was in 3 sections, with a total length of 15 inches when assembled. The hollow cylindrical section, 7 inches long with outer diameter 0.975 inch and wall thickness 0.050 inch, formed the test section. The middle 4 inches of this section was coated on the outside with the porcelain enamel under test. The ends of the specimen fitted into the test section by expansion joints which could be tightened with the tapered plug. Each end piece had a square section for a length of 1.75 inches to permit clamping. Only the middle section need be changed to test various coatings. A torque wrench was used to ensure a maximum torque of 70 inch pounds to tighten the nuts which drew in the tapered plug, in order to maintain consistent conditions for all specimens. The specimen was horizontal and clamped at one end to a

massive steel base. A light steel disc, with radial arms diametrically opposed, was clamped to the free end of the specimen. One of the arms carried a piezoelectric accelerometer at its end. The excitation from a magnetic coil was applied to the end of the other arm. The excitation frequency was varied until steady state resonant vibration was reached. The system was allowed to decay freely by cutting off the power to the driving coil and the decay rate was measured. The assembly shown in figure (A5.2) had a natural frequency of 600 Hz. The fundamental frequency was changed by clamping steel weights to the free end of the specimen. The frequencies so obtained were 430 Hz, 340 Hz and 165 Hz.

A cylindrical electric furnace was used to heat the specimen. The furnace had a bore of 2.5 inches and was 10 inches long so that 2.5 inches of the specimen projected outside the furnace at either end for clamping, measurement and control. Insulating plates were used at either end to close the furnace chamber. The furnace winding was tapped at a number of points and brought out to terminals on the outside of the furnace. Certain sections of the furnace winding could be shunted to maintain a uniform temperature distribution in the furnace. Three chromel-

alumel thermocouples, their lead wires enclosed in refractory tubes, could be inserted into the furnace chamber through holes in the wall of the furnace. They covered a length of about 3 inches in the middle of the furnace and could be radially adjusted to be about 0.03 inch away from the specimen surface. The middle thermocouple was used to control the furnace temperature and was also the indicating thermocouple during the damping tests. A temperature survey was conducted with thermocouples mounted at various positions on the apparatus with an uncoated specimen as shown in figure (A5.3). Thermocouple #7 was located at the position of the accelerometer and a blower was used to keep its temperature within the safe operating range of the accelerometer. The resistance shunts across the various sections of the furnace winding were adjusted, until the temperature variation in the middle 4 inches of the specimen was less than 20F (11C). The indicating thermocouple (#8) was found to show a temperature 20F (11C) higher than that of the specimen. A soak time test showed that it took at least two hours to reach temperature equilibrium for the first, relatively large, temperature change, and about 45 minutes for each subsequent smaller temperature change.

The accelerometer and a charge amplifier were used to produce a voltage signal proportional to the vibration amplitude. The signal was displayed on an oscilloscope to monitor the wave shape and indicate the vibration amplitude. The frequency was measured with a counter. A level recorder was used to measure the decay rate. The magnetic coil used to excite the system was driven by a low frequency oscillator and audio amplifier.

A calibration of the stress level versus the angular displacement at the free end was made on an uncoated specimen. 45° strain gages for shear measurements were mounted at either end of the test section of the specimen. Torque was applied by hanging weights from the end of a lever arm fastened to the free end of the specimen. A dial gage showed the linear displacement at the end of a light aluminum arm; for small displacements, this reading divided by the distance to the center of the specimen gives the angular displacement. Figure (A5.4) is a graph of the average strain in the specimen versus the angular displacement at the free end.

The lowest frequency of 165 Hz was obtained with this apparatus by clamping a solid steel disc shown in figure (A5.5) to the end of the specimen. The

loss coefficient at this frequency was found to be amplitude dependent. The apparatus was set up so that the specimen was vertical, to eliminate static deflection of the specimen due to the heavy weight at the end; the non-linearity, however, still remained. Damping measurements at room temperature were made on a solid steel specimen, 0.75 inches in diameter and 15 inches long. This showed no dependence of the loss coefficient on vibration amplitude. Apparently, the expansion fits of the test section with the end grips caused this non-linearity. The temperature dependence of the loss coefficient of the system with a coated and an uncoated specimen was determined at various stress levels. The temperature dependence of the loss coefficient due to the coating alone was determined at various stress levels as the difference in the damping value between the coated and uncoated specimens at the same stress amplitude. Figure (A5.6) shows the measured system damping for the coated and bare specimens at two different temperatures as functions of amplitude. Since the difference in η_s between the coated and uncoated specimens is independent of amplitude, the damping in the coating alone is not amplitude dependent; the non-linearity is due entirely to mechanical misfit in the expansion

joints. All damping values for this frequency were determined at an amplitude corresponding to about 0.1 volts on the abscissa in figure (A5.6) which corresponds to a shear stress level of 50 psi on the surface of the specimen. Similar amplitude surveys were made with other discs at higher frequencies and no such non linearity was observed.

Natural Frequency

The test specimen is shown in Figure (A5.2). It was held at one end by a clamp 1.75 inches long, so that the effective length of the specimen was 13.25 inches. The stiffness distribution in the specimen was used to calculate the strain energy for data reduction. The measured and computed natural frequencies were compared to verify the strain distribution in the test section.

The Holzer method [47] was used for the frequency calculation. Experience shows that calculated mass polar moments of inertia are quite accurate, but that torsional stiffnesses are more difficult. The stiffnesses of the specimen, between the support and three different points on the specimen, were measured by applying a known torque, and measuring the corresponding angular displacement. These

points, A, B and C were at 4.25 inches, 7.25 inches and 12.50 inches respectively from the support. Figure (A5.7) shows the graph of the measured angular displacement at these points versus the applied torque. The slopes in this graph give the stiffnesses between the support and the corresponding points.

The stiffnesses K_A , K_B and K_C were also calculated from the polar moment of inertia.

Now,

$$1/K_A = \theta_A/M = \frac{1}{G} \int_0^{4.25} 1/I_p dx$$

where G is the shear modulus, and I_p is the polar moment of inertia. Then:

$$\begin{aligned} 1/K_A &= 1/G \ 97.04 = 1/(11 \times 10^6) \times 97.04 \\ &= 8.73 \times 10^{-6} \text{ radians/inch pound} \end{aligned}$$

or

$$K_A = 11.45 \times 10^4 \text{ inch pound/radian}$$

Similarly, $K_B = 5.95 \times 10^4$ inch pound/radian, $K_C = 3.56 \times 10^4$ inch pound/radian. The measured stiffnesses, with superscript m , from Figure (A5.7) are

$$K_A^m = 6.0 \times 10^4 \text{ inch pound/radian, } K_B^m = 3.96 \times 10^4 \text{ inch pound/radian and } K_C^m = 2.13 \times 10^4 \text{ inch pound/radian.}$$

The measured stiffnesses in each case were about 0.6 times the stiffness calculated from the polar moment of inertia. The difference was probably due to the end support not being perfectly rigid and

some loss of stiffness in the expansion joints between the test section and the end grips. In the calculation of the natural frequency, the stiffnesses obtained from the polar moment of inertia were used after correcting them by the factor of 0.6. The specimen was divided into 53 segments each of length 0.25 inches. The mass moment of inertia of the driving arm was added to that of disc #1. Figure (A5.8) shows the graph of assumed frequency versus the residual angular displacement at the clamped end. The natural frequency of the system can be read off as 644 Hz. Figure (A5.9) shows the mode shape at that frequency. The measured frequency of the specimen was 605 Hz.

The lower frequency of 170 Hz was obtained by fastening a heavy disc near the free end of the specimen, at the point C. Dividing the specimen into N parts as before, the total kinetic energy of the system is

$$KE = \omega^2 \left(\sum_{i=1}^N J_i \theta_i^2 + J_m \theta_m^2 \right) / 2$$

where J_m = mass moment of inertia of the heavy disc and J_i = mass moment of inertia of the discs of the Holzer division. θ 's are the corresponding angular displacements and ω = frequency in radians/sec.

J_1 includes the driving arm; but each of the J_i 's

for $i = 2 \dots N$ is negligibly small compared to J_m .

Therefore,

$$KE = \omega^2 (J_1 \theta_1^2 + J_m \theta_m^2) / 2$$

Then for

$$\theta_m = 1, \theta_1 \approx (13.25) / 12.5 = 1.06$$

$$J_1 = 1.0 \times 10^{-3} \text{ inch pound second}^2$$

$$J_m = 19 \times 10^{-3} \text{ inch pound second}^2$$

Therefore,

$$KE = \omega^2 \times 10.1 \times 10^{-3} \text{ inch pound}$$

The potential energy = $K_C \theta_m^2 / 2$.

$$K_C, \text{ measured} = 2.13 \times 10^4 \text{ inch pound/radian}$$

Therefore,

$$PE = 1.07 \times 10^4 \text{ inch pound}$$

Equating kinetic and potential energies,

$$\omega^2 = 1.06 \times 10^6 \text{ (radians)}^2$$

Therefore,

$$\text{frequency } f = 166 \text{ Hz.}$$

The measured frequency with this mass was 175 Hz.

Appendix 6. Details of Experimental Procedures

This appendix describes the various procedural problems that were encountered during the experiments and the measures taken to overcome them.

In order to reduce variability in system measurements from test to test, consistent mounting conditions had to be maintained for all specimens and extraneous damping had to be reduced to a minimum. A torque wrench was used to tighten bolts and nuts to the same torque. In the bending apparatus, the high temperature bolts used were tightened to a torque of 120 inch pounds, and those in the high frequency torsion apparatus to 70 inch pounds. In assembling the latter specimen a jig, exactly 15 inches long was used so that the end grips could be positioned correctly inside the center hollow cylinder. In both the torsion experiments the weights and the driving arm had to be fastened at the free end of the specimen at the same point from test to test. In the high frequency torsion experiment the driving arm was placed at the very end of the specimen. The clearance between the insulating plates enclosing the furnace and the driving coil support was only an inch; the weights were positioned in the middle of this clearance.

In the torsion pendulum apparatus, the position of the weight and driving arm was determined by a pair of cylinders placed on the fixed floor of the apparatus.

To reduce the room temperature damping of the systems, they were isolated from the building vibration using rubber pads (isomode pads). The various parts of the apparatus had to be properly aligned. The ball bearing in the torsion pendulum case was particularly difficult to align. The slightest misalignment there caused the system damping at room temperature to increase from 0.0002 to 0.001. The cable from the accelerometer was taped to the base after adjusting the tension and position of the cable to give minimum damping. Room temperature measurements were always made with the furnace chamber closed with the insulating plates so that variations in air friction between room temperature and higher temperatures were minimized. The lowest room temperature damping measured was about 0.00015; the highest was over 0.002 for the high frequency torsion experiment. The high frequency electronic noise from the instrumentation used and the line frequency noise were filtered out using a band-pass filter.

All temperature measurements were made with chromel-alumel thermocouples. The same thermocouple was used to indicate the specimen temperature for about 10 tests, after which the thermocouple junction was renewed. The drift in the indicated temperature due to the on-off furnace cycle was about 1C. In the torsion experiments the indicating thermocouple was not in contact with the specimen, but about 0.03 inch away from the surface of the specimen. Before the damping tests were conducted, a temperature survey was done using several thermocouples as shown in figures (A3.4) and (A5.3), fastened along the length of specimen. These thermocouples had their junctions in good contact with the specimen. The temperatures indicated by these thermocouples were compared with the temperature indicated by the thermocouple used in the damping tests at a number of different temperatures in the range of interest. It was found that the temperature indicated during the tests was 11C lower for the torsion pendulum apparatus and 11C higher for the high frequency torsion apparatus when the furnace resistances were set to give uniform temperature across the 4 inch test section of the specimens. During the tests, sufficient time was

allowed for the specimen to attain temperature equilibrium - 2 hours for the first temperature change and 45 minutes for each subsequent temperature change.

The accelerometer used in the earlier tests had a maximum safe operating temperature of 180C. It had to be kept within that limit by blowing air over it. The blower was used even during the temperature surveys. It lowered the temperature of the specimen by about 3C. For some later experiments, a high temperature accelerometer capable of operating safely up to 400C was used and the blower was then not required.

In order to avoid geometry changes due to differences in thermal expansion, all parts of any apparatus subjected to high temperatures were made of the same material. High temperature bolts and nuts were used. To prevent binding of screw threads exposed to high temperatures, a coating of ceric oxide was used on them. Care was taken not to exceed a torque of 70 inch pounds in tightening the high temperature bolts which draw in the tapered plug in the high frequency torsion experiment. A higher torque at room temperature did not change the system damping appreciably; too high a torque

might cause the different parts of the specimen to weld together when heated to temperatures exceeding 1000C.

The frequency measurements were made with a counter whose gate could be set for a 1, 10 or 100 second measurement. For very low frequencies as in the torsion pendulum experiments, the decay was sufficiently slow that the measurement could be made over a 100 second interval. However, the chances of stray noise signals being picked up and counted were also increased. The count on the instrument had to be watched carefully over the entire measurement interval to ensure that no stray signals were counted. By taking an average of several such frequency measurements, the error in the frequency at 1.2 Hz could be controlled to 0.2%. For the frequencies 170 Hz and above, since a magnetic driver was used to excite the system, the resonant frequency could be measured before cutting off the power to the driver. By making a 10 second measurement, the error was limited to a maximum of 0.1%. When using a magnetic driver, the output of the oscillator and the signal from the accelerometer were fed to the horizontal and vertical terminals of the oscilloscope respectively. The

resonant frequency of the system was determined from the Lissajous figure displayed on the oscilloscope. To ensure that the system was being driven exactly at resonance before making the frequency measurement, the system was allowed to decay freely by cutting off the power to the oscillator. The collapse of the Lissajous figure on the oscilloscope was watched for any phase changes indicated by a change in shape of the figure. The frequency of the driver was adjusted so that the Lissajous figure decayed vertically without changing shape. The least accurate of the frequency measurements were the ones made at 47 Hz. The decay rate in the transition region was too high to permit a 10 second measurement. By taking an average of about 30 measurements over a 1 second interval, the error could be controlled to 0.3%.

The thickness of the coating could not be controlled accurately during application. It had therefore to be measured after application. It was obtained as the difference in specimen thicknesses (diameters) before and after application of the coating. A micrometer with a least count of 10^{-4} inch was used for the torsion specimens. However, for the bending specimens, a micrometer was not found

satisfactory because of the taper. A jig was devised to measure the thickness of the bending specimen. It consisted of a plate with V-grooves exactly 1.3 inches apart which was the gage length of the bending specimen. Two roller pins, with radius slightly less than the radius of the fillets at the two ends of the test section of the specimen, were placed one in each groove. The specimen was then laid over the pins so that the lower surface of the test section was horizontal at the level of the top of the pins. A dial gage with a least count of 10^{-4} inch was used to measure the specimen thickness. The reading at the top of the two pins was the same and set to zero. The specimen thickness was then read off the dial gage at various points on the specimen. Care was taken to see that the readings were taken at the same points with both coated and uncoated specimens. For the torsion specimens also, the thickness was measured very precisely at several points and an average taken. The error in the specimen thickness so obtained is not expected to exceed 0.05%.

TABLE (2.1)
COMPOSITION OF ENAMEL FRITS

		C.V.#12325,%	C.V.#16845,%
Silicon Dioxide	(SiO ₂)	33.68	27.46
Aluminum Oxide	(Al ₂ O ₃)	3.25	3.09
Iron Oxide	(Fe ₂ O ₃)	0.24	0.28
Sodium Oxide	(Na ₂ O)	13.27	13.63
Calcium Oxide	(CaO)	5.19	5.47
Zinc Oxide	(ZnO)	3.11	5.69
Barium Oxide	(BaO)	12.72	12.32
Potassium Oxide	(K ₂ O)	18.64	18.85
Boron Oxide	(B ₂ O ₃)	8.50	8.50
Magnesium Oxide	(MgO)	0.15	1.01
Lead Oxide	(PbO)	0.02	0.02
Antimony Oxide	(SbO)	-	1.76
Manganese Oxide	(MnO ₂)	-	0.01
Molybdenum Oxide	(MoO ₂)	-	0.74
Trace Constituents		Antimony	Titanium
		Titanium	Chromium
		Copper	
		Manganese	
		Silver	

TABLE 2.2

VALUES OF $F(x', \beta) - M'(x')/M'(0)$

x'	Distribution Width Parameter β												
	0	0.5	1.0	1.5	2.0	2.5	3.0	3.5	4.0	4.5	5.0	5.5	6.0
0	1.0	1.0	1.0	1.0	1.0	1.0	1.0	1.0	1.0	1.0	1.0	1.0	1.0
0.25	.8544	.8766	.9127	.9386	.9555	.9667	.9743	.9797	.9836	.9865	.9887	.9904	.9918
0.5	.5749	.6177	.7030	.7792	.8348	.8739	.9015	.9214	.9361	.9472	.9557	.9624	.9677
0.75	.3447	.3815	.4728	.5784	.6693	.7396	.7925	.8321	.8621	.8852	.9032	.9175	.9289
1.0	.1980	.2215	.2903	.3905	.4953	.5875	.6625	.7218	.7685	.8053	.8346	.8581	.8771
1.25	.1121	.1257	.1694	.2451	.3413	.4393	.5273	.6018	.6631	.7132	.7540	.7874	.8148
1.5	.0631	.0711	.0966	.1462	.2213	.3105	.4003	.4825	.5542	.6150	.6661	.7089	.7447
1.75	.0355	.0400	.0546	.0846	.1366	.2086	.2905	.3725	.4487	.5165	.5755	.6262	.6696
2.0	.0199	.0225	.0307	.0481	.0813	.1340	.2021	.2772	.3521	.4225	.4863	.5429	.5924
2.25	.0112	.0127	.0173	.0272	.0472	.0829	.1351	.1990	.2681	.3368	.4020	.4618	.5157
2.5	.0063	.0071	.0097	.0153	.0270	.0498	.0872	.1382	.1981	.2618	.3251	.3856	.4417
2.75	.0035	.0040	.0054	.0086	.0153	.0292	.0545	.0929	.1422	.1984	.2573	.3160	.3723
3.0	.0020	.0022	.0030	.0048	.0086	.0168	.0332	.0606	.0993	.1467	.1994	.2542	.3088

TABLE 2.3

VALUES OF $2f(0, \beta) = 2M''(0)/\delta M$

β	$2f(0, \beta)$
0.0	1.0000
0.5	0.9454
1.0	0.8344
1.5	0.7231
2.0	0.6279
2.5	0.5499
3.0	0.4865
3.5	0.4346
4.0	0.3918
4.5	0.3560
5.0	0.3258
5.5	0.3001
6.0	0.2780

TABLE 2.4

VALUES OF $2f(x', \beta) = 2M''(x')/M_U$

x'	0	0.5	1.0	2.0	3.0	4.0	5.0	6.0
0	1.0	.9454	.8344	.6279	.4865	.3918	.3258	.2780
0.25	.8544	.8287	.7615	.5999	.4739	.3853	.3221	.2757
0.5	.5749	.5839	.5865	.5241	.4385	.3773	.3113	.2688
0.75	.3447	.3606	.3945	.4202	.3855	.3377	.2942	.2582
1.0	.1980	.2094	.2422	.3109	.3223	.3010	.2719	.2438
1.25	.1121	.1188	.1413	.2143	.2565	.2598	.2456	.2265
1.50	.0631	.0672	.0806	.1389	.1947	.2171	.2170	.2070
1.75	.0355	.0378	.0455	.0857	.1413	.1758	.1874	.1861
2.0	.0199	.0212	.0256	.0510	.0983	.1379	.1584	.1646
2.25	.0112	.0120	.0144	.0296	.0657	.1050	.1309	.1433
2.50	.0063	.0067	.0080	.0169	.0424	.0776	.1059	.1227
2.75	.0035	.0037	.0045	.0096	.0265	.0557	.0838	.1034
3.0	.0020	.0020	.0025	.0053	.0161	.0389	.0649	.0858

TABLE 2.5
VALUES OF $f_1(x', \beta) = (M'/M_0 - 0.5)$

x'	Distribution Width Parameter β												
	0	0.5	1.0	1.5	2.0	2.5	3.0	3.5	4.0	4.5	5.0	5.5	6.0
0	0.0	0.0	0.0	0.0	0.0	0.0	0.0	0.0	0.0	0.0	0.0	0.0	0.0
0.25	.2597	.2390	.1992	.1631	.1354	.1146	.0988	.0866	.0769	.0691	.0626	.0573	.0527
0.5	.4090	.3923	.3492	.2993	.2554	.2198	.1916	.1691	.1510	.1361	.1238	.1134	.1046
0.75	.4693	.4618	.4359	.3946	.3497	.3086	.2735	.2441	.2197	.1992	.1820	.1673	.1547
1.0	.4901	.4874	.4761	.4511	.4157	.3775	.3414	.3091	.2811	.2569	.2360	.2179	.2022
1.25	.4968	.4959	.4918	.4769	.4568	.4266	.3942	.3628	.3339	.3079	.2849	.2645	.2465
1.5	.4990	.4987	.4973	.4923	.4797	.4589	.4330	.4051	.3777	.3518	.3280	.3065	.2870
1.75	.4996	.4995	.4991	.4973	.4912	.4785	.4596	.4369	.4126	.3884	.3652	.3435	.3235
2.0	.4999	.4998	.4997	.4990	.4964	.4894	.4769	.4597	.4395	.4180	.3965	.3756	.3558
2.25	.4999	.4999	.4999	.4997	.4986	.4951	.4874	.4752	.4594	.4413	.4221	.4027	.3838
2.5	.4999	.4999	.4999	.4999	.4995	.4979	.4935	.4854	.4736	.4590	.4426	.4253	.4077
2.75	.5000	.5000	.4999	.4999	.4998	.4991	.4968	.4917	.4834	.4721	.4586	.4436	.4278
3.0	.5000	.5000	.5000	.4999	.4999	.4996	.4985	.4955	.4899	.4815	.4707	.4581	.4443

TABLE 3.1
VALUES OF R AND η_A/η_B

Sp. # and Coating Type	Coating Thickness x 10 ⁻³ in.	Freq Hz	f Hz	f- \tilde{f} Hz	r/2 = $\frac{f-\tilde{f}}{\tilde{f}}$	$\eta_{\max} \times 10^3$	R = $\frac{r_A}{r_B}$	$\frac{\eta_A}{\eta_B}$
5;S9919D	2.4	47	46	1.5	0.0326	14.0	2.0	1.84
		170	153	2.5	0.0163	7.6		
7;S9919D	5.7	47	46.7	3.0	0.064	41.0	1.69	2.0
		170	158.5	6.0	0.0379	20.5		
15;CV-145-S(b)	2.0	47	47	1.2	0.0255	7.4	1.67	1.8
		170	163	2.5	0.0153	4.1		
16;325(Bb)	1.85	47	45.4	1.6	0.035	11.5	1.84	1.91
		170	159	3.0	0.019	6.0		
4X;CV-145-S(B)	4.0	47	44.8	1.6	0.0357	19.2	1.65	2.02
		170	161.5	3.5	0.0217	9.5		

TABLE 4.1

MANUFACTURERS OF COATING FRITS

Type of Coating	Firing Temperature, °C	Manufacturer
AL-2(A)	550	Ferro
S5-8A	550	Solar
CV-145-S(B) or #16845	600	Chicago
325(Bb) or #12325	730	Chicago
S9919D	900	Solar
S6100M	980	Solar

Addresses:

Ferro: Ferro Corporation
One Erieview Plaza
Cleveland, Ohio 44114

Solar: Solar, Division of International Harvester Company
2200 Pacific Highway
San Diego, California 92112

Chicago: Chicago Vitreous Corporation
1425 South 55th Court
Cicero, Illinois 60650

TABLE 4.2

MAXIMUM DAMPING AND TEMPERATURE DATA - TORSION PENDULUM

SP#	Coating Type	Coating Thickness r_2 ins	1.2 HZ		8.4 HZ		14.25 HZ		η_c max / r_2 per inch	1/2 max peak width η_c (AV)
			T, °C	η_c max	T, °C	η_c max	T, °C	η_c max		
1	325 (Bb) or #12325	0.0045	574	0.00725	589	0.0072	593	0.0067	1.6	50
2	"	0.0029	570	0.00445	585	0.0045	592	0.0042	1.55	50
3	CV-145-S(B) or #16845	0.00173	459	0.00192	474	0.00192	482	0.00192	1.11	50

TABLE 4.3
MAXIMUM DAMPING AND TEMPERATURE DATA - BENDING

Sp#	Coating	Coat.Th. d ₂ in.	11 Hz		33 Hz		47 Hz		170 Hz		η _c /d ₂ per in	peak width at 1/2 max in	°C
			T, °C	η _c max	T, °C	η _c max	T, °C	η _c max	T, °C	η _c max measured			
1	S5-8A	.0017			410	0.0062							
2	"	.0016	398	0.007	410	0.0064	425	0.0071	424	0.0044	0.0079	4.4	60
3	"	.0026			416	0.011						4.2	
4	"	.0022	396	0.0089	407	0.0117	413	0.009	413	0.0065	0.0117	4.1	
2X	AL-2(A)	0.0028	427	0.014			430	0.014				5.0	
AR9	"	0.003	427	0.014	436	0.0144	436	0.0146				4.8	
4X	CV-14.5-S(B)	0.004	461	0.018	455	0.0125	458	0.0194	464	0.0094	0.0169	4.5	64
15	"	0.002	443	0.007	441	0.01	461	0.0077	464	0.004	0.0072	3.6	60
15A	"	0.0023	462	0.009			469	0.0094	478	0.0047	0.0086	3.91	60
6X	325(Bb)	0.002			585	0.0148						7.4	
16	"	0.00185	575	0.0106	585	0.011	582	0.0122	591	0.0059	0.0106	6.0	65
16A	"	0.0029	593	0.0124			603	0.013	603	0.0068	0.0124	4.3	60
18A	"	0.0048							585	0.0155	0.0279	5.8	77
22	"	0.004	585	0.0142			593	0.0146	591	0.0082	0.0146	3.65	60
5	S9919D	0.0024	626	0.0136	648	0.0143	651	0.0142	659	0.0072	0.013	5.7	83
6	"	0.0030	612	0.0178	628	0.016	634	0.0182				6.0	
7	"	0.0057	623	0.041	637	0.035	640	0.037	662	0.0207	0.037	6.5	85
8	"	0.0053	631	0.0415	640	0.0368	640	0.0405				7.6	
10	S6100M	0.0009	732	0.006	759	0.005	753	0.004				5.6	
11	"	0.0011			682	0.0088	693	0.005				4.6	
12	"	0.0025	676	0.0155	676	0.014	687	0.016				6.4	
13	"	0.0028			676	0.015						5.4	

TABLE 4.4

MAXIMUM DAMPING AND TEMPERATURE DATA -
HIGH FREQUENCY TORSION

SPECIMEN #1

COATING TYPE: #12325

COATING THICKNESS: 0.0057 INS

165 HZ		340 HZ		430 HZ		600 HZ	
T, °C	η_c max	T, °C	η_c max	T, °C	η_c max	T, °C	η_c max
587	0.0054	599	0.0056	599	0.0056	601	0.003

TABLE 4.5

VALUES OF G_2' AND G_2'' - TORSION PENDULUM

SP.#	Coating Type	Coating Thickness r_2 ins.	G_2' psi $\times 10^{-6}$ at room T.	G_2'' psi $\times 10^{-6}$ maximum
1	#12325	0.0045	5.5	0.75
2	"	0.0029	5.0	0.73
3	#16845	0.00173	-	0.53

TABLE 4.6

VALUES OF E_2' AND E_2'' - BENDING

SP.#	Coating Type	Coating Thickness d_2 , ins.	E_2' psi $\times 10^{-6}$ at Room T.	E_2'' psi $\times 10^{-6}$ Maximum
5	S9919D	0.0024	10.0	1.75
7	"	0.0057	9.5	1.84
16	#12325	0.00185	13.5	1.98
16A	"	0.0029	10.0	1.34
22	"	0.004	8.2	1.08
15	#16845	0.002	9.0	1.28
15A	"	0.0023	9.0	1.30

Note: The modulus values have been corrected for anticlastic curvature by multiplying the measured values by 0.9. This corresponds to a Poisson's ratio, ν , of 0.31.

TABLE 4.7

BENDING RESULTS

SP.#	Coating Type	Coating Thickness ins.	E''_{max} psi $\times 10^{-6}$	E_U psi $\times 10^{-6}$	f_m , Hz	T_0 °C	β	Q kcal/mole	$\frac{2E''_{max}}{E_U}$
5	S9919D	0.0024	1.75	8.2	50	648	3	104	.426
7	"	0.0057	1.84	8.2	50	648	3	102	.449
16	#12325	0.00185	1.98	11.7	50	585	5	223	.338
16A*	"	0.0029	1.34	9.0	50	599	6	300	.300
15	#16845	0.002	1.28	7.7	50	461	5	120	.33
15A*	"	0.0023	1.30	7.7	50	471	5	150	.341

* Coated at the University of Minnesota.

TABLE 4.8

TORSION PENDULUM RESULTS

SP. #	Coating Type	Coating Thickness ins.	G_2^{max} psi $\times 10^{-6}$	G_U psi $\times 10^{-6}$	f_m , Hz	T_0 °C	β	$\frac{Q}{\text{kcal/mole}}$
1*	#12325	0.0045	0.75	3.6	50	602	4	190
2*	"	0.0029	0.72	3.6	50	602	4	200
3*	#16845	0.00173	0.53	3.1	50	488	4	135

* Coated at the University of Minnesota.

TABLE 4.9

COMPOSITION OF BASE METALS

	Hastelloy X %	Multimet Alloy %
Nickel	Balance (~ 45)	19 - 21
Cobalt	0.5 - 2.5	18.5 - 21
Chromium	20.5 - 23	20 - 22.5
Molybdenum	8 - 10	2.5 - 3.5
Tungsten	0.2 - 1	2 - 3
Iron	17 - 20	Balance (~ 32)
Carbon	0.05 - 0.15	0.08 - 0.16
Silicon	1. (max)	1
Manganese	1. (max)	1 - 2
Nitrogen	-	0.1 - 0.2
Columbium	}	0.75 - 1.25
Tantalum		

References

1. Lazan, B. J.; "Damping of Materials and Members in Structural Mechanics", Pergamon Press, New York, 1968.
2. Plunkett, R.; "Vibration Damping," in "Applied Mechanics Surveys", Abramson, Liebowitz, Crowley and Juhasz, eds., Spartan Books, Washington D.C., 1966 pp. 691-702.
3. Plunkett, R.; "Measurement of Damping", in "Structural Damping", Ruzicka, ed, ASME, Dec. 1959, p. 117.
4. Entwistle, K. M.; "The Damping Capacity of Metals", in "The Physical Examination of Metals", Chalmers and Quarrell, eds., Arnold, London, 2nd Ed., 1961, p. 487.
5. Bradfield, G.; "Measurements of Elasticity using Mechanical Waves", in "The Physical Examination of Metals", Chalmers and Quarrell, eds, Arnold, London, 2nd Ed., 1961, p. 559.
6. Andrews, A.I.; "Porcelain Enamels", The Garrard Press, Champaign, Illinois, 1961.
7. Wirt, L. S.; "Development of High Temperature Vibration Damping Coatings", Airesearch Technical Report, U.S. Army Contract Da-44-009-AMC-838(T), Airesearch Manufacturing Company of Arizona, Phoenix, Arizona, February 1966.
8. Lee, C. T.; "Damping Characteristics of Composite Engineering Structures", Ph.D. Dissertation, University of Minnesota, 1969.
9. Zachariasen, W. H.; "The Atomic Arrangement in Glass", Journal of the American Chemical Society, 54, 1932, p. 3841.
10. Warren, B. E.; "X-Ray Determination of the Structure of Glass", Journal of the American Ceramic Society, 17, 1934, p. 249.
11. Morey, G. W.; "The Properties of Glass", Reinhold Publishing Corporation, 2nd Ed. 1954.

12. Jones, G. O.; "Glass", Chapman and Hall Ltd., 2nd Ed., 1971.
13. Fitzgerald, J. V., K. M. Laing, and G. S. Bachman; "Temperature Variation of the Elastic Moduli of Glass", Journal of the Society of Glass Technology, 36, 1952, p. 90.
14. Spinner, S.; "Elastic Moduli of Glasses at Elevated Temperatures by a Dynamic Method," Journal of the American Ceramic Society, 39(3), 1956, p. 113.
15. McCormick, J. M.; "Apparatus for the Measurement of the Viscoelastic Properties of Glass", Journal of the American Ceramic Society, 38(8), 1955, p. 288.
16. Forry, K. E.; "Two peaks in the Internal Friction as a Function of Temperature in some Soda-silicate Glasses", Journal of the American Ceramic Society, 40(2), 1957, p. 90.
17. Kirby, P.L.; "The Mechanical Relaxation of Alkali Ions in a Borosilicate Glass", Journal of the Society of Glass Technology, 39, 1955, p. 385T.
18. Moore, D. N. and D. E. Day; "Temperature Variation in the Distribution of Relaxation Times in Aluminosilicate Glasses", Physics and Chemistry of Glasses, 12(3), 1971, p. 75.
19. Copley, G. J. and D. R. Oakley; "Internal Friction Studies of the Stabilization of Sheet-Glass", Physics and Chemistry of Glasses, 9(5), 1968, p. 141.
20. Kadota, K., S. Saito and T. Sakaino; "Stress Relaxation Mechanism of Sodium Phosphate Glasses", Yogyo-Kyokai-Shi, Japan, 80[5], 1972, p. 179.
21. Arrhenius, S.; "On the Reaction Rates in the Inversion of Sucrose with Acids", Zeitschrift Für Physikalische Chemie, 4, 1889, p. 226.
22. Yager, W. A.; "Distribution of Relaxation Times in Typical Dielectrics", Journal of Applied Physics, 7(12), 1936, pp. 434-450.

23. Nowick, A. S. and B. S. Berry; "Lognormal Distribution Function for describing Anelastic and other Relaxation Processes", IBM Journal of Research and Development, 5, 1961, pp. 297 and 312.
24. Ke, T. S.; "A Grain Boundary Model and the Mechanism of Viscous Slip", Journal of Applied Physics, 20, 1949, p. 274.
25. Ke, T. S.; "Internal Friction of Metals at Very High Temperatures", Journal of Applied Physics, 21, 1950, p. 414.
26. Wachtman, J. B. and D. G. Lam; "Young's Modulus of Various Refractory Materials as a Function of Temperature", Journal of the American Ceramic Society, 42, 1959, p. 254.
27. Chang, R.; "The Elastic and Anelastic Properties of Refractory Materials for High Temperature Applications", in "Mechanical Properties of Engineering Ceramics", Kriegel and Palmour, eds., Interscience, New York, 1961, p. 209.
28. "Symposium on Porcelain Enamels and Ceramic Coatings and Engineering Materials", ASTM Special Technical Publication No. 153, 1954.
29. Cowan, R. W., A. W. Allen and A. L. Friedberg; "Effect of Temperature on Modulus of Elasticity of Porcelain Enameled Steel", Journal of the American Ceramic Society, 39(9), 1956, p. 293.
30. See for example:
Tobolsky, A. V.; "Properties and Structure of Polymers", Wiley, New York, 1960.
31. Bartenev, G. M.; "The Structure and Properties of Inorganic Glasses", Walters-Noordhoff Publishing, The Netherlands, 1970.
32. Engel, W. H., R. A. Eppler and D. W. Parsons; "Transmission Electron Microscopy of TiO₂ Opacified Porcelain Enamels", American Ceramic Society Bulletin, 49(2), 1970, p. 175.
33. Aklonis, J. J., W. J. MacKnight and M. Shen; "Introduction to Polymer Viscoelasticity", Wiley-Interscience, New York, 1972.

34. McCrum, N. G., B. E. Read and G. Williams; "Anelastic and Dielectric Effects in Polymeric Solids", Wiley, New York, 1967.
35. Ferry, J. D.; "Viscoelastic Properties of Polymers", Wiley, New York, 2nd Ed., 1970.
36. Chicago Vitreous Corporation, 1425 South 55th Court, Cicero, Illinois, 60650; Private Communication.
37. Dietz, E. D.; "The Glassy State", Science and Technology, Nov. 1968, p. 10.
38. Mackenzie, J. D.; "Recent Advances in Glass Science and Technology", in "Vistas in Science", Arm. ed., The University of New Mexico Press, Albuquerque, 1968, p. 94.
39. Litovitz, T. A.; "Liquid Relaxation Phenomena and the Glass State", in "Non-Crystalline Solids", Frechette, ed., Wiley, New York, 1960, p. 252.
40. Nowick, A. S. and B. S. Berry; "Anelastic Relaxation in Crystalline Solids", Academic Press, New York, 1972.
41. Zener, C.; "Elasticity and Anelasticity of Metals", University of Chicago Press, Chicago, 1948.
42. Van Oort, W. P.; "A Method for the Measurement of Dynamic Mechanical Properties of Small Samples of Plastic Materials", Microteknic, 7(5), 1952, p. 246.
43. Nashif, A. D.; "New Method for Determining Damping Properties of Viscoelastic Materials", Shock and Vibration Bulletin, #36, pt. 4, 1967, p. 37.
44. Snowdon, J. D.; "Vibration and Shock in Damped Mechanical Systems", Wiley, New York, 1968.
45. Visser, T. J. M. and J. M. Stevels; "Rheological Properties of Boric Oxide and Alkali Borate Glasses", Journal of Non-Crystalline Solids, 7, 1972, p. 376.

46. Hopkins, I. L. and C. R. Kurkjian; "Relaxation Spectra and Relaxation Processes in Solid Polymers and Glasses", in "Physical Acoustics", Vol. IIB, Mason, ed., Academic Press, New York, 1965.
47. Den Hartog, J. P.; "Mechanical Vibrations", McGraw-Hill, New York, 1947, p. 235.

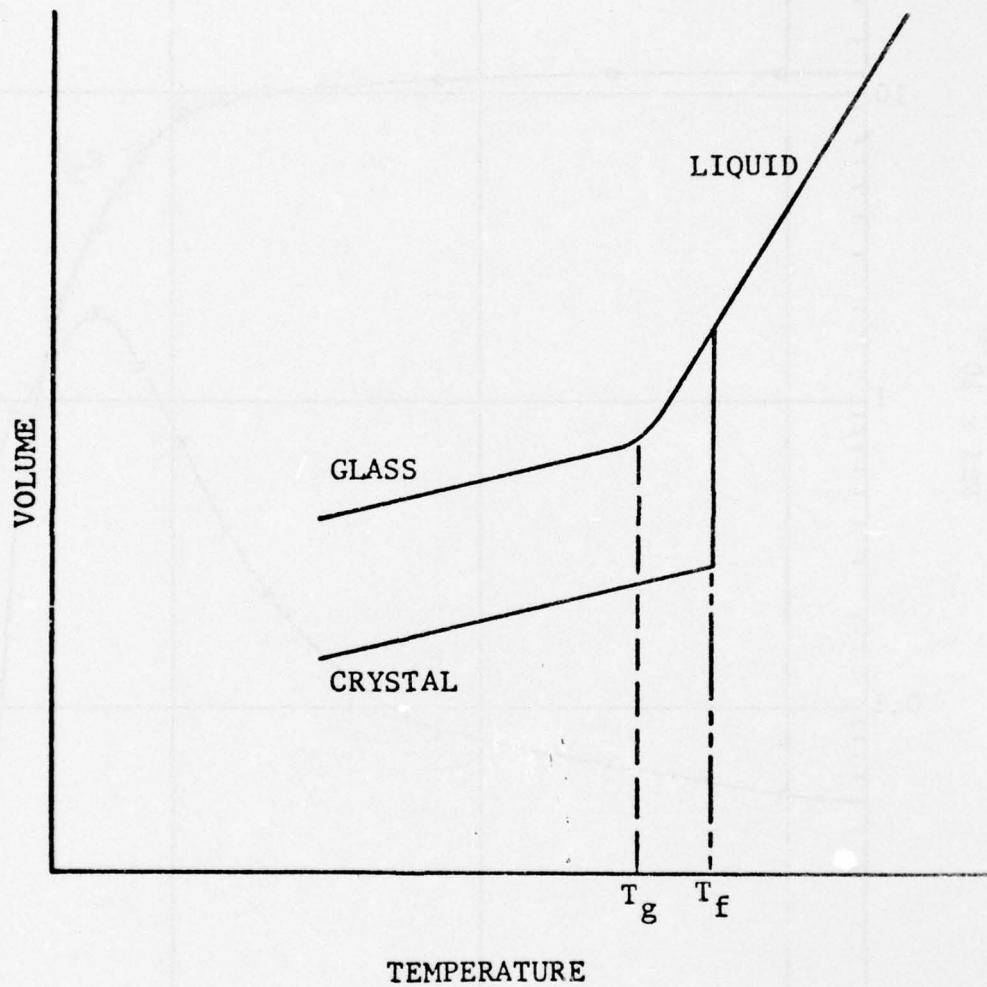


FIG. 2.1. VOLUME VS TEMPERATURE FOR GLASS.

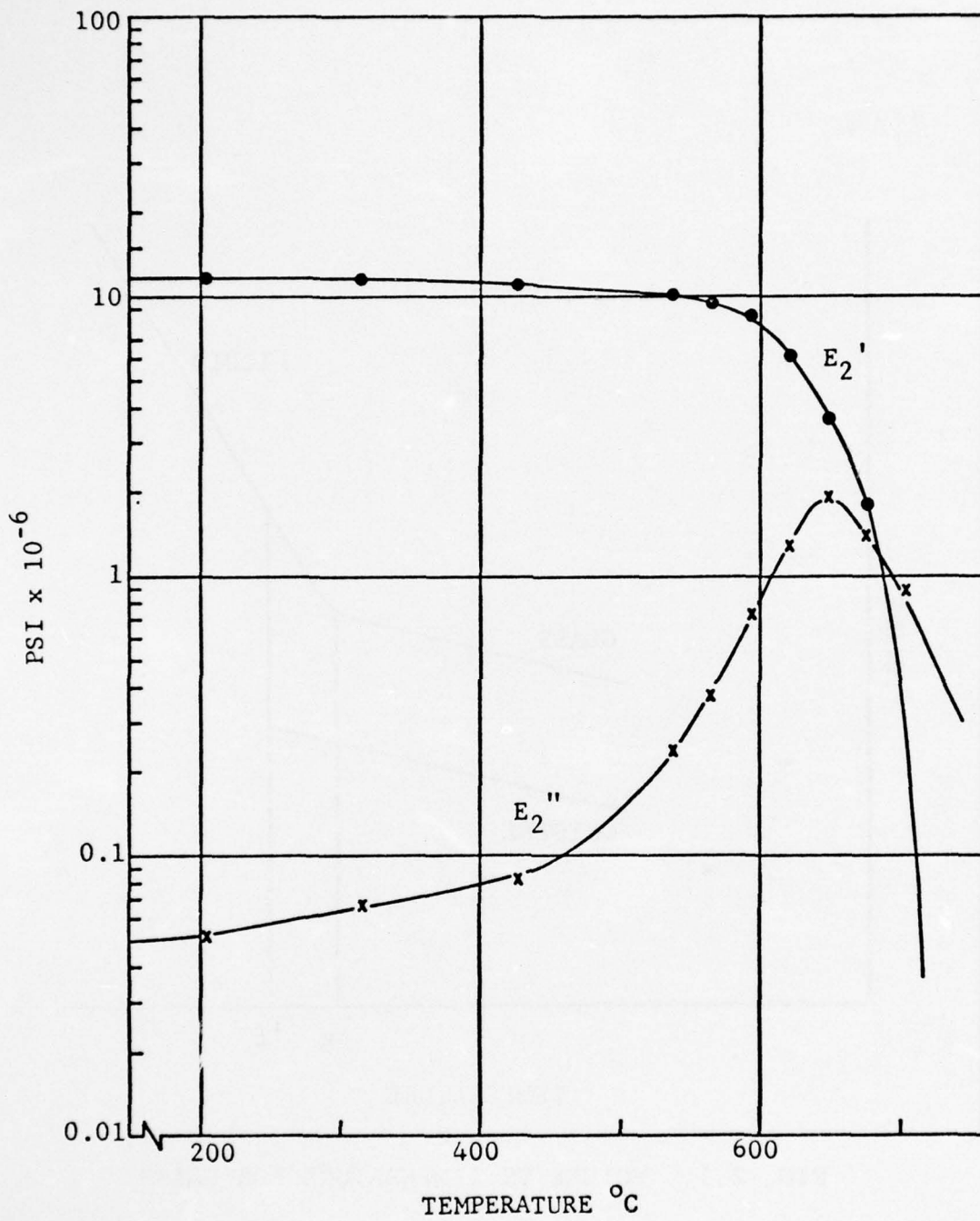


FIG. 2.2. E_2' AND E_2'' VS TEMPERATURE;
 COATING S9919D, SP #5, B.

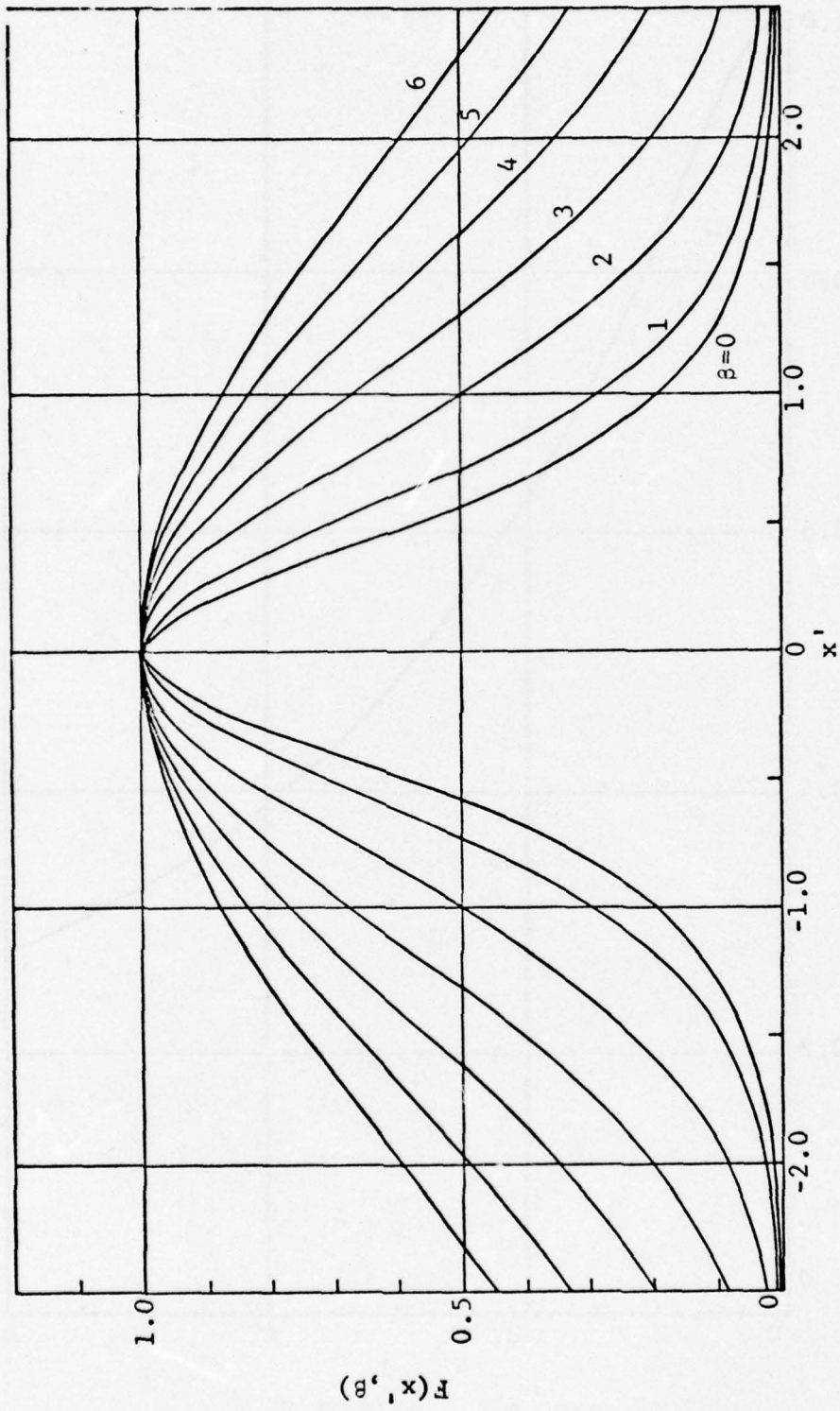


FIG. 2.3. $F(x', \beta)$ VS x' FOR VARIOUS β 's.

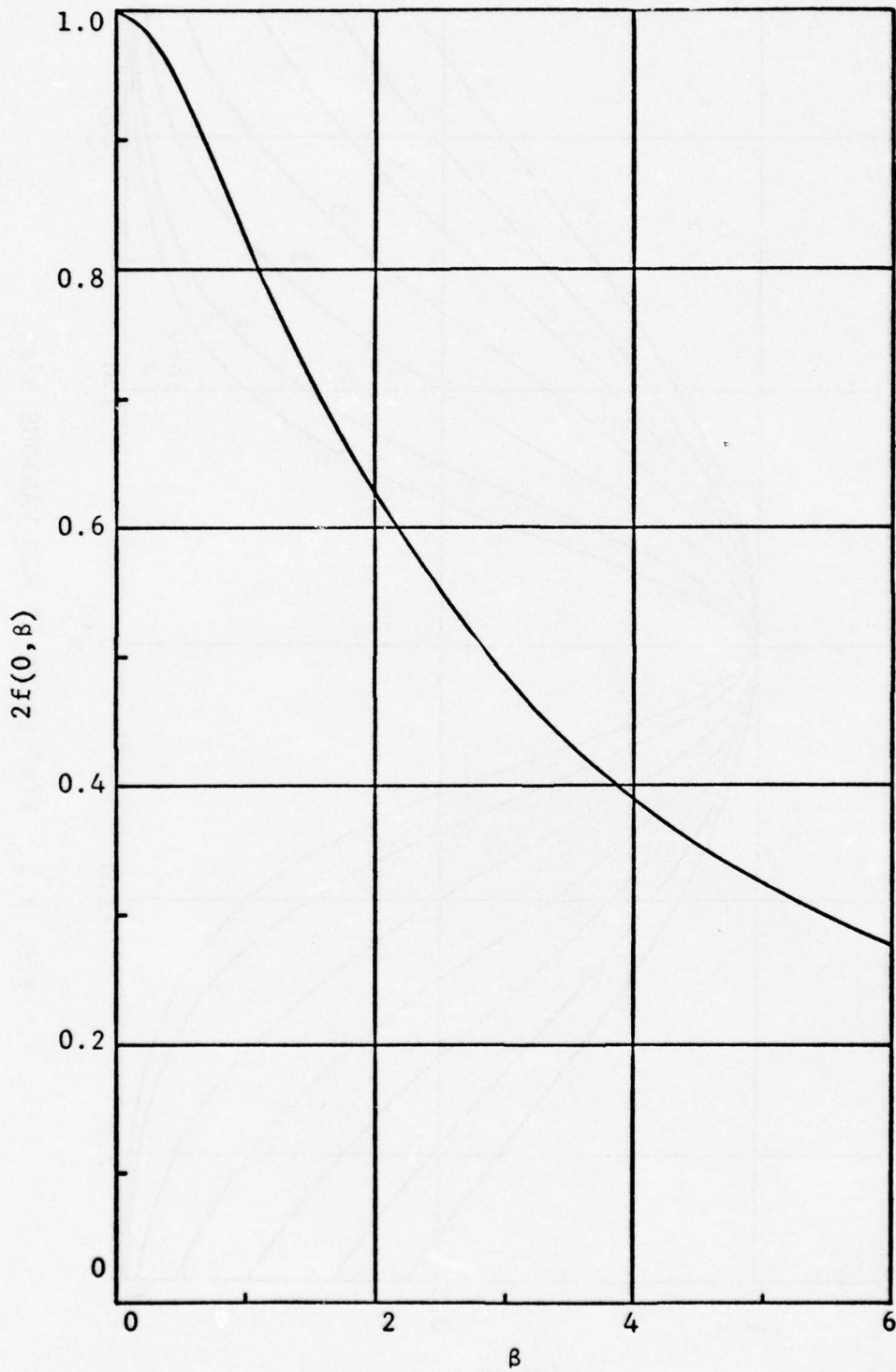


FIG. 2.4. $2f(0, \beta)$ vs β

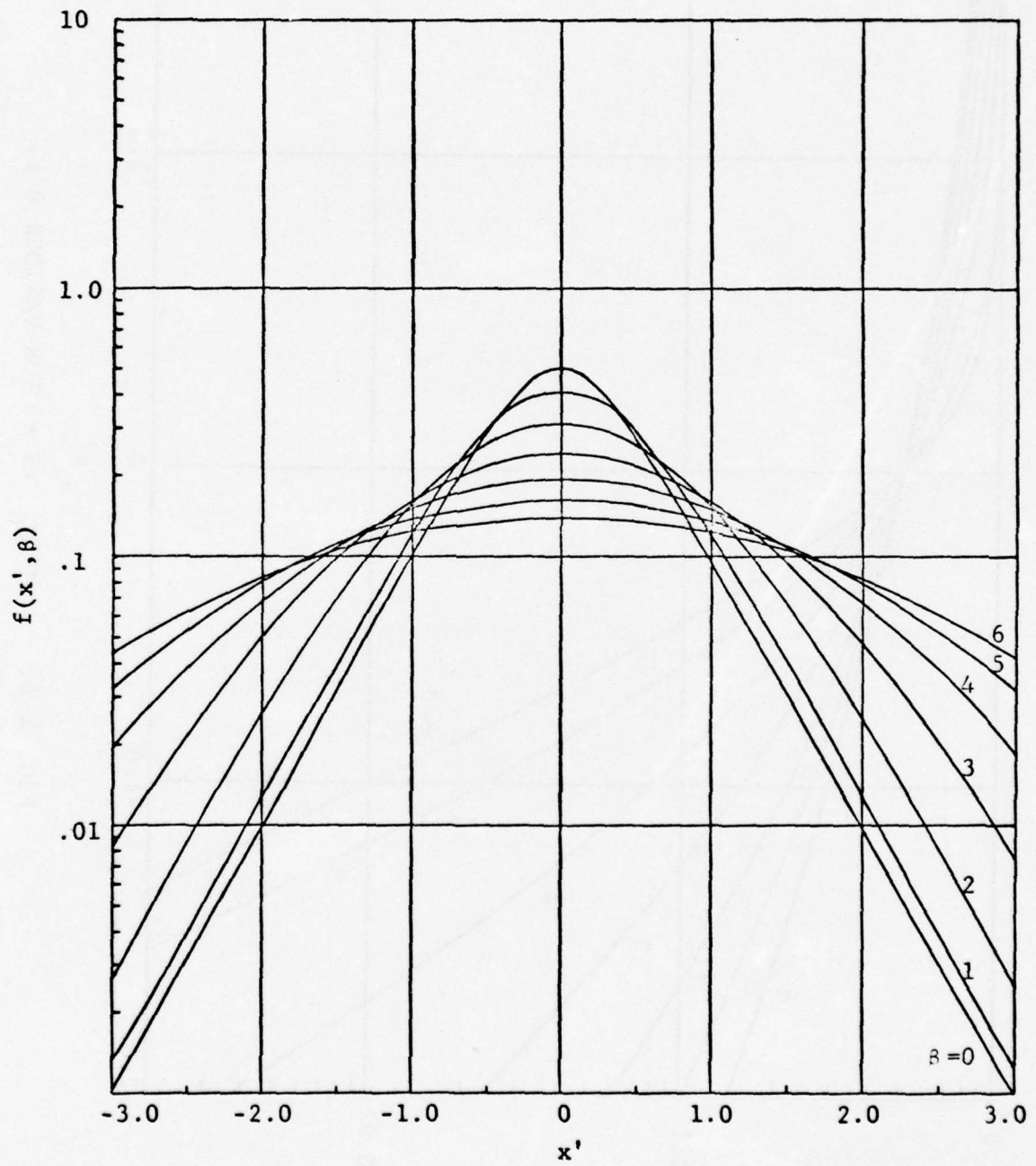


FIG. 2.5. $f(x', \beta)$ vs x' FOR VARIOUS β 'S

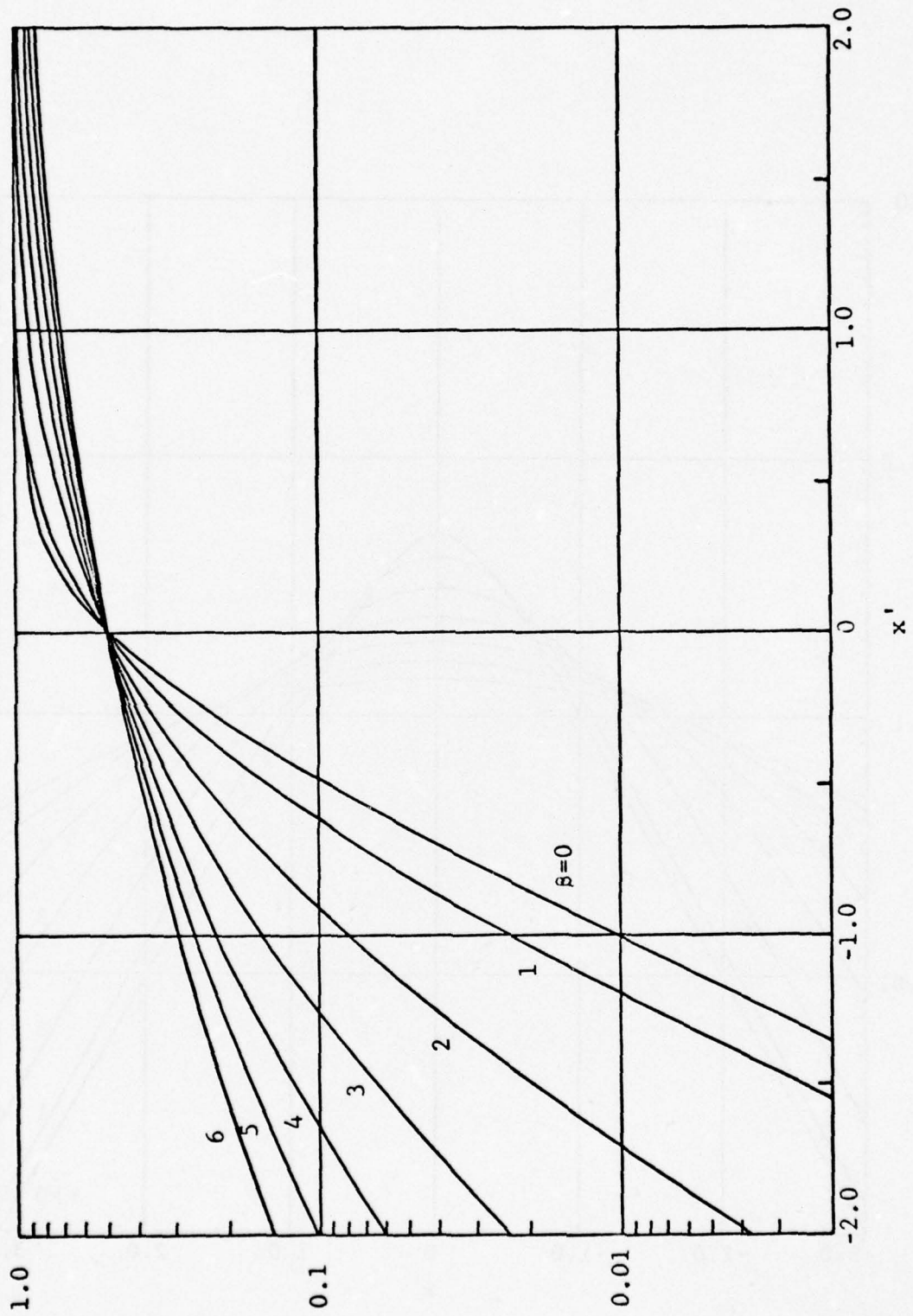


FIG. 2.6. M'/M_U VS x' FOR VARIOUS β 's.

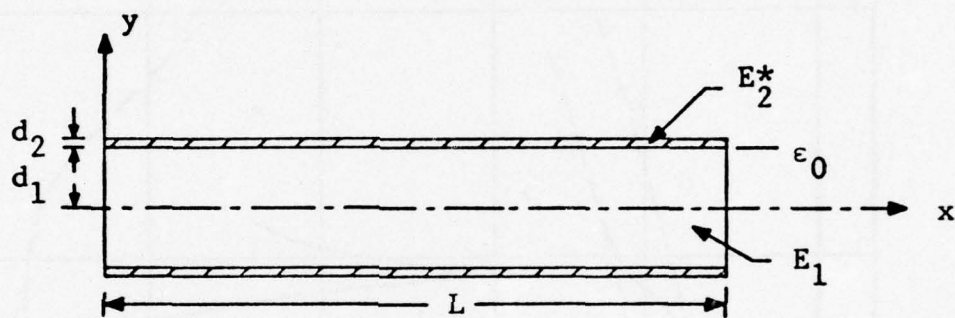


FIG. 3.1. BEAM OF UNIFORM THICKNESS

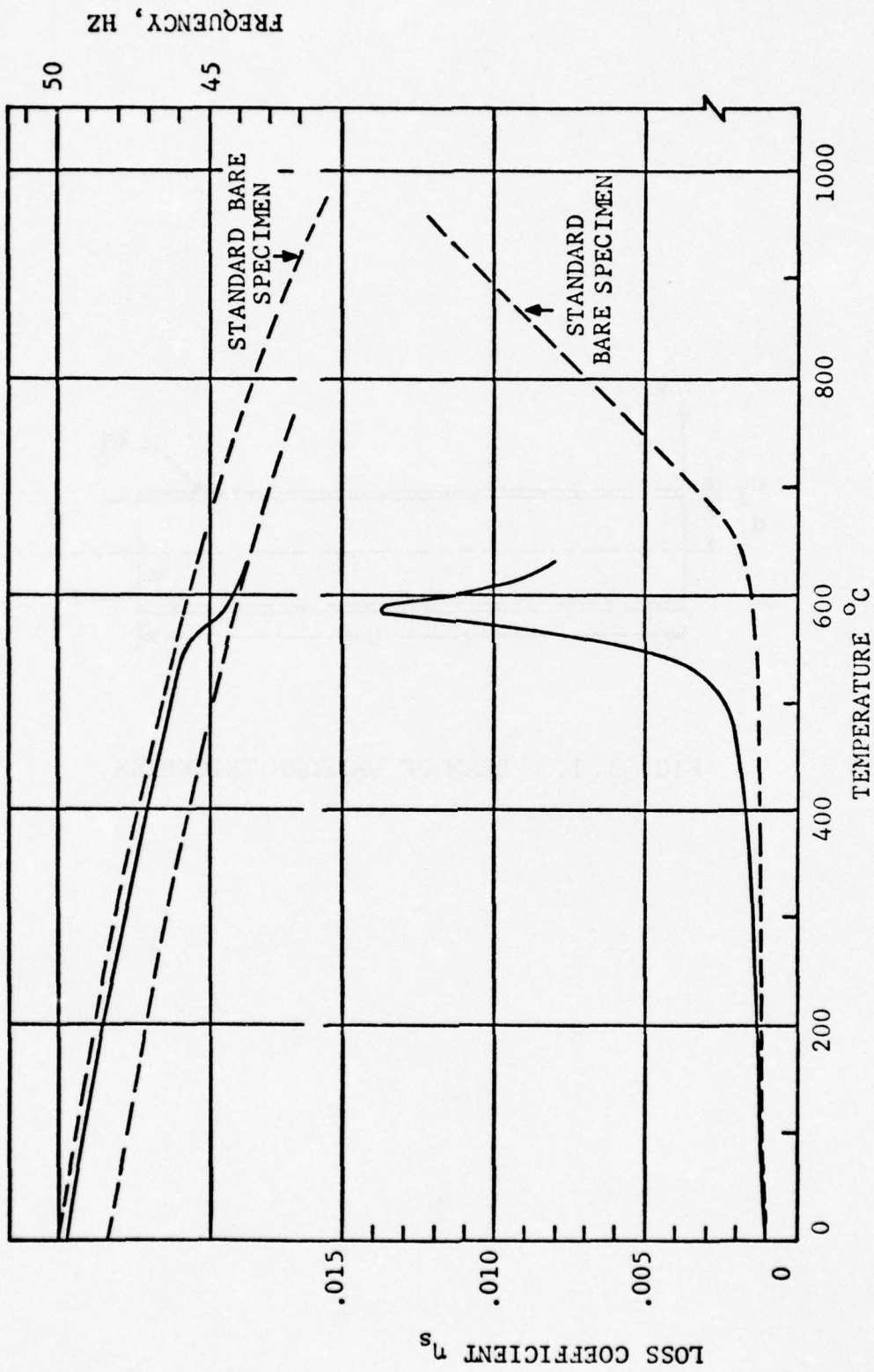


FIG. 3.2. η_s AND f VS TEMPERATURE; $f = 47$ HZ, SP. #16, B

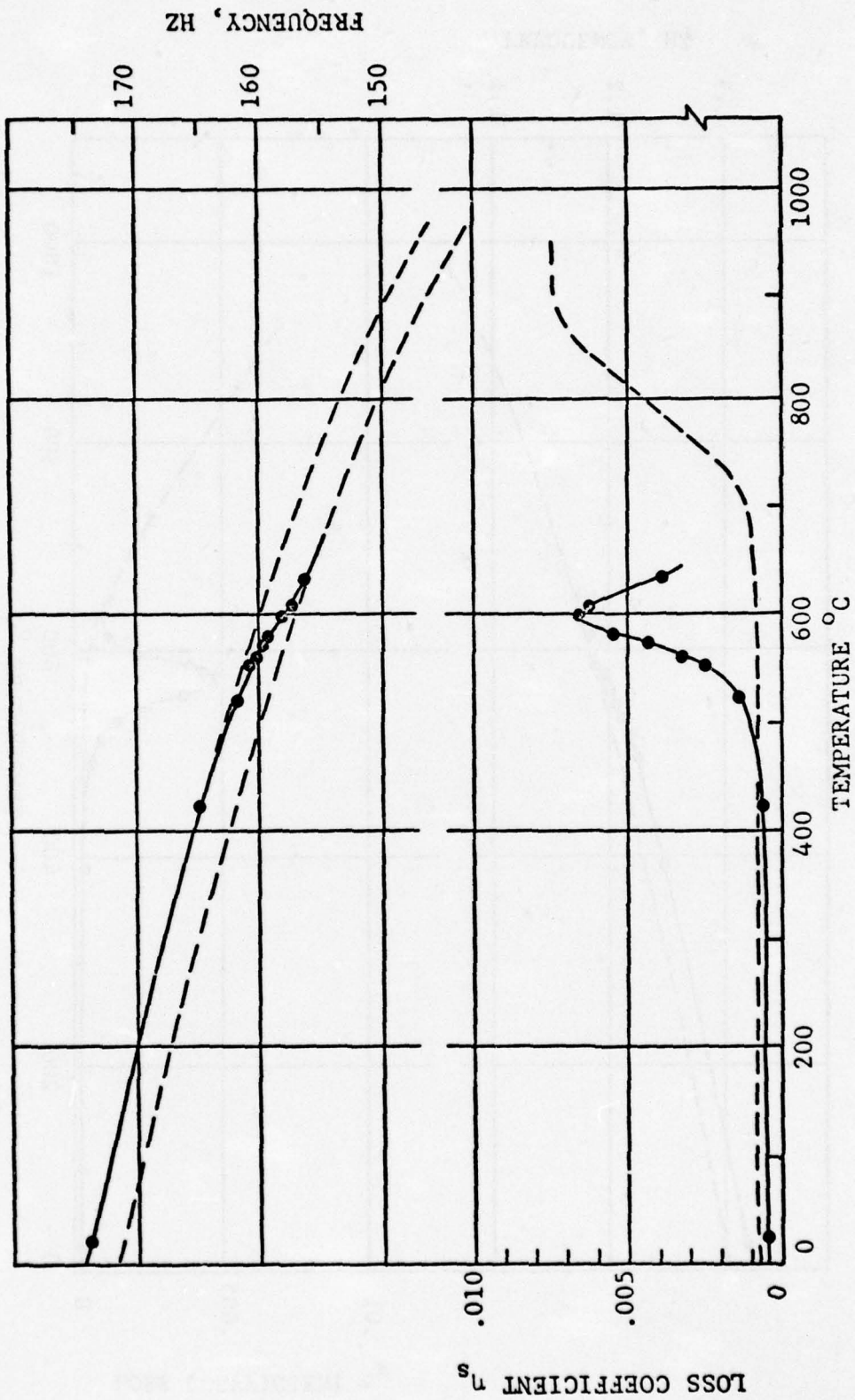


FIG. 3.3. η_s AND f VS TEMPERATURE; $f = 170$ HZ, SP. #16, B.

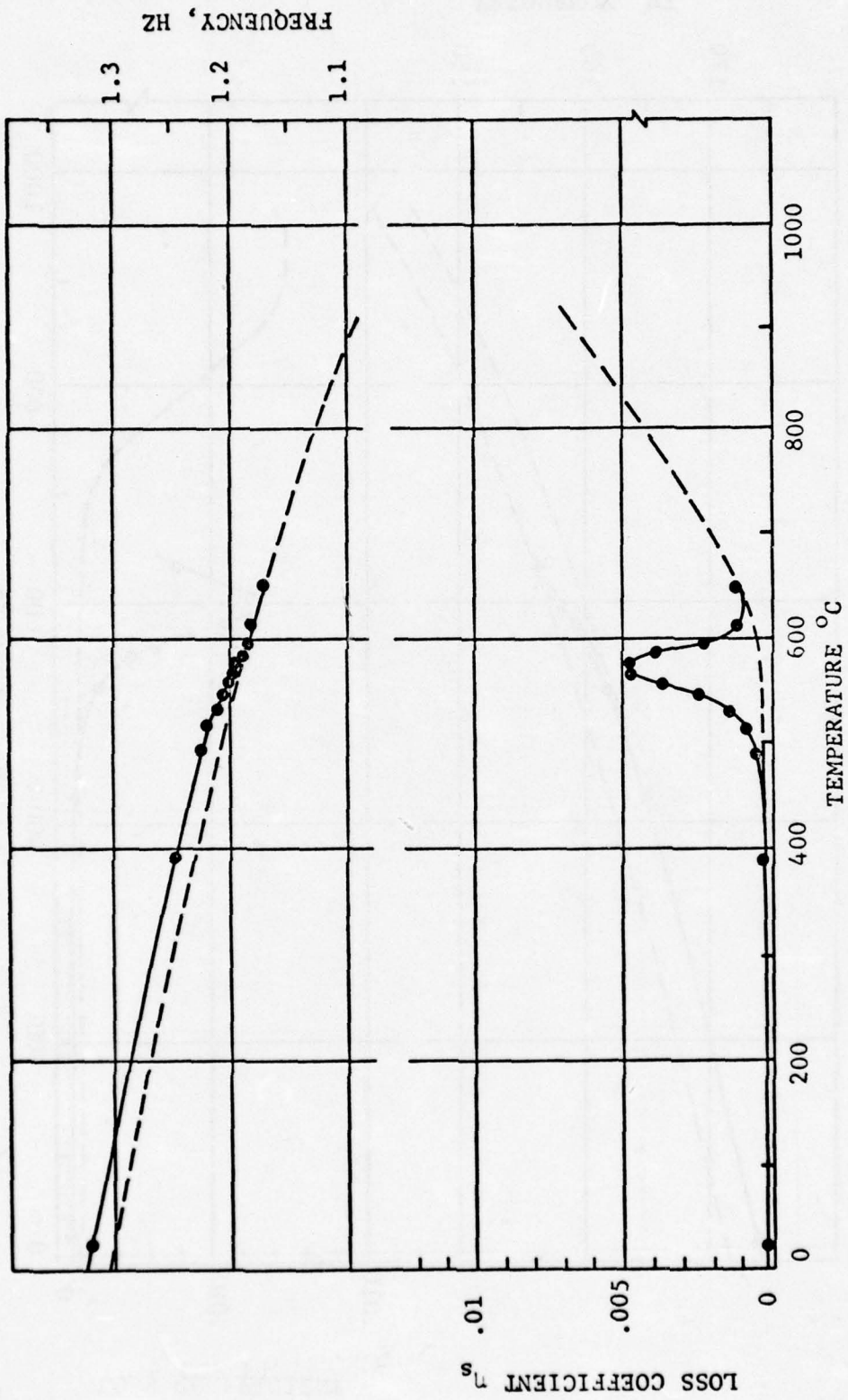


FIG. 4.1.1. η_s AND f VS TEMPERATURE; $f = 1.2$ HZ, SP. #2, TP.

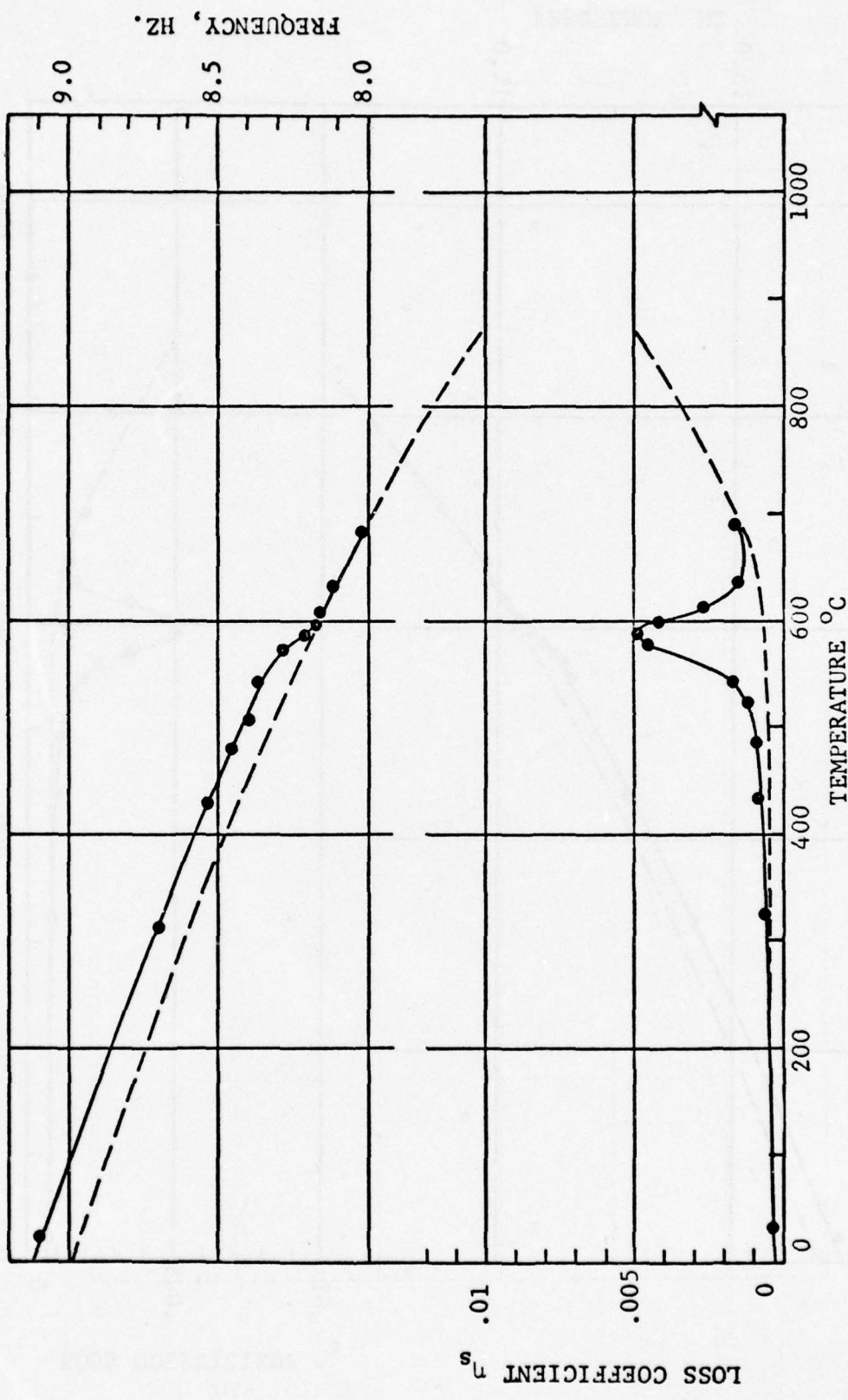


FIG. 4.2. η_s AND f VS TEMPERATURE; $f = 8.4$ HZ, SP. #2, TP.

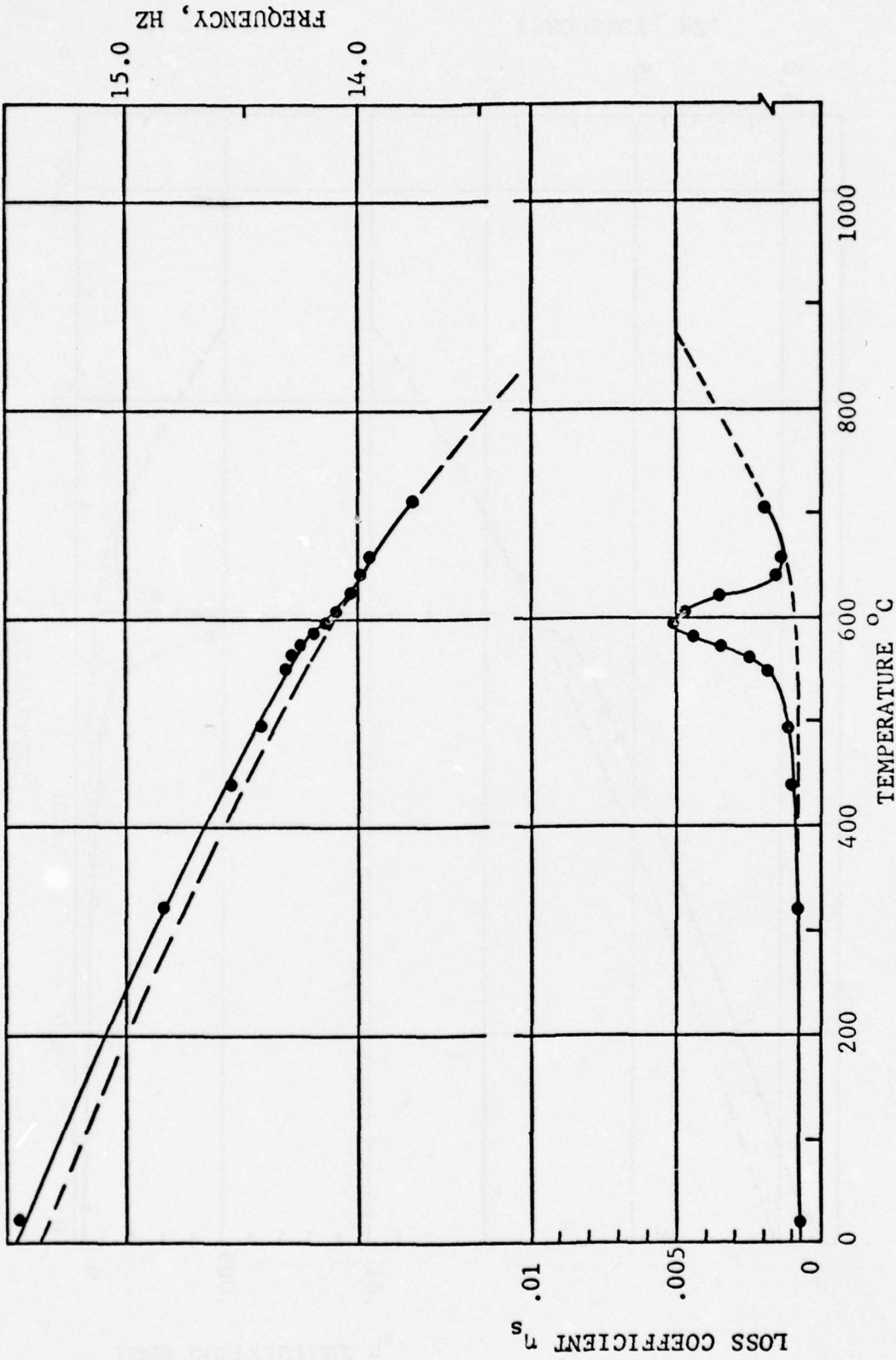


FIG. 4.3. η_s AND f VS TEMPERATURE; $f = 14.25$ HZ, SP. #2, TP.

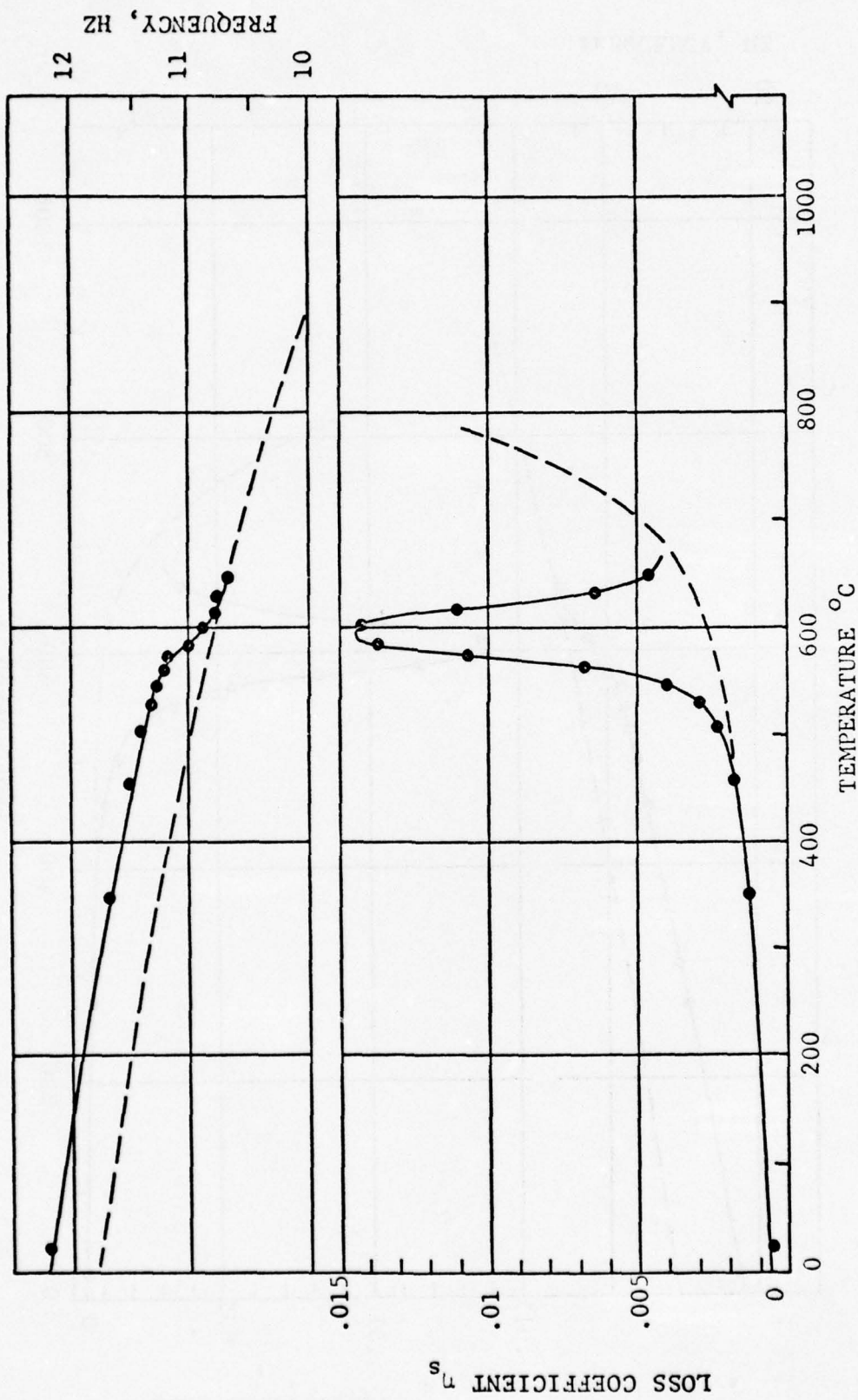


FIG. 4.4. η_s AND f VS TEMPERATURE; $f = 11$ HZ, SF. #16 A, B.

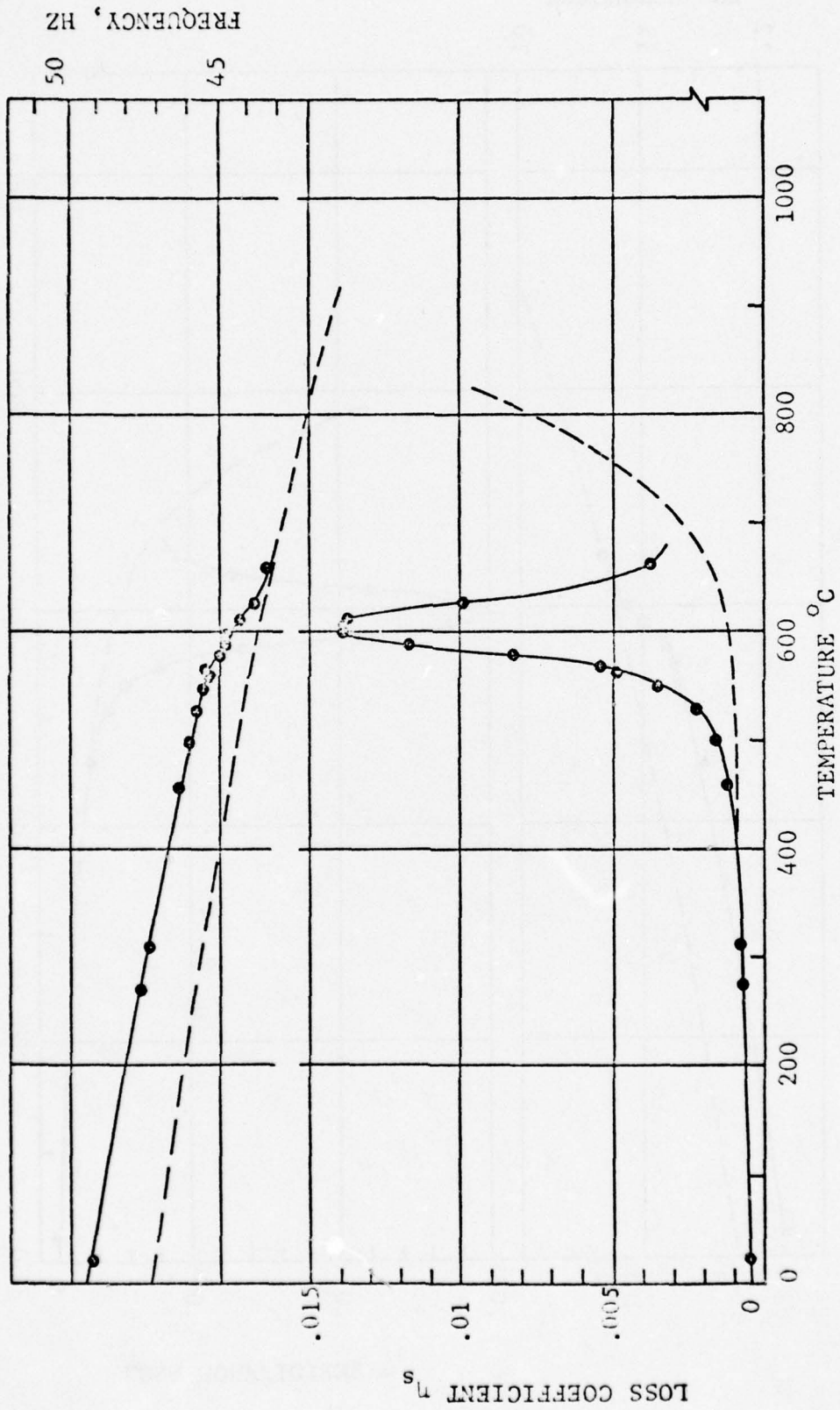


FIG. 4.5. η_s AND f VS TEMPERATURE; $f = 47$ HZ, SP. #16 A, B.

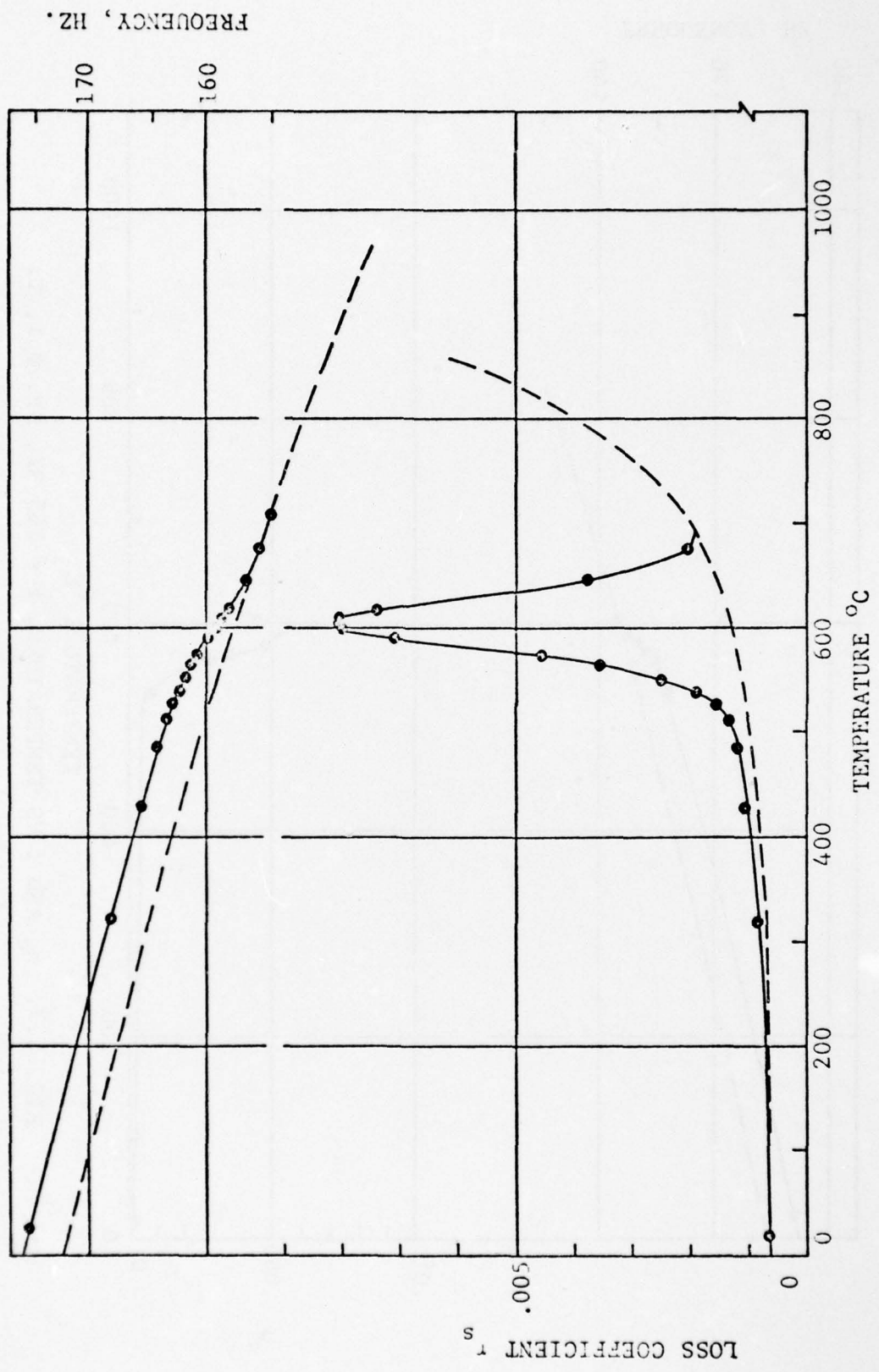


FIG. 4.6. η_s AND f VS TEMPERATURE; $f = 170$ HZ, SP. # 16A, B.

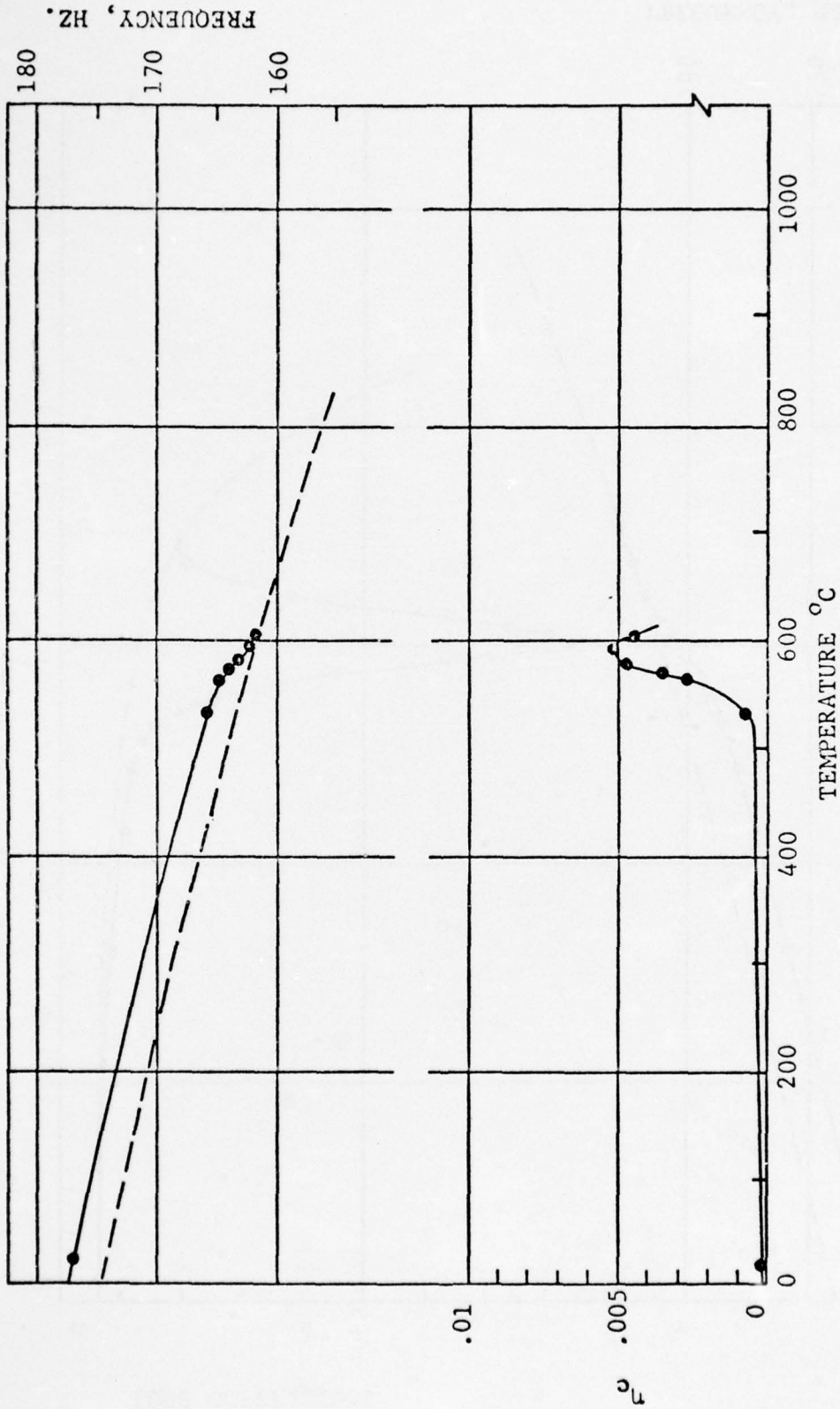


FIG. 4.7. η_c AND f VS TEMPERATURE; $f = 165$ HZ, SP. # 1, T.

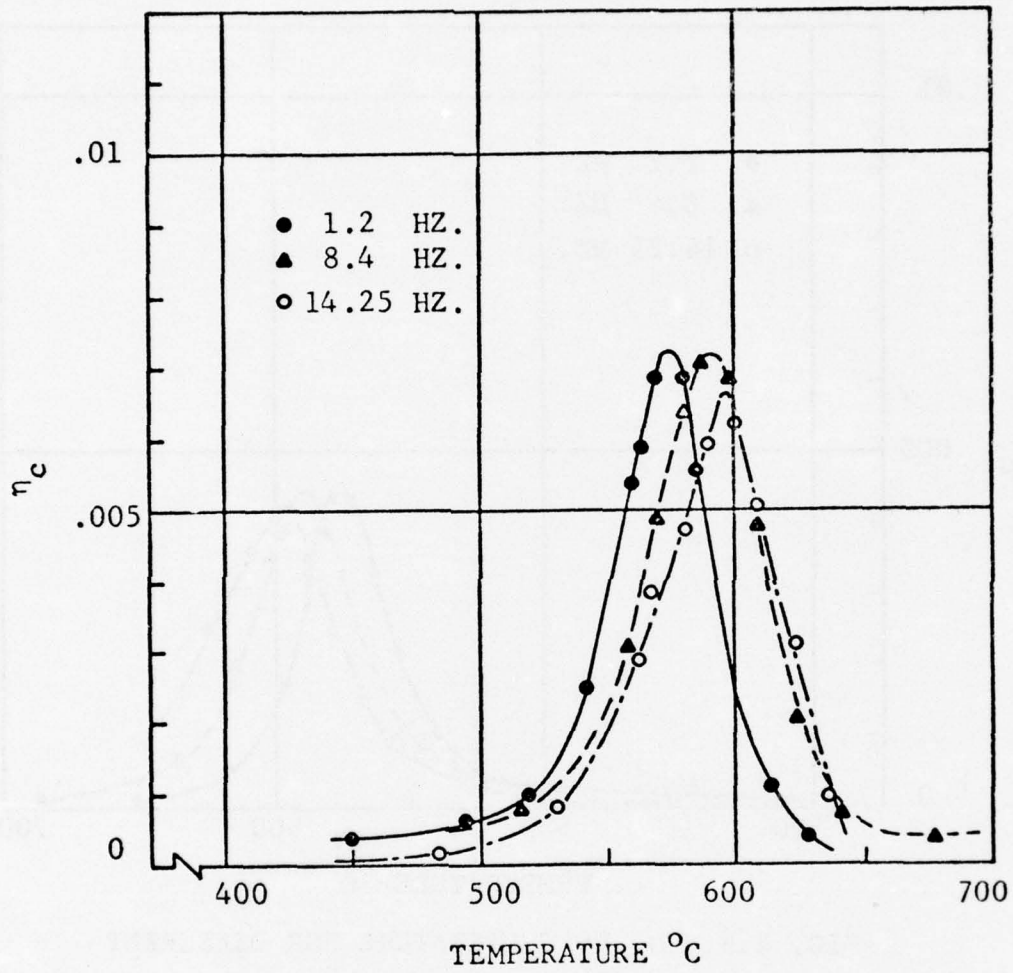


FIG. 4.8 η_c VS TEMPERATURE FOR DIFFERENT FREOUENCIES; SP. #1, TP

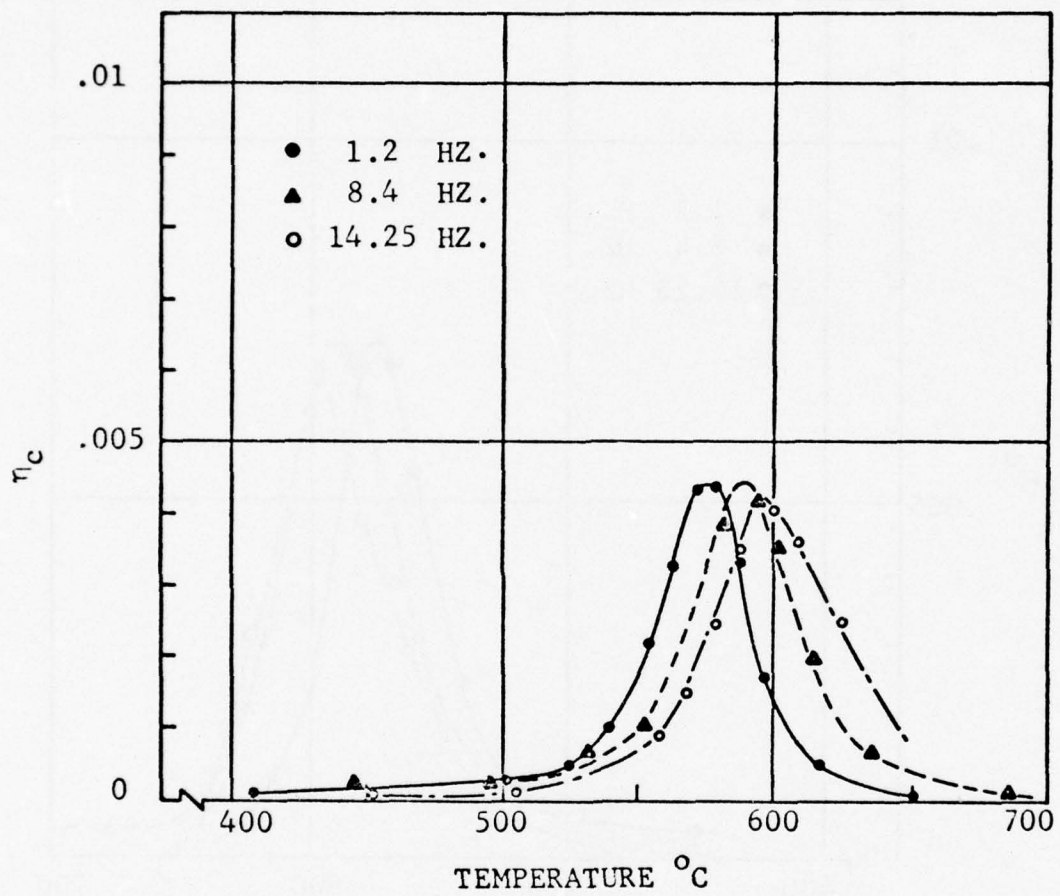


FIG. 4.9. η_c VS TEMPERATURE FOR DIFFERENT FREQUENCIES; SP. #2, TP

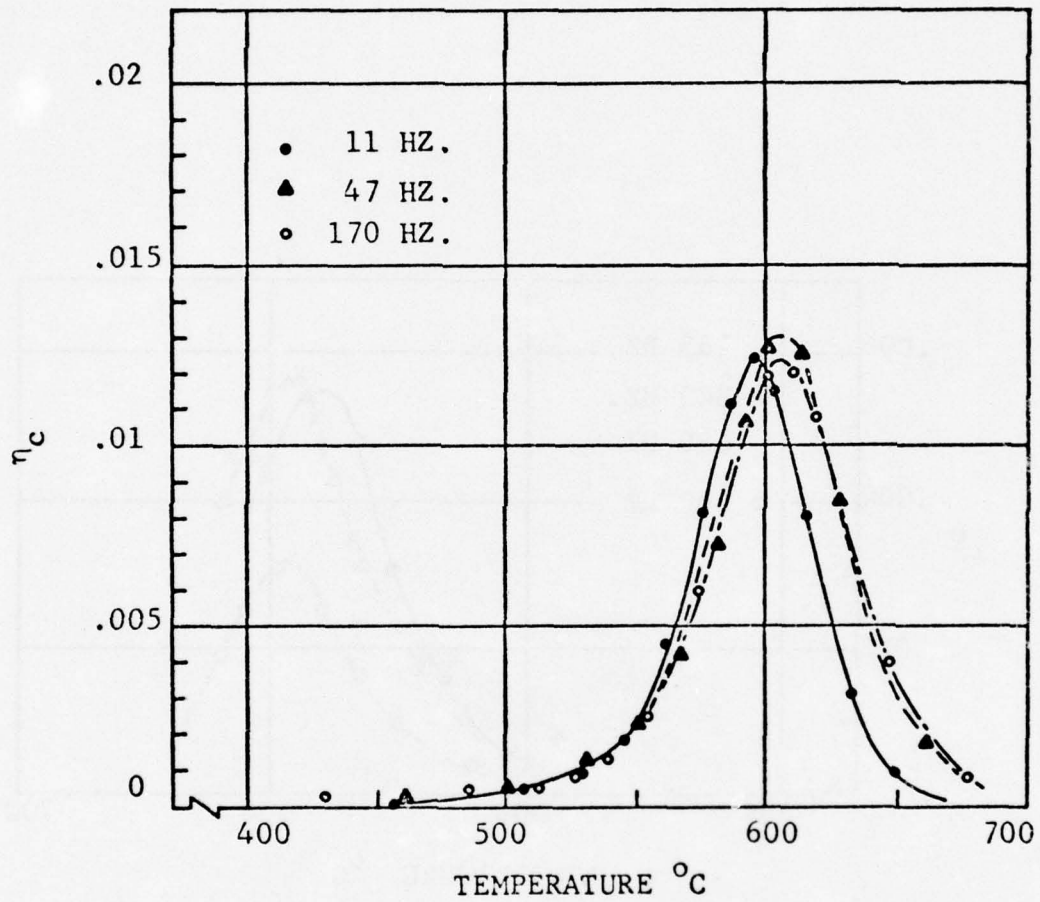


FIG. 4.10. η_c VS TEMPERATURE FOR DIFFERENT FREQUENCIES; SP. #16A, B.

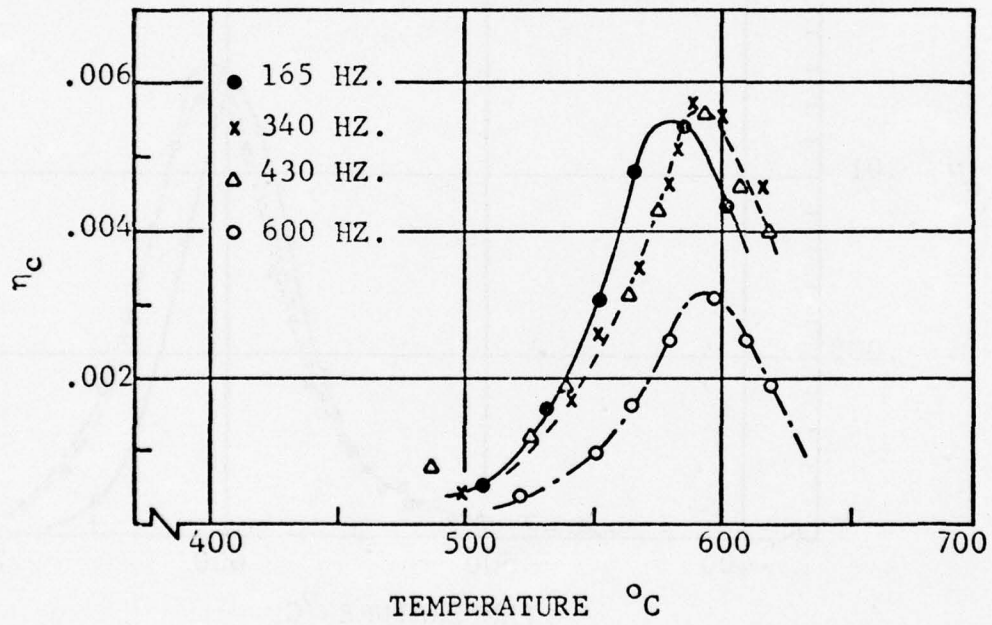


FIG. 4.11. η_c VS TEMPERATURE FOR DIFFERENT FREQUENCIES; SP. #1, T.

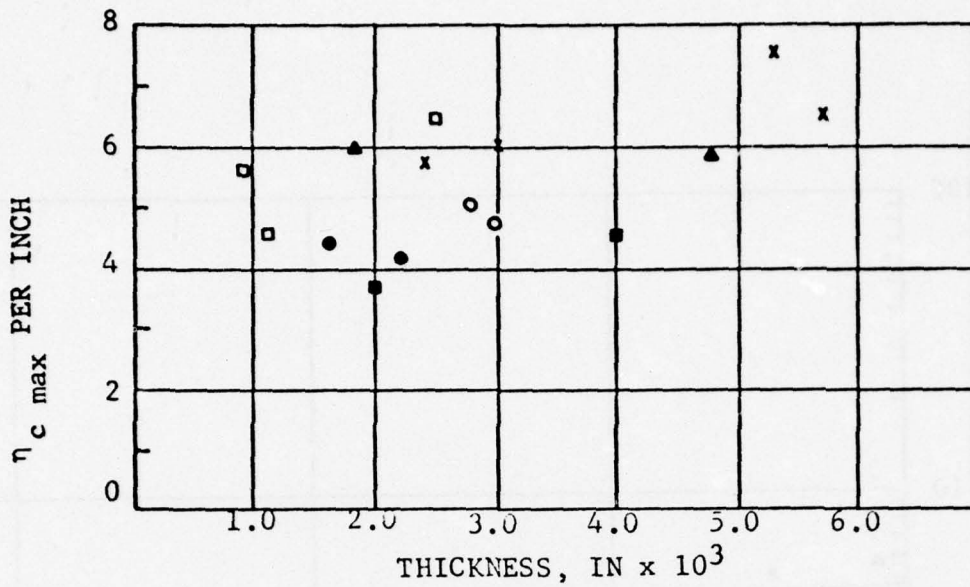


FIG. 4.12. $\eta_c \text{ max}$ PER INCH VS THICKNESS OF COATING, BENDING

- S5-8A
- AL-2(A)
- CV-145 s(B)
- ▲ 325(Bb)
- × S9919D
- S6100M

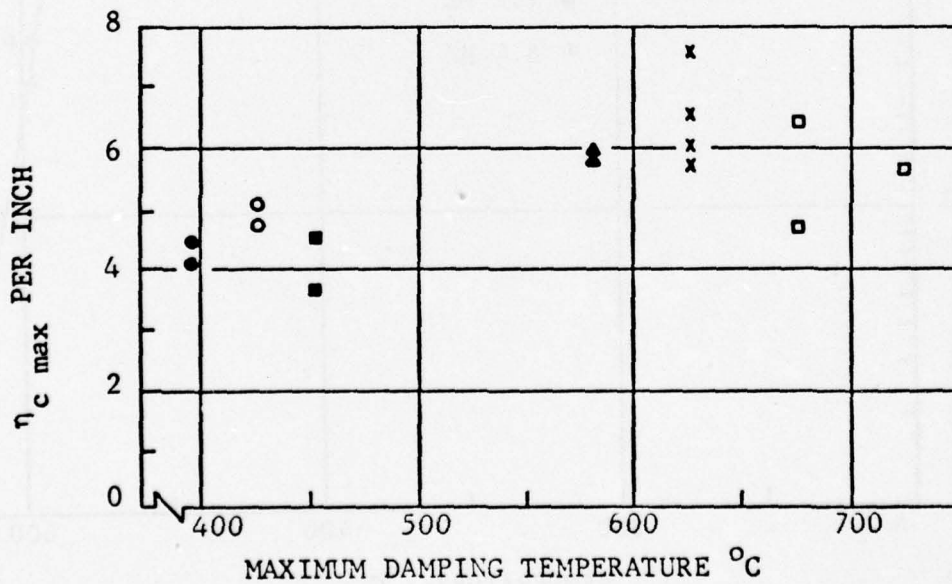


FIG. 4.13. $\eta_c \text{ max}$ PER INCH VS TEMPERATURE OF MAXIMUM DAMPING, BENDING

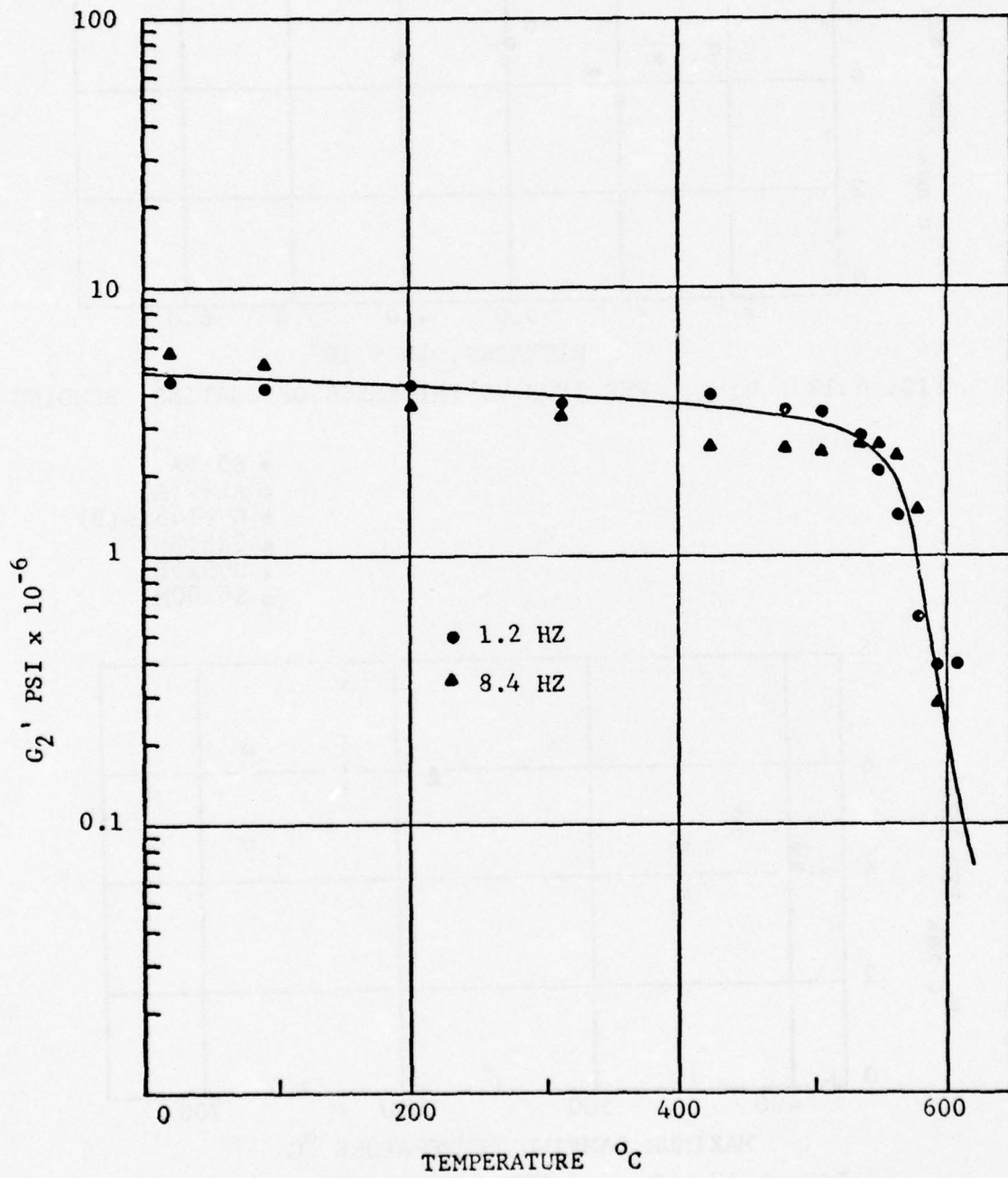


FIG. 4.14. G_2' VS TEMPERATURE; COATING #12325, SP. #2, TP.

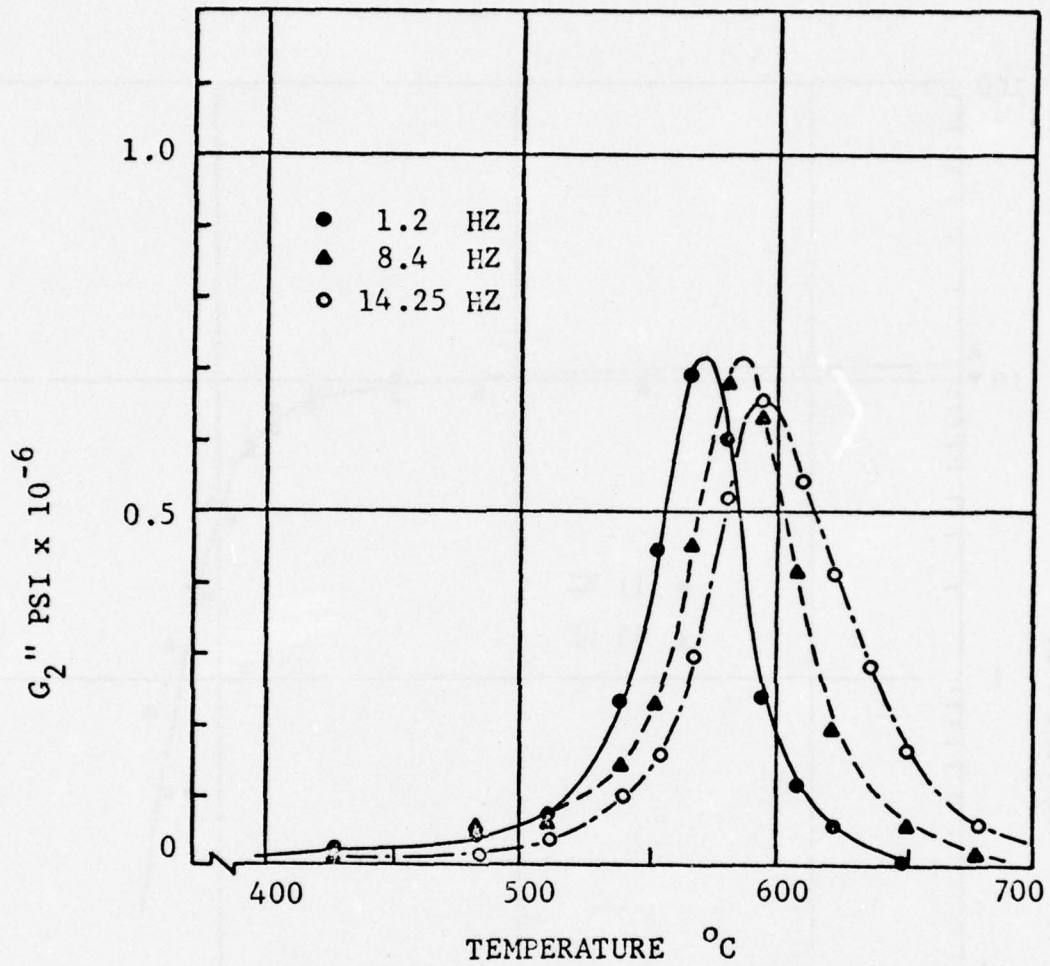


FIG. 4.15. G_2'' VS TEMPERATURE FOR DIFFERENT FREQUENCIES; SP. #2, TP

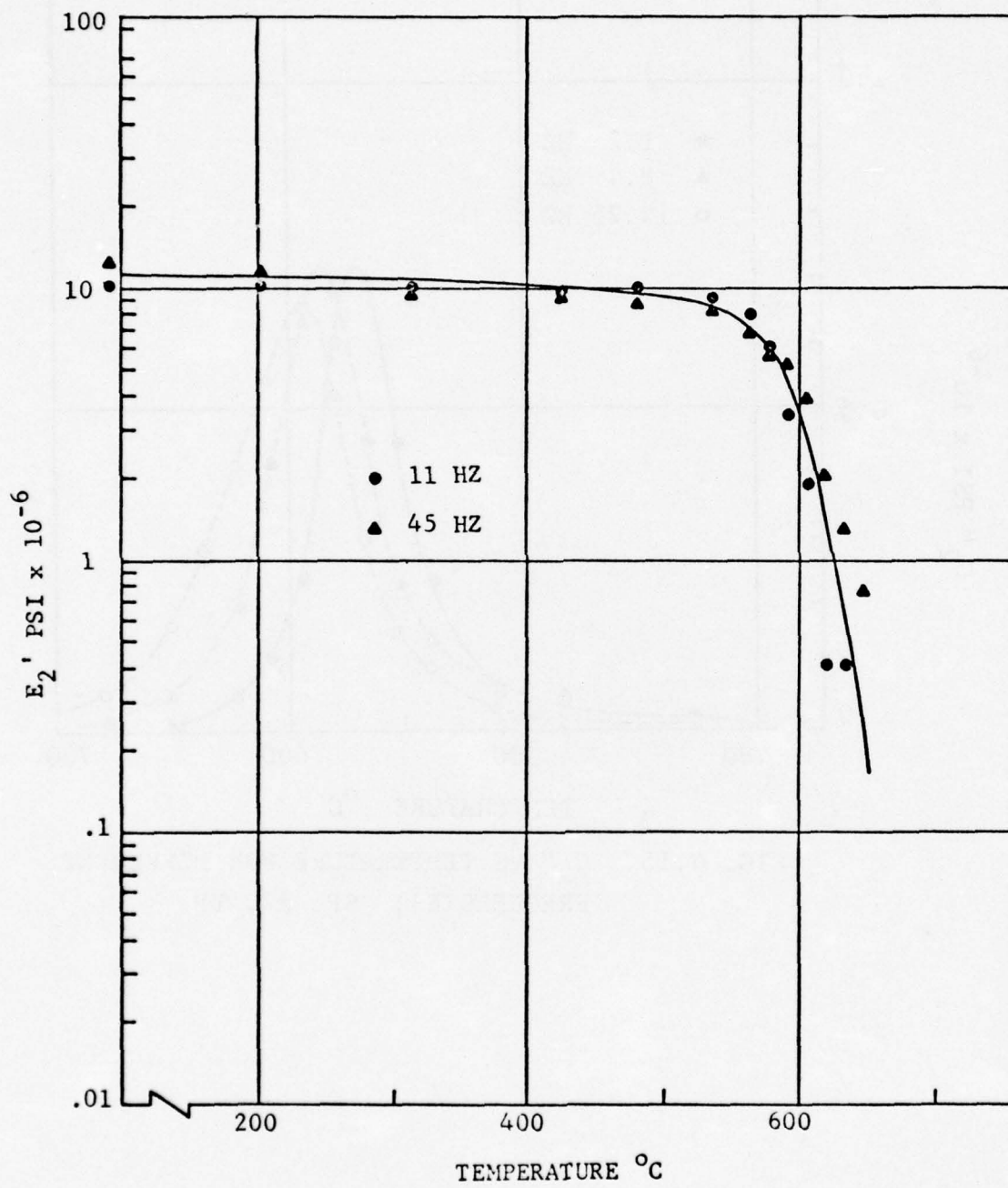


FIG. 4.16. E₂' VS TEMPERATURE; COATING #12325, SP.#16A,B.

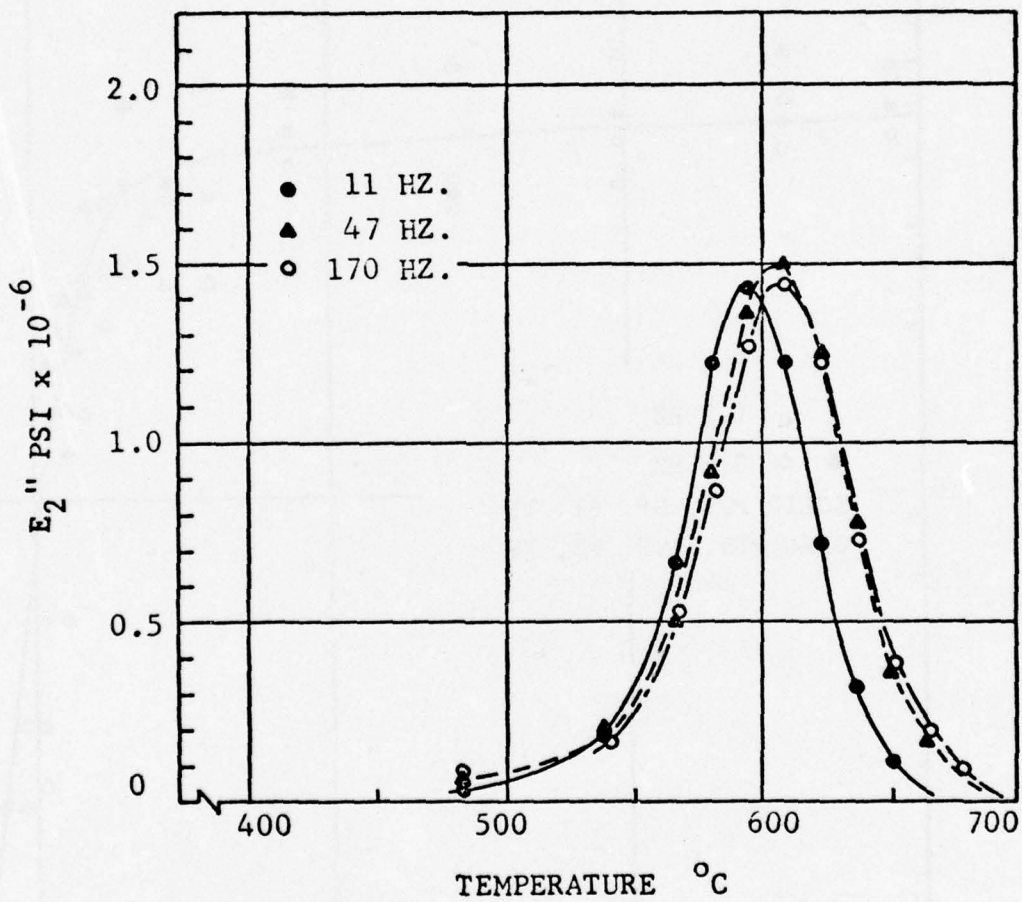


FIG. 4.17. E_2'' VS TEMPERATURE FOR DIFFERENT FREQUENCIES; SP. #16A, B.

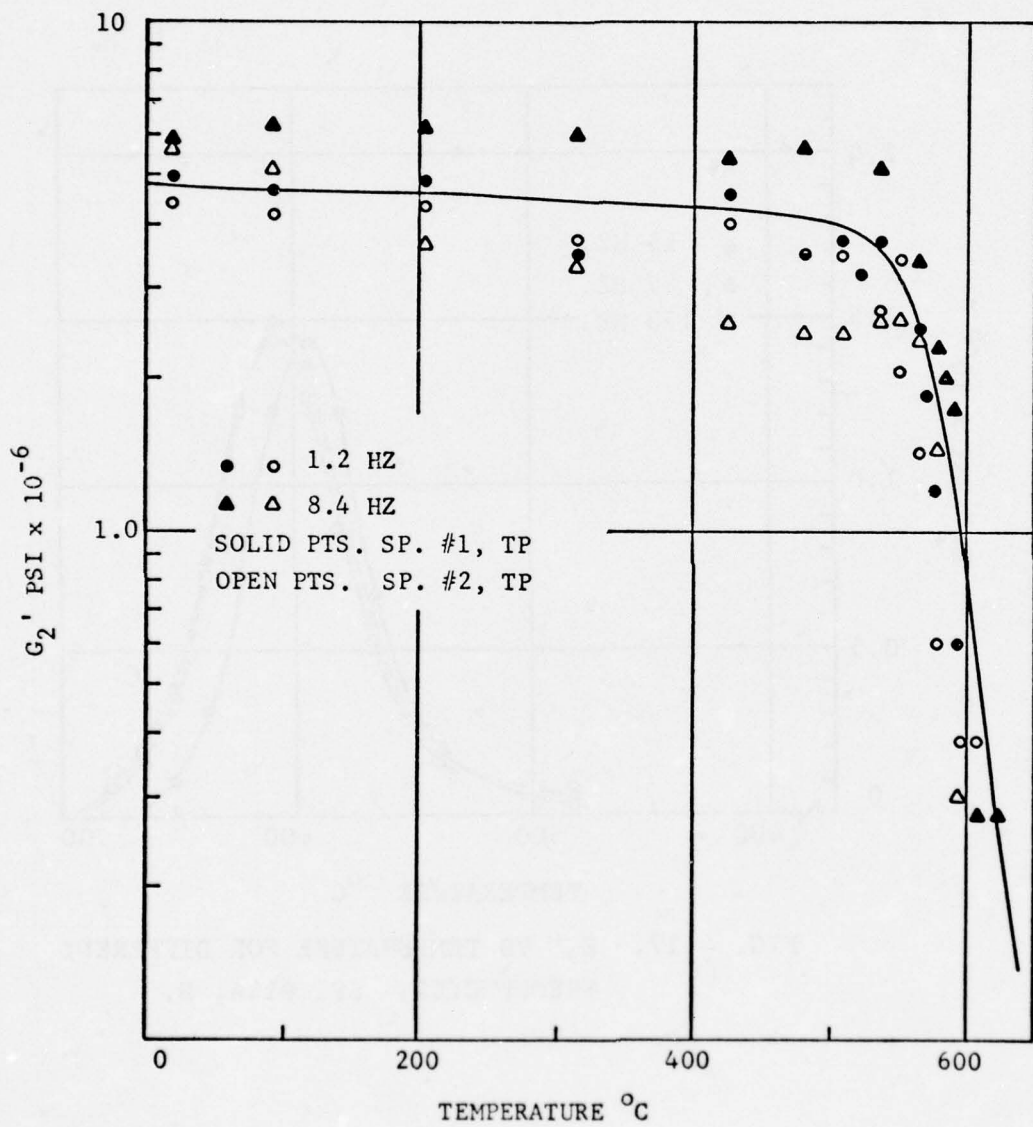


FIG. 4.18. G_2' VS TEMPERATURE; COATING #12325

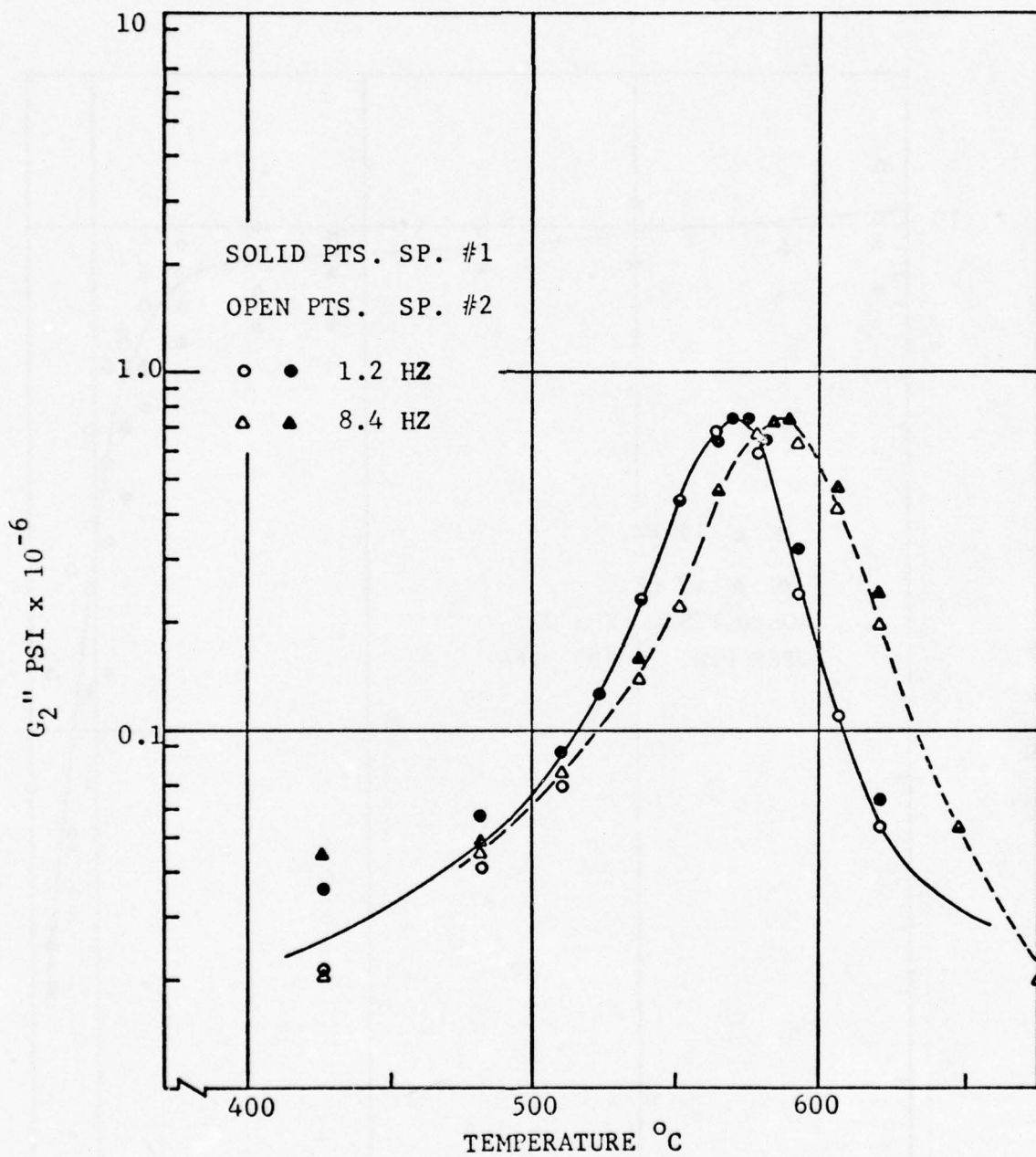


FIG. 4.19. G₂'' VS TEMPERATURE; COATING #12325

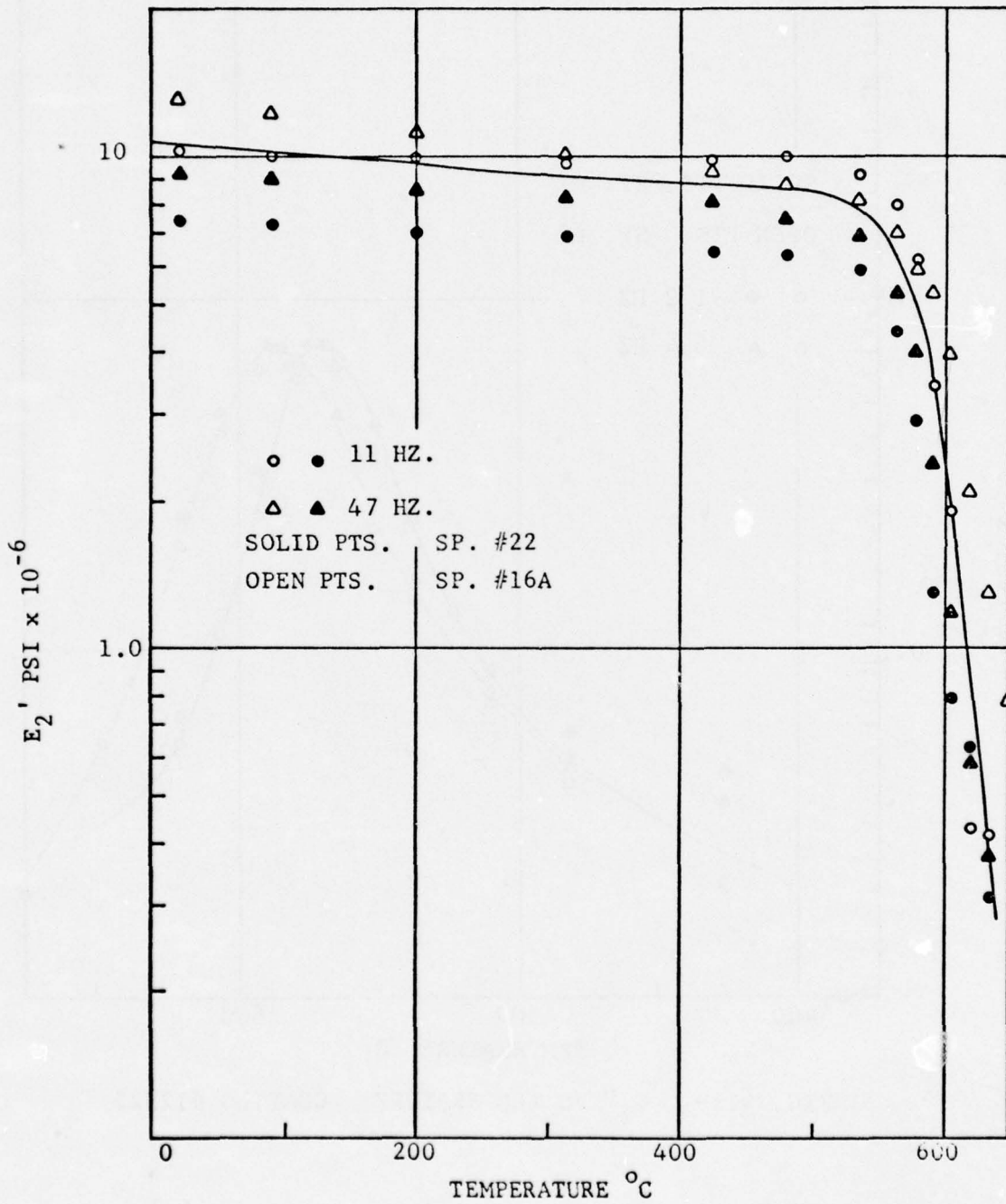


FIG. 4.20. E_2' VS TEMPERATURE; COATING #12325

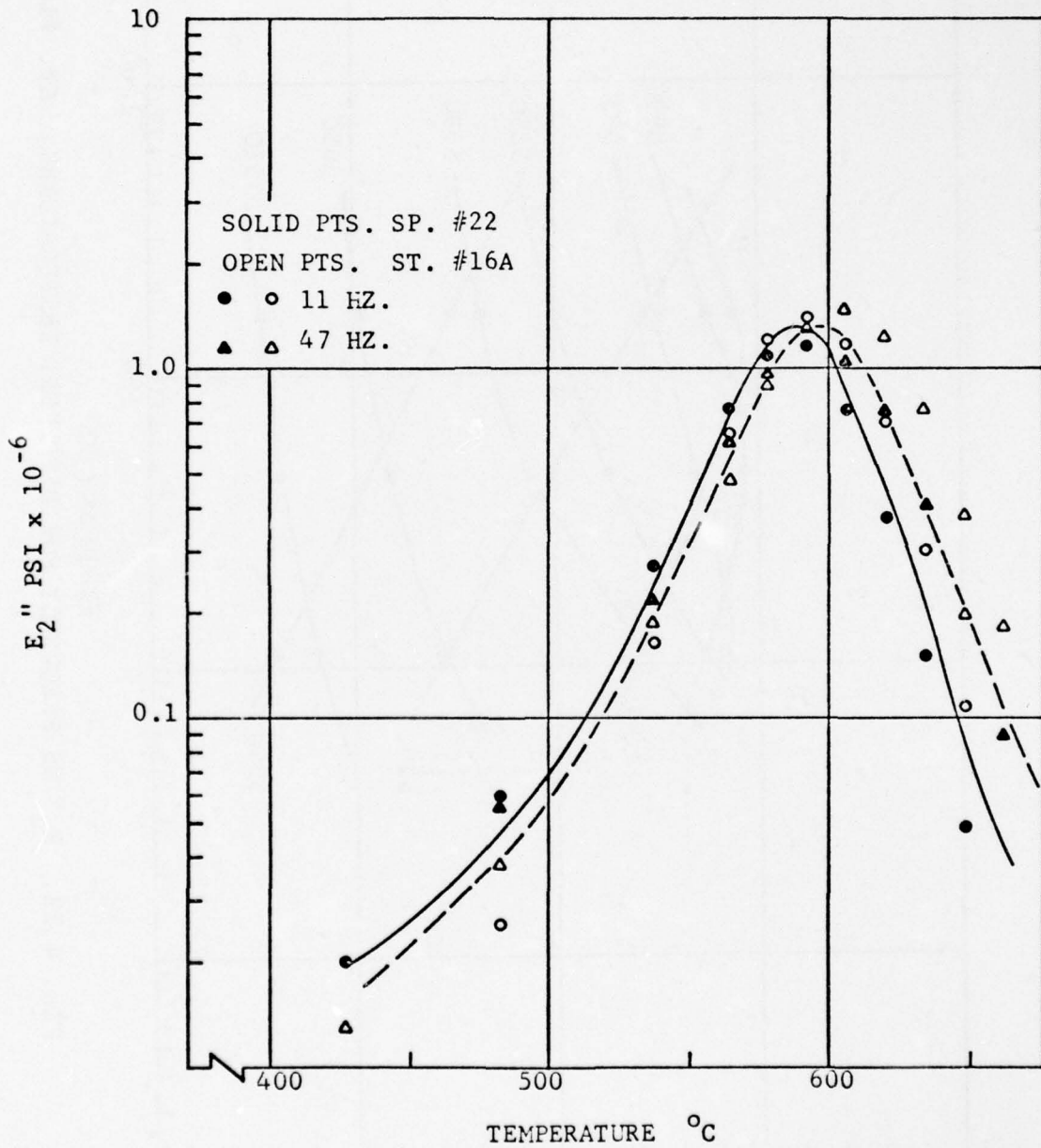


FIG. 4.21. E_2'' VS TEMPERATURE; COATING #12325

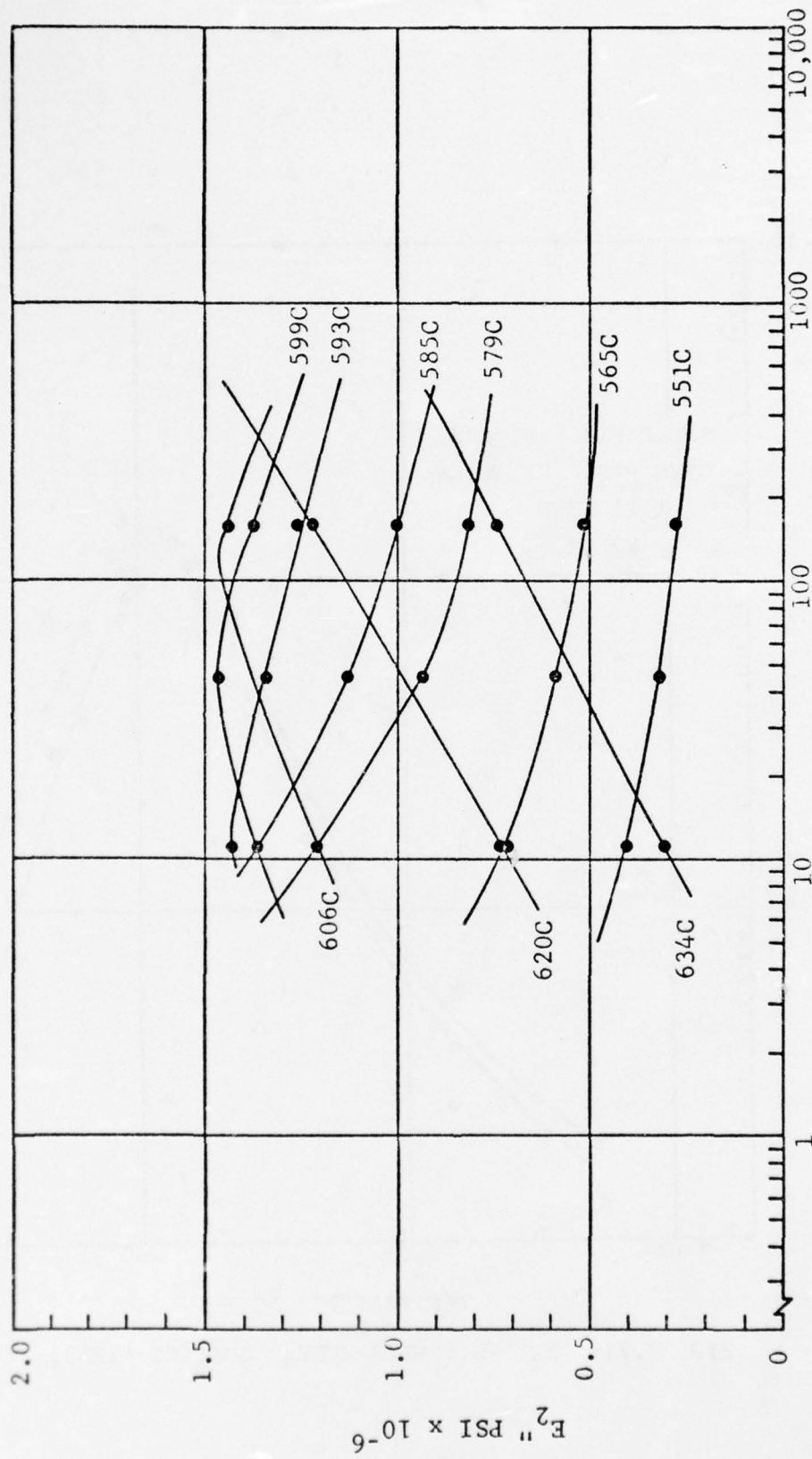


FIG. 4.22. E_2'' VS FREQUENCY FOR DIFFERENT TEMPERATURES; SP. #16A, B

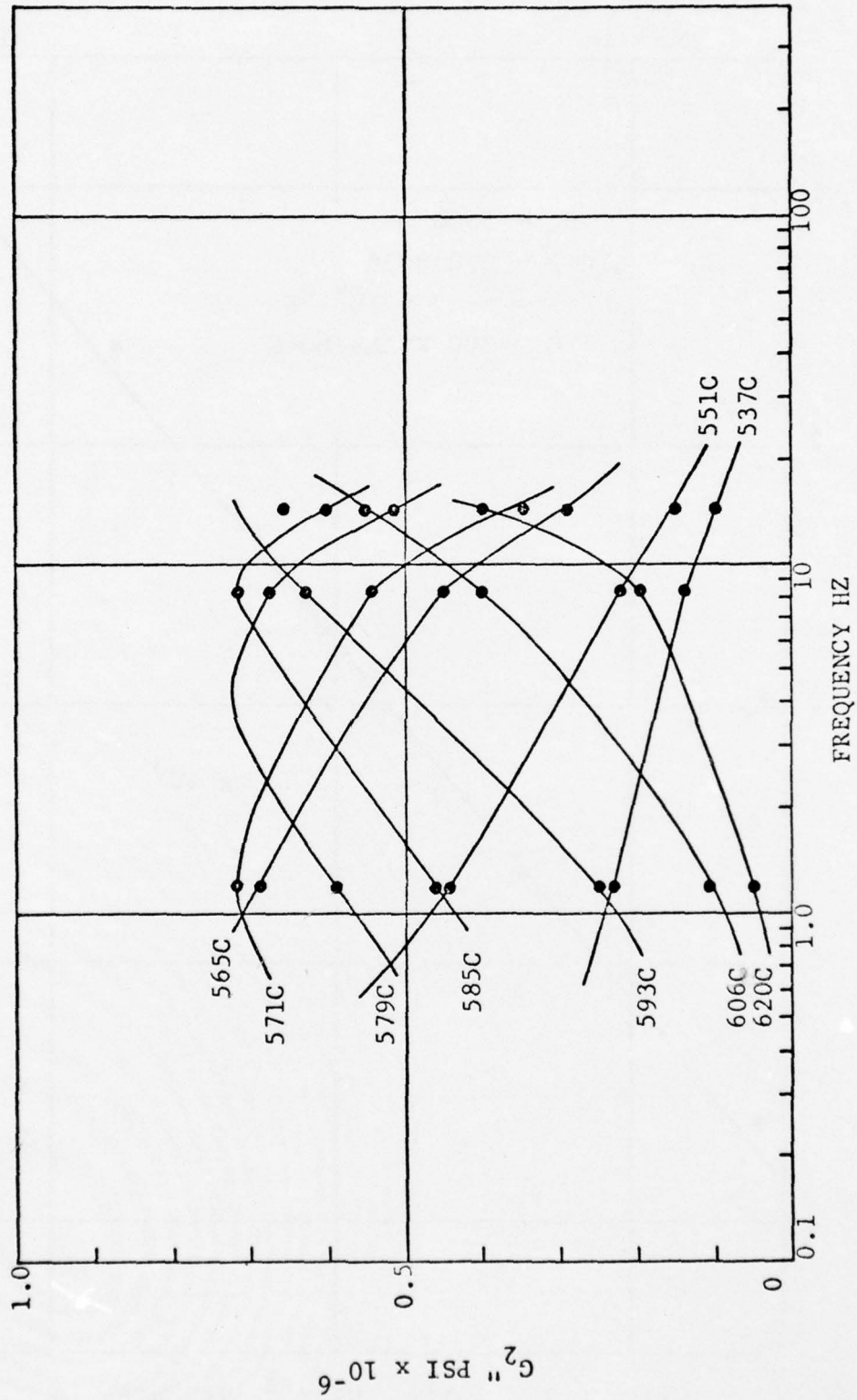


FIG. 4.23. G_2 VS FREQUENCY FOR DIFFERENT TEMPERATURES; SP. #2, TP.

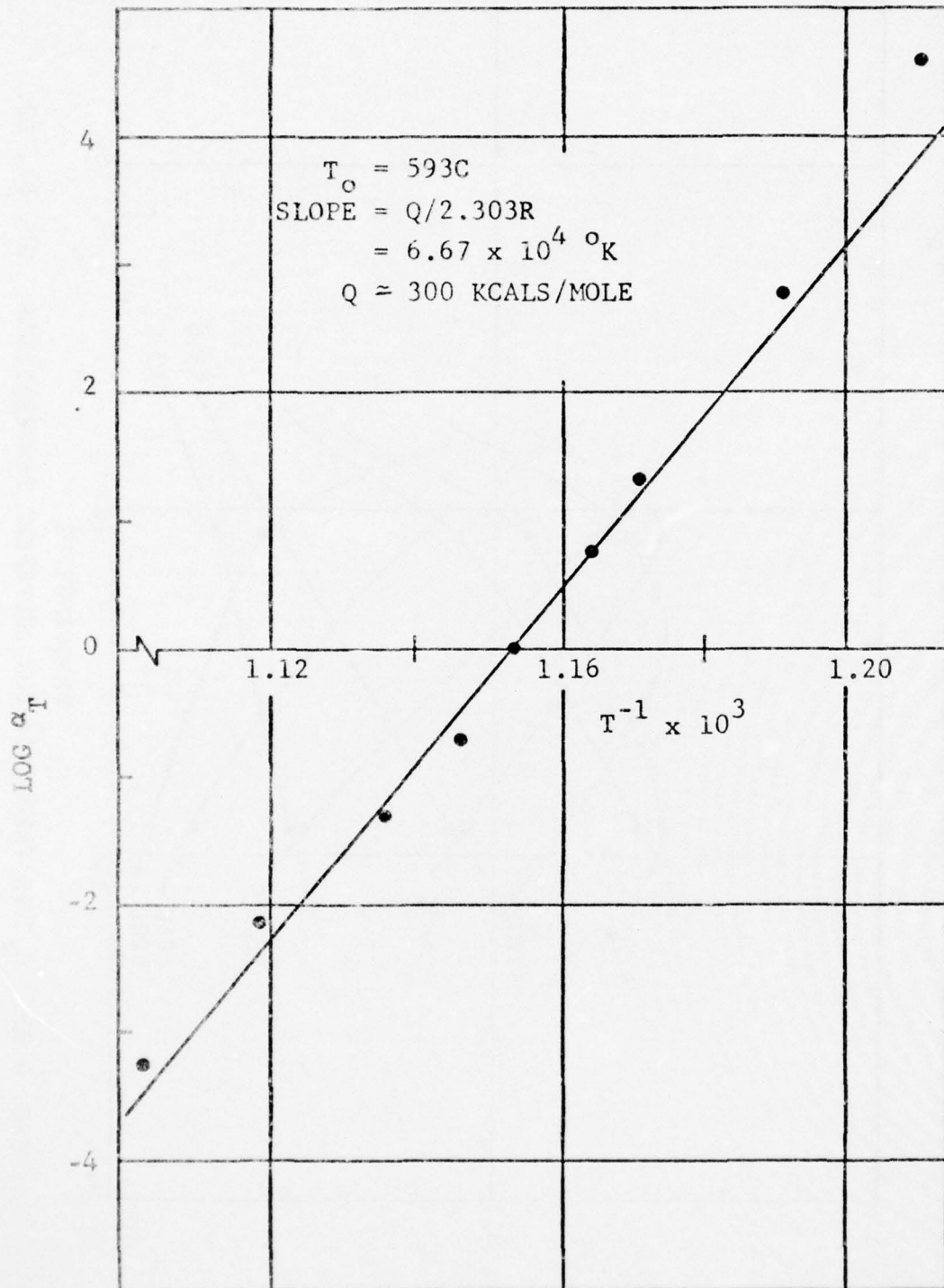


FIG. 4.24. $\text{LOG } \alpha_T$ VS T^{-1} ; SP. #16A, B.

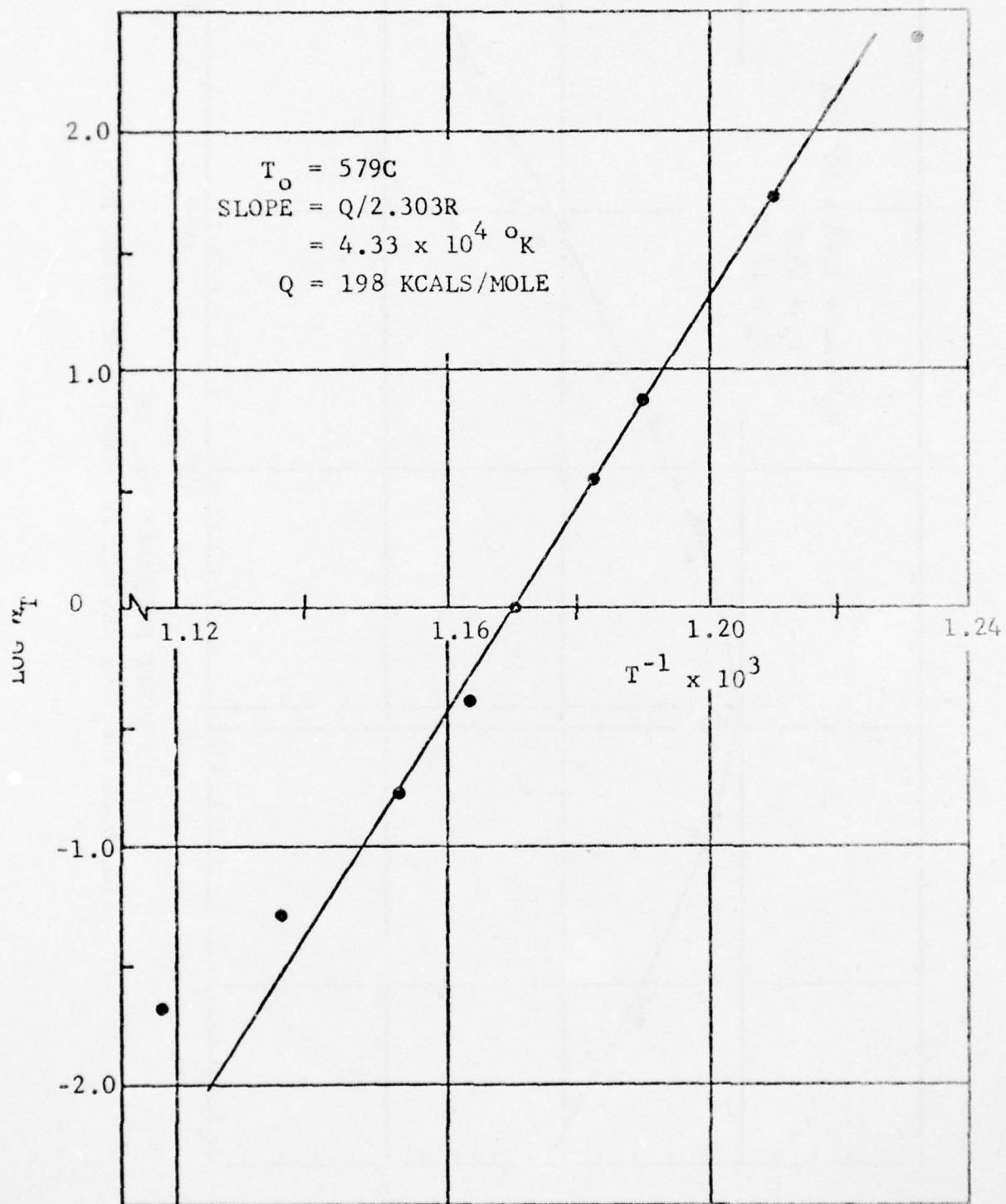


FIG. 4.25. $\text{LOG } \alpha_T$ VS T^{-1} ; SP. #2, T.P.

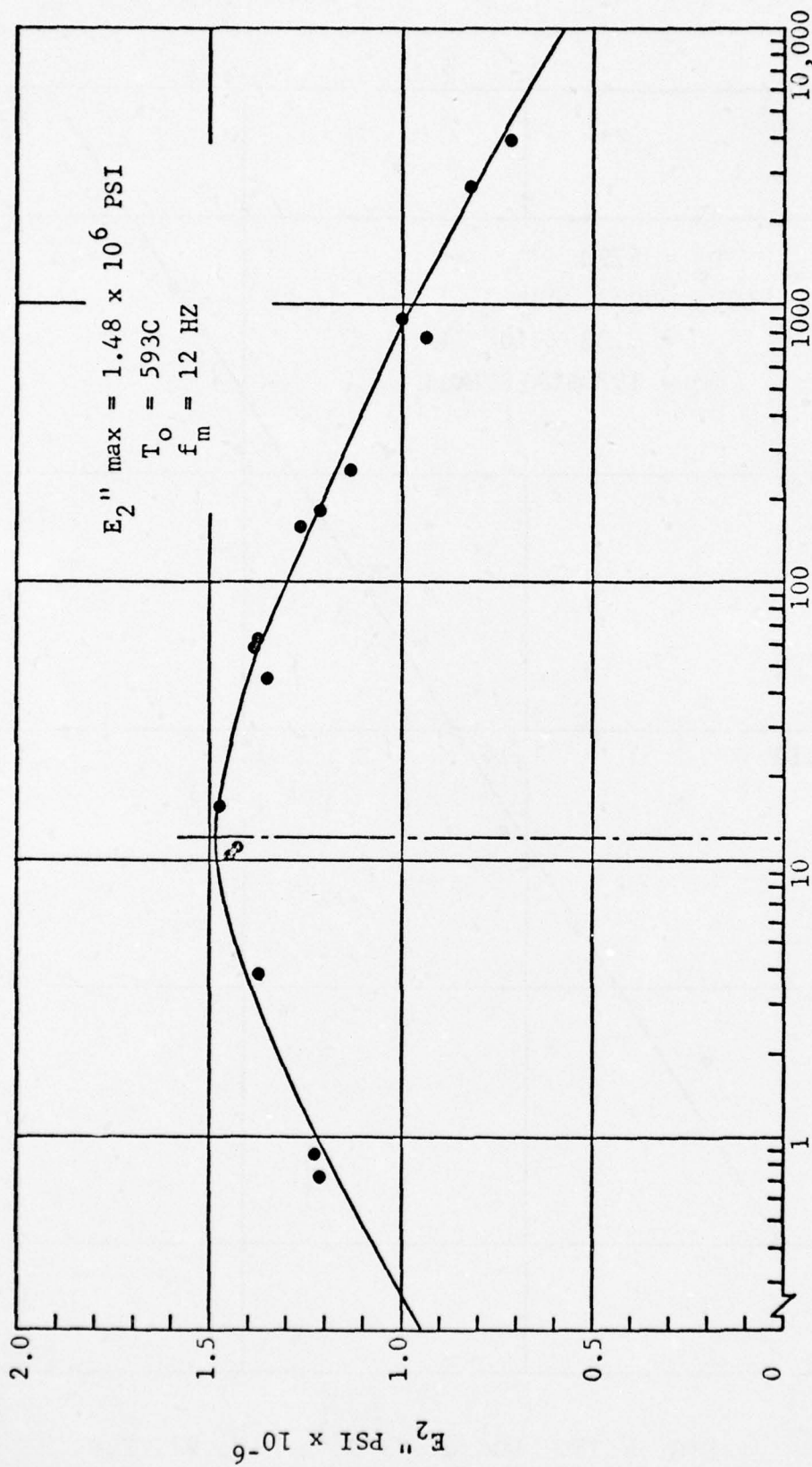


FIG. 4.26. E_2'' VS REDUCED FREQUENCY; SP. #16A, B.

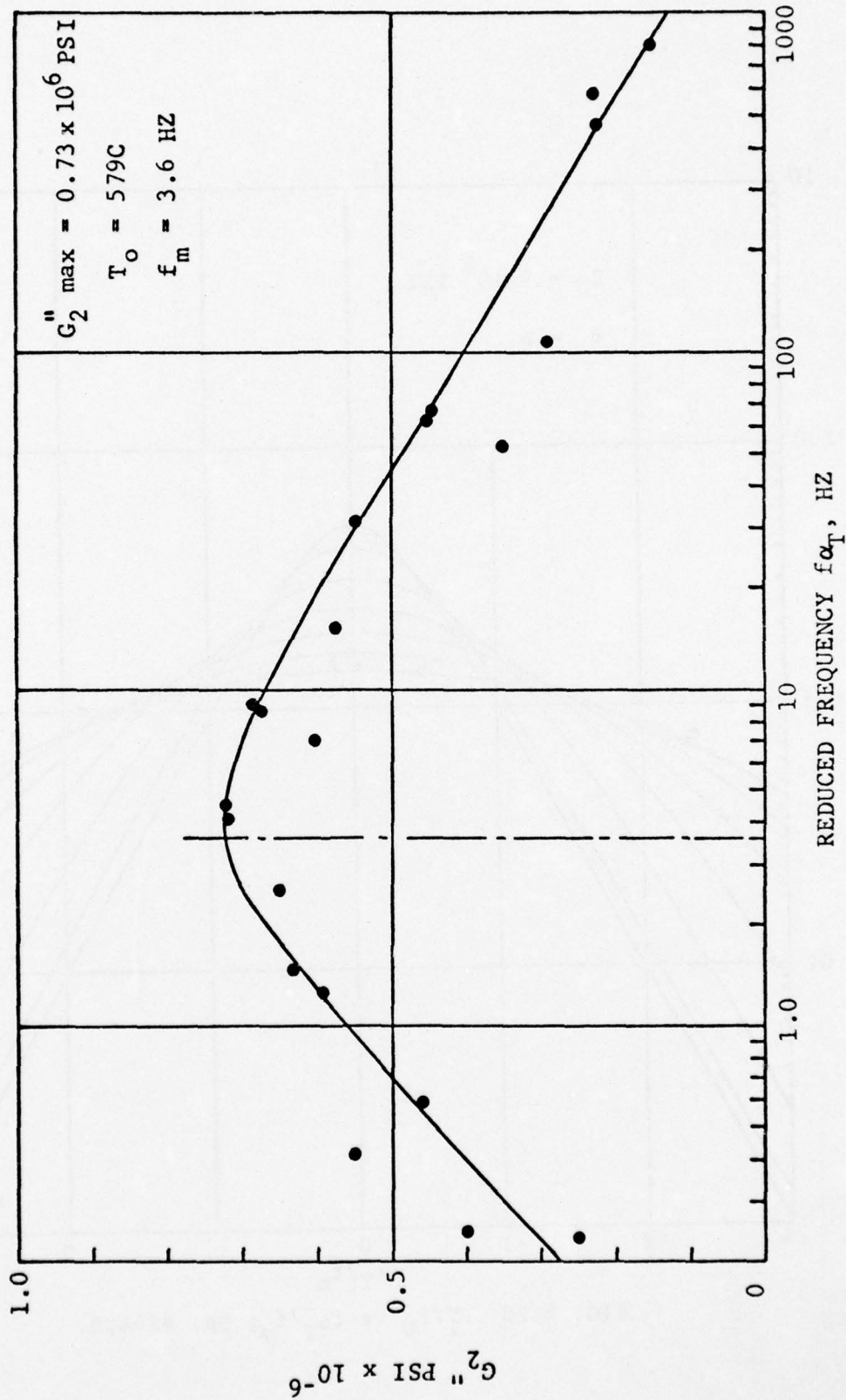


FIG. 4.27. G_2'' VS REDUCED FREQUENCY; SP. #2, TP

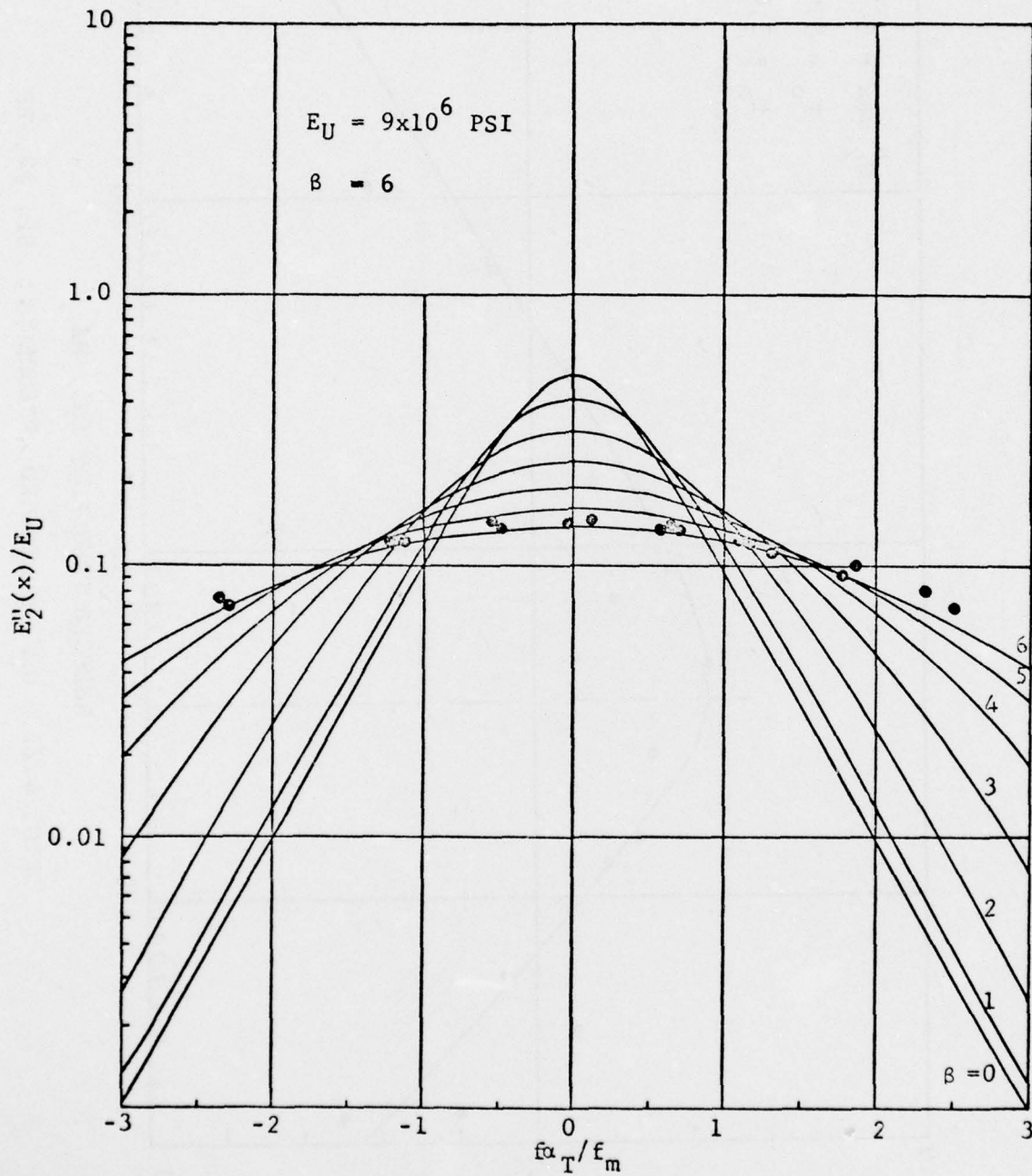


FIG. 4.28. E'_2/E_U vs f_{α_T}/f_m ; Sp. #16A,B.

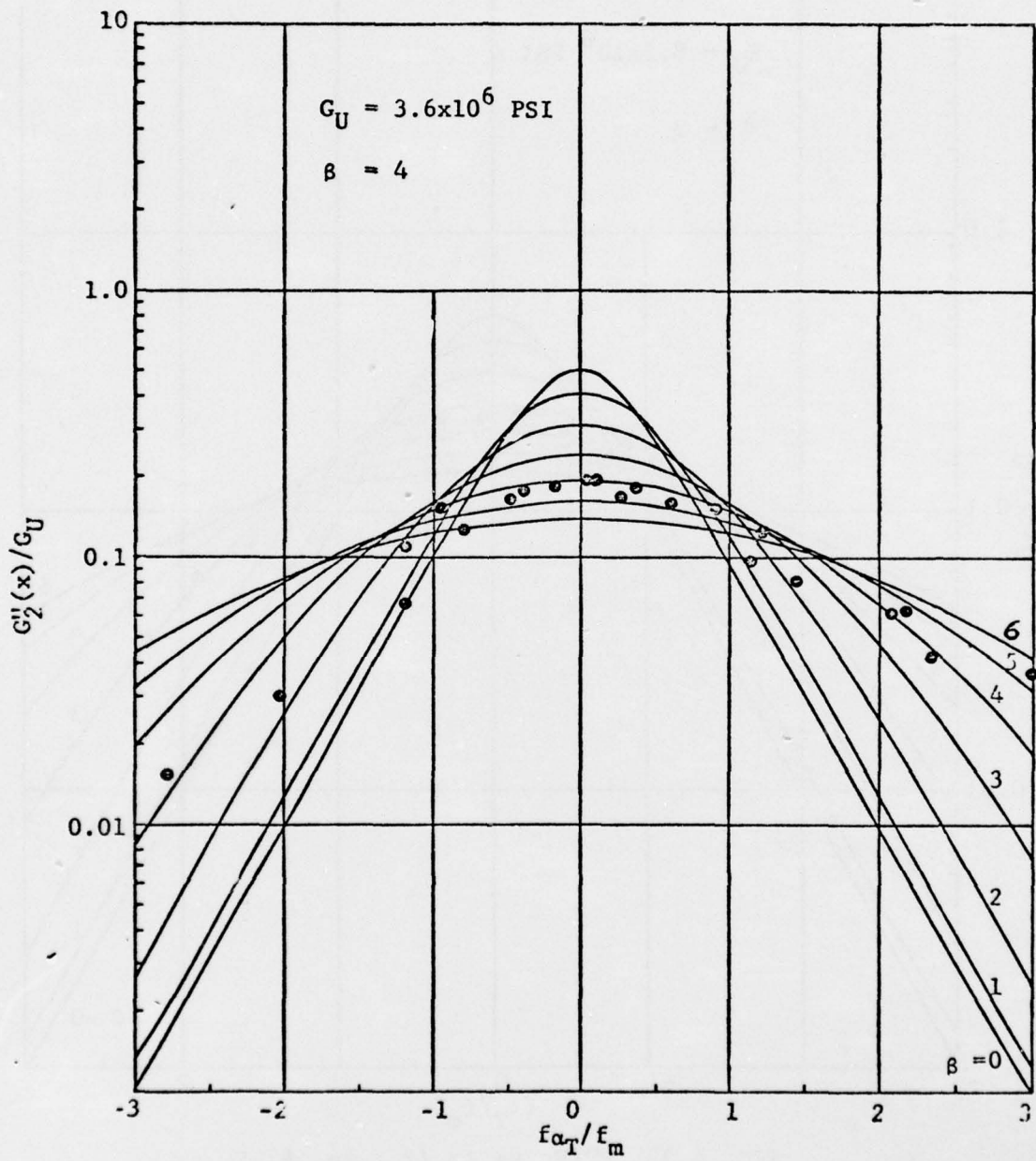


FIG. 4.29 G''/G_U vs f_{α_T}/f_m ; Sp. 42, TP

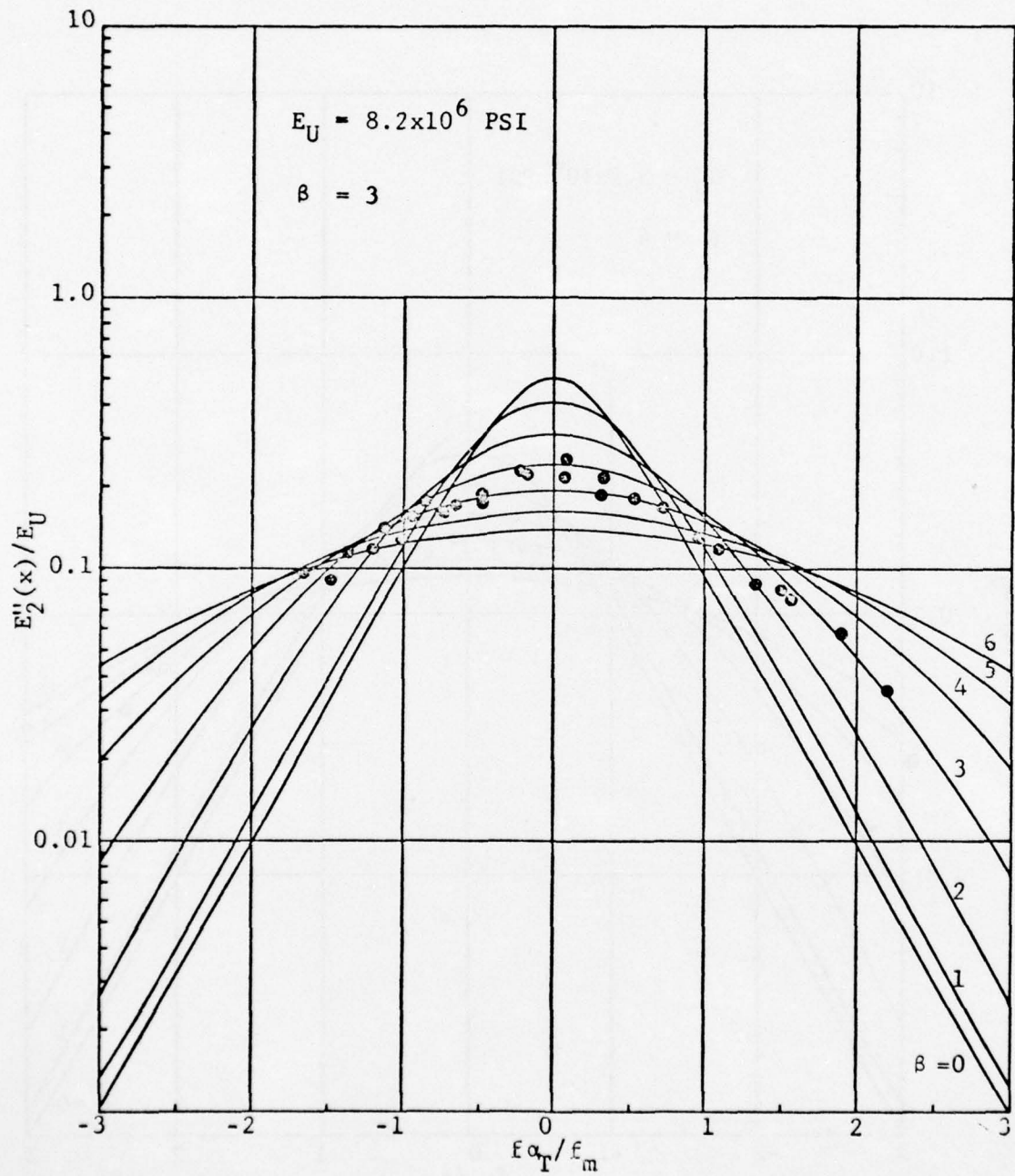


FIG. 4.30. E''_2/E_U vs $f\alpha_T/\epsilon_m$; Sp. #7, B.

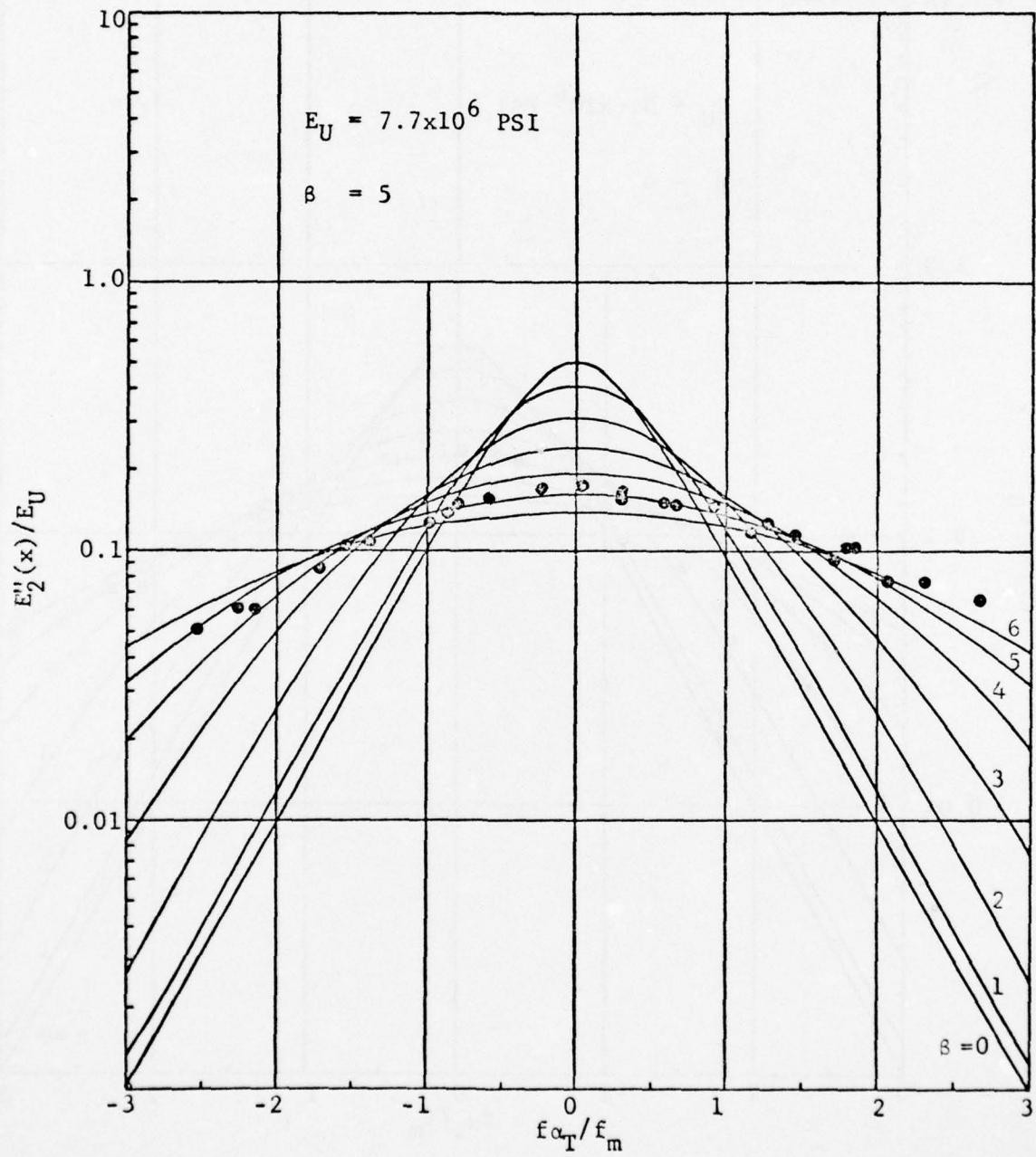


FIG. 4.31. E''_2/E_U vs f_{α_T}/f_m ; Sp. #15A, B.

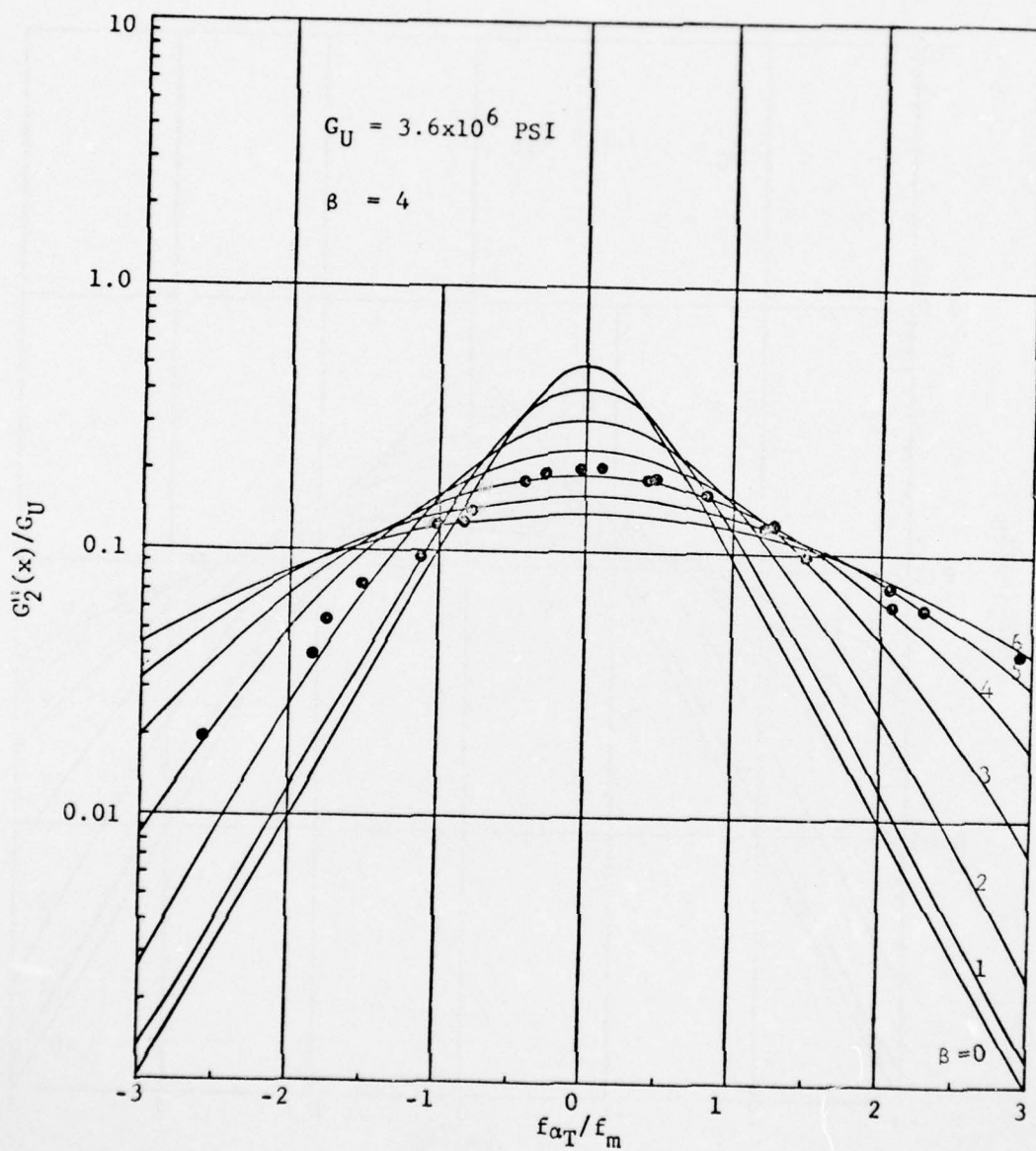


FIG. 4.32. G_2''/G_U vs $f\alpha_T/\bar{\epsilon}_m$; Sp. #1, TP.

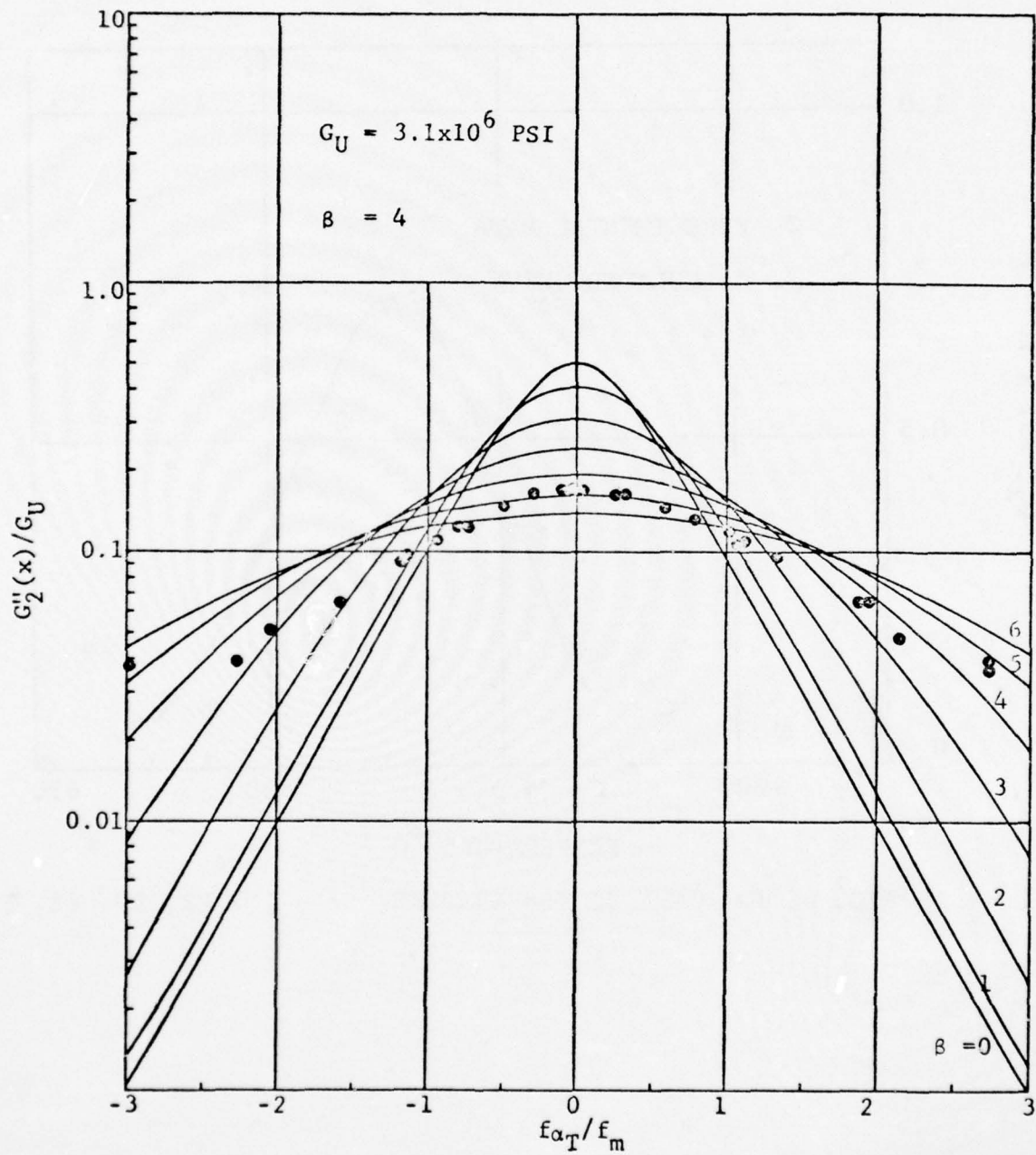


FIG. 4.33. G_2''/G_U vs f_{α_T}/f_m ; Sp. #3, TP.

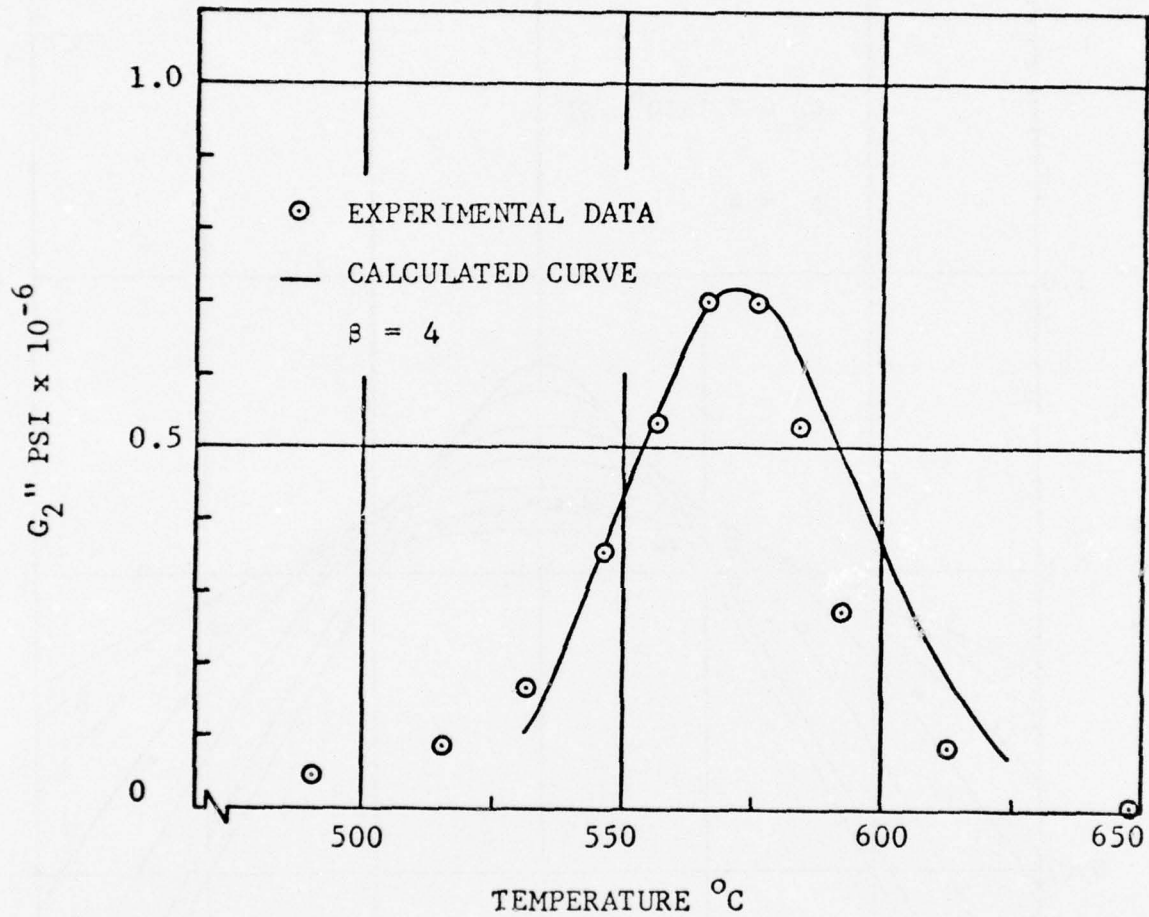


FIG. 4.34a, G_2'' VS TEMPERATURE; $f = 1.2$ HZ, SP. #2, TP

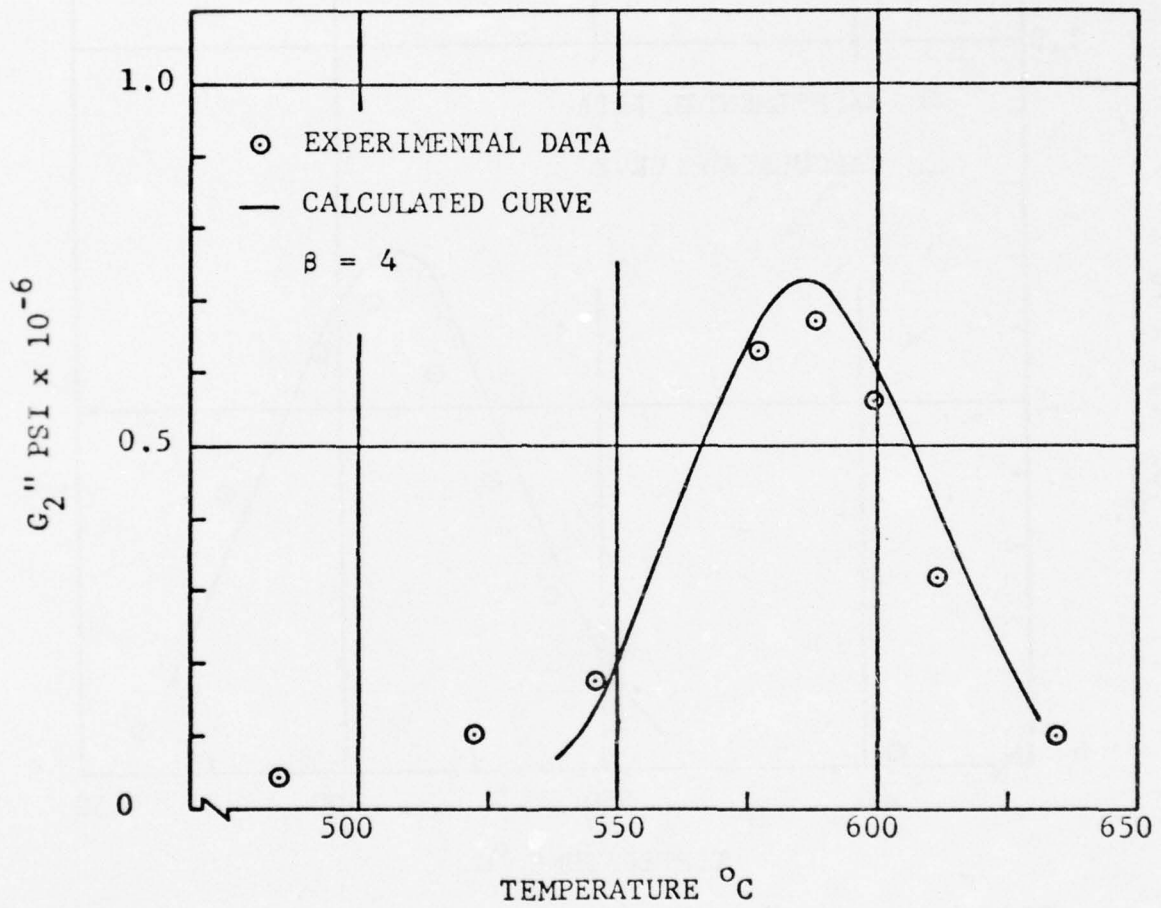


FIG. 4.34b. G_2'' VS TEMPERATURE; $f = 8.4$ HZ, SP. #2, TP

AD-A031 774

MINNESOTA UNIV MINNEAPOLIS DEPT OF AERONAUTICS AND --ETC F/G 11/2
DAMPING IN PORCELAIN ENAMEL COATINGS.(U)
JUL 76 P I SRIDHARAN

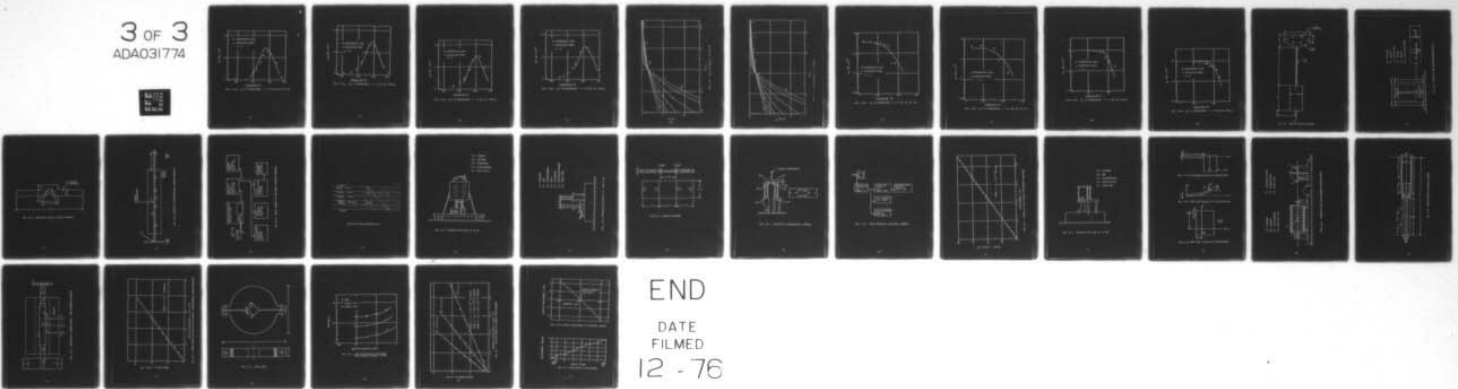
F33615-72-C-1315

UNCLASSIFIED

AFML-TR-74-191

NL

3 of 3
ADA031774



END
DATE
FILMED
12 - 76

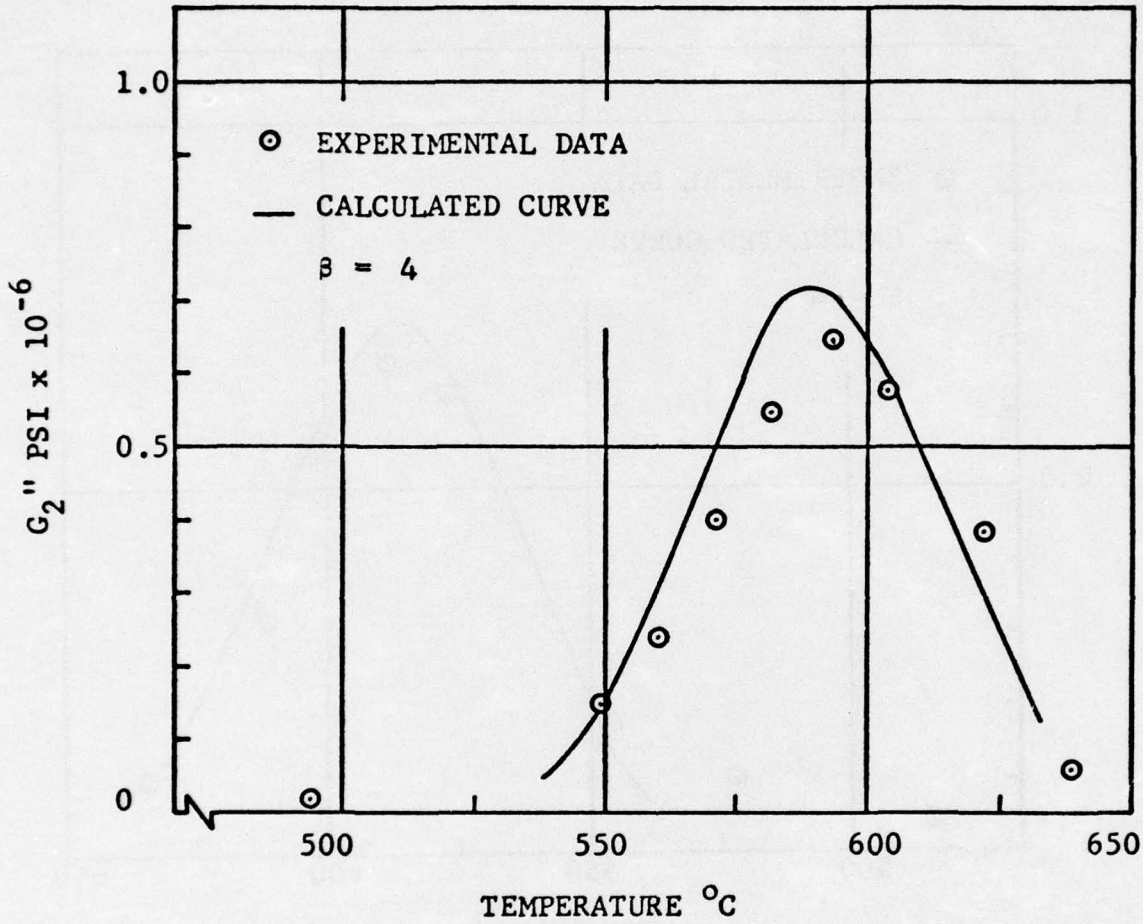


FIG. 4.34c. G_2'' VS TEMPERATURE; $f = 14.25$ HZ, SP. #2, TP

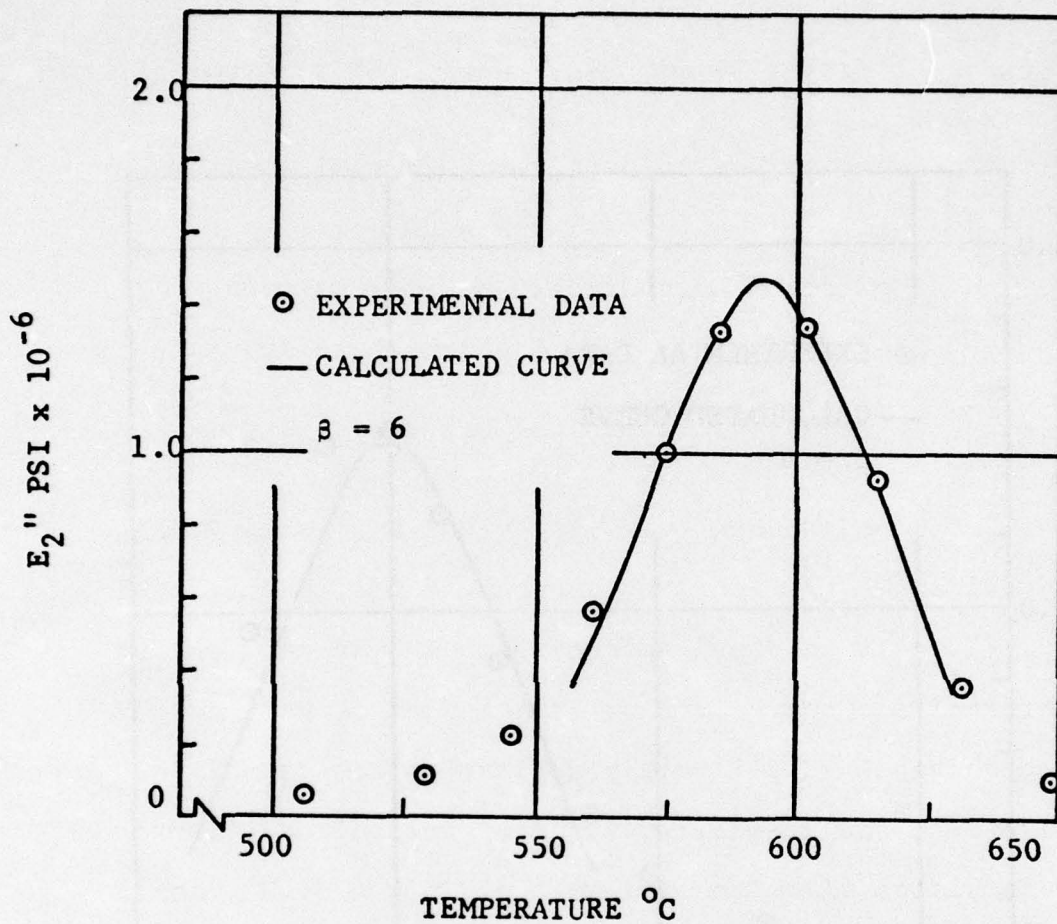


FIG. 4.35a. E_2'' vs TEMPERATURE; $f = 11$ HZ, SP. #16A,B.

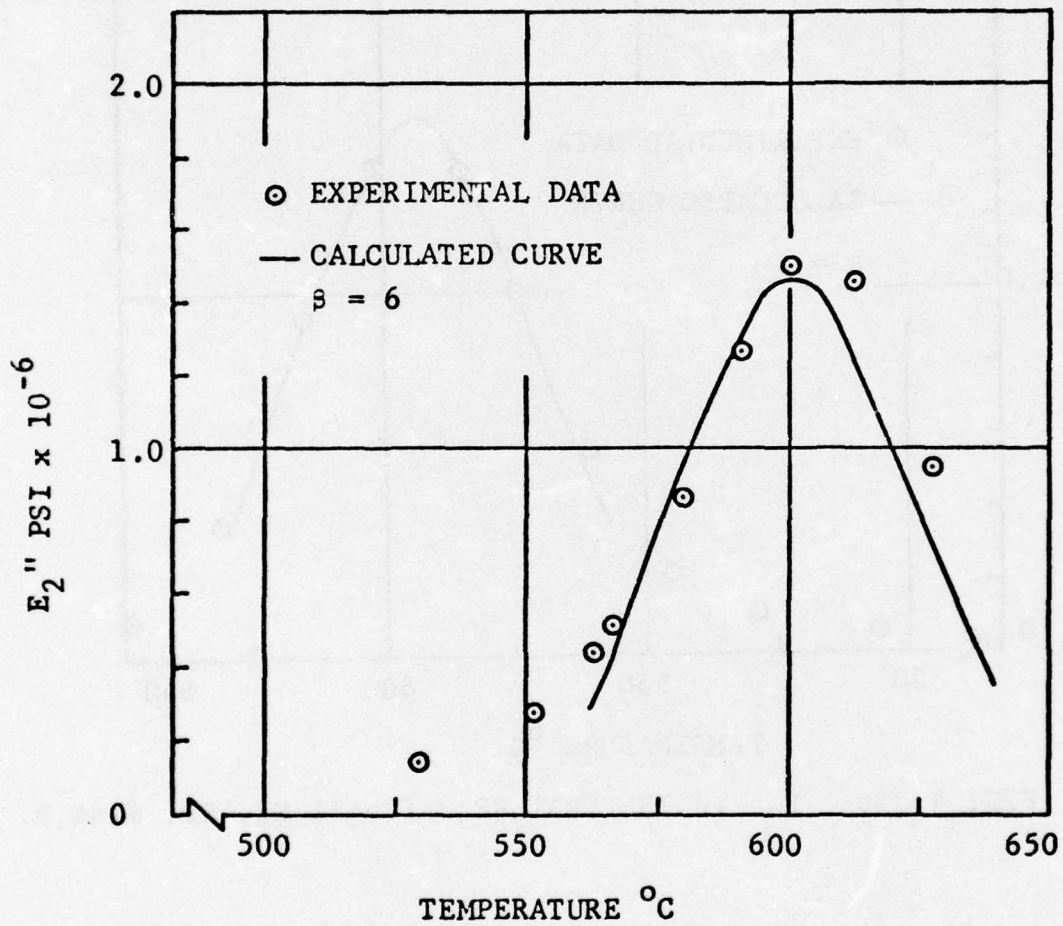


FIG. 4.35b. E_2'' VS TEMPERATURE; $f = 47$ HZ, SP. #16A,B.

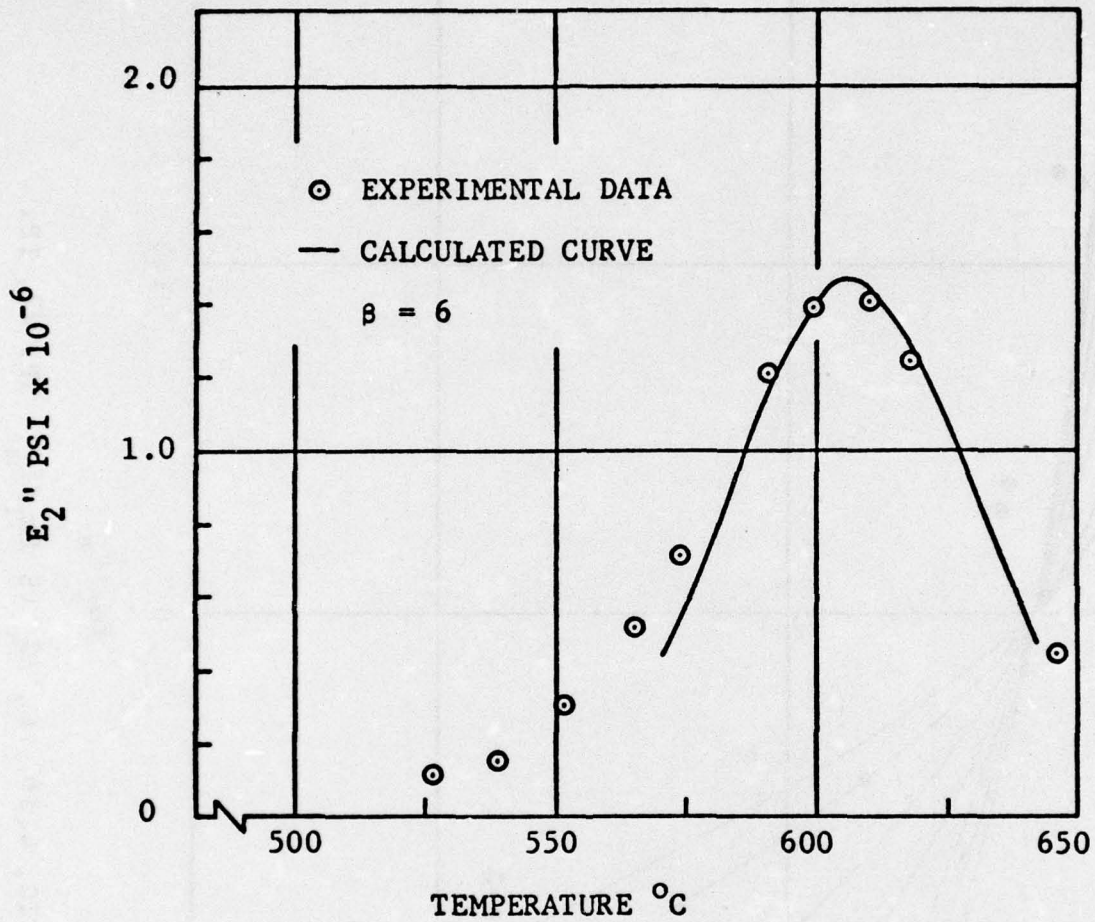


FIG. 4.35c. E_2'' VS TEMPERATURE; $f = 170$ HZ, SP. #16A,B.

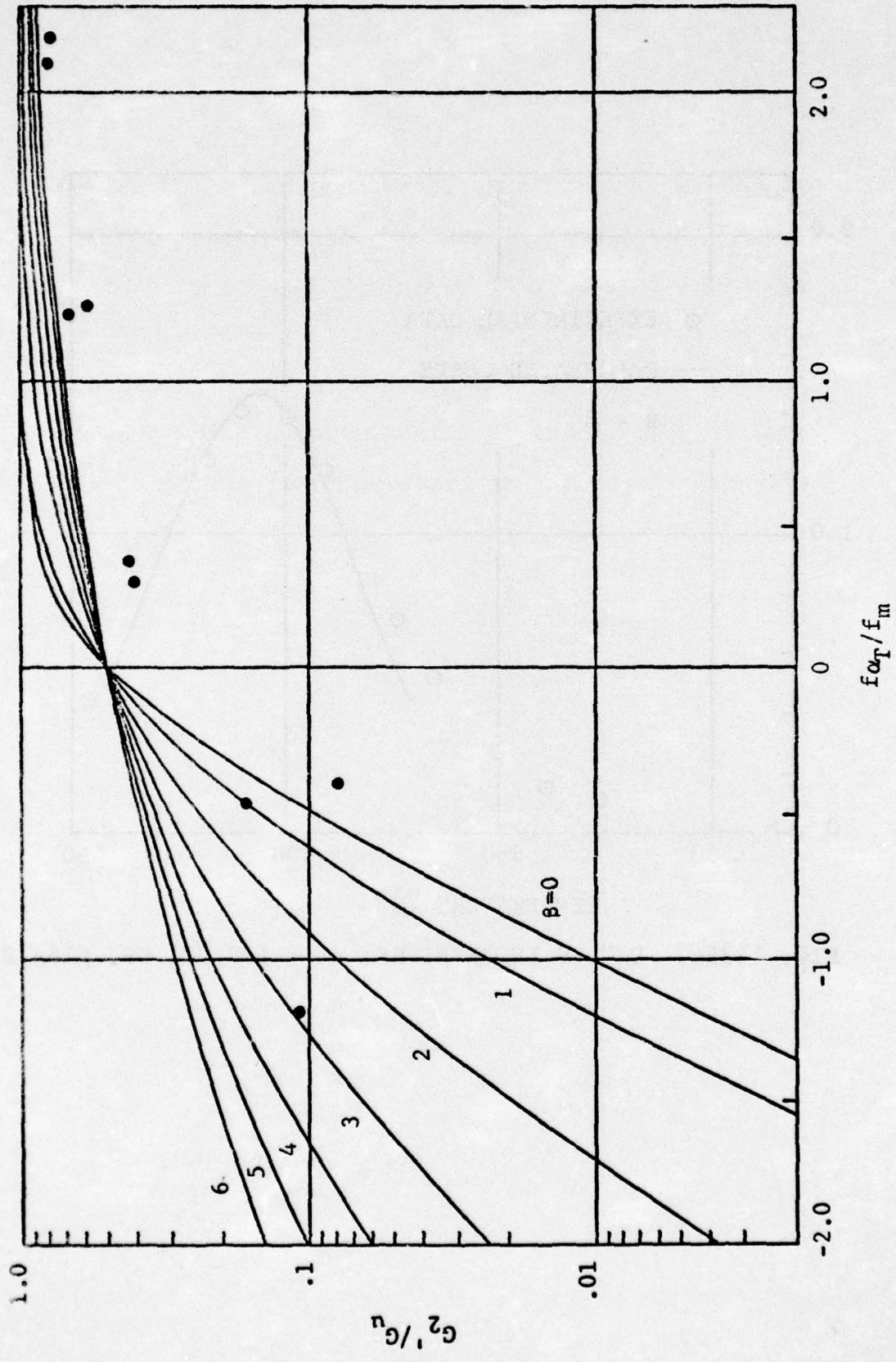


FIG. 4.36. G_2'/G_u VS $f\alpha_T/f_m$; SP. #2, TP.

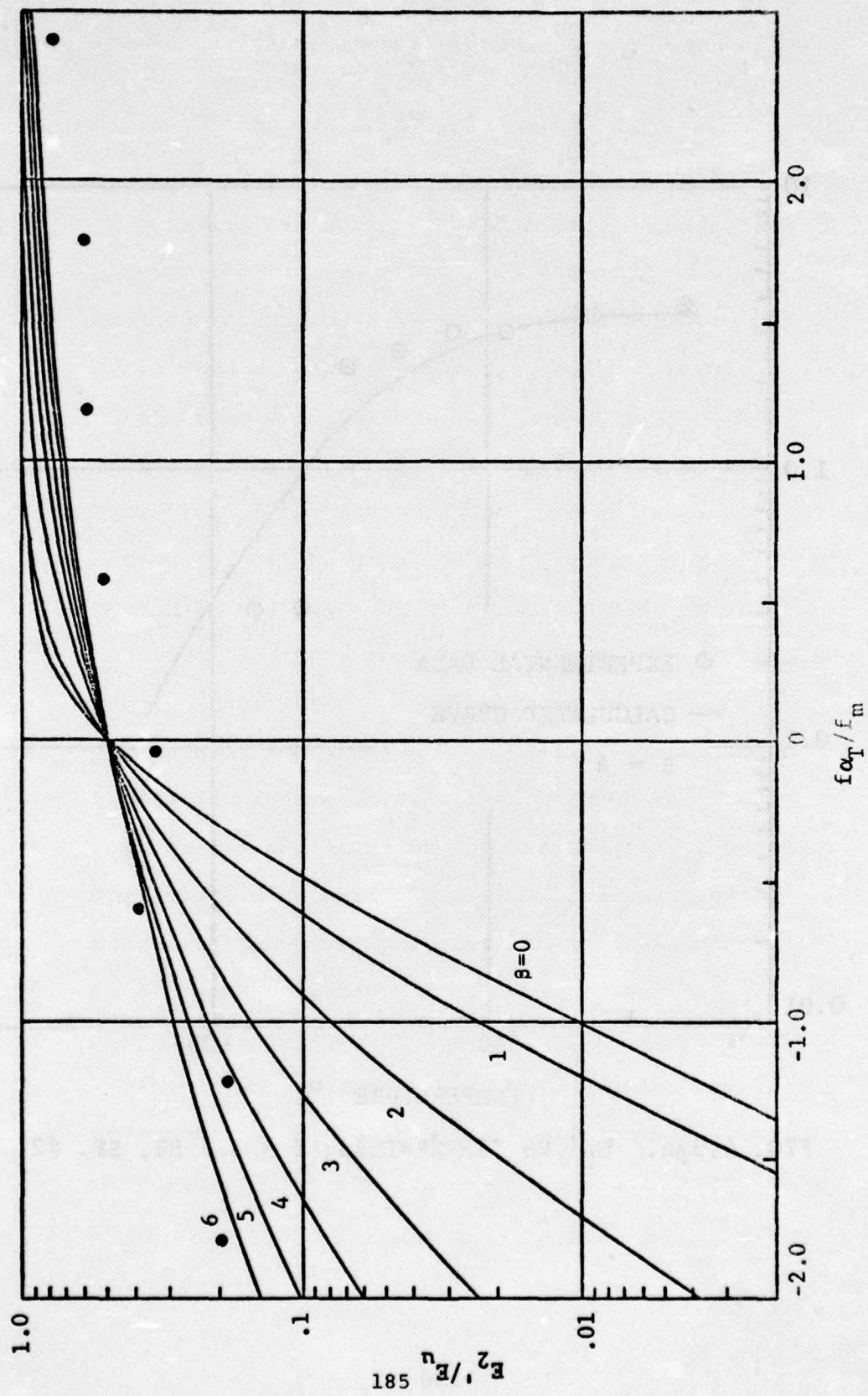


FIG. 4.37. E_2'/E_u VS $f\alpha_T/f_m$; SP. #16A,B.

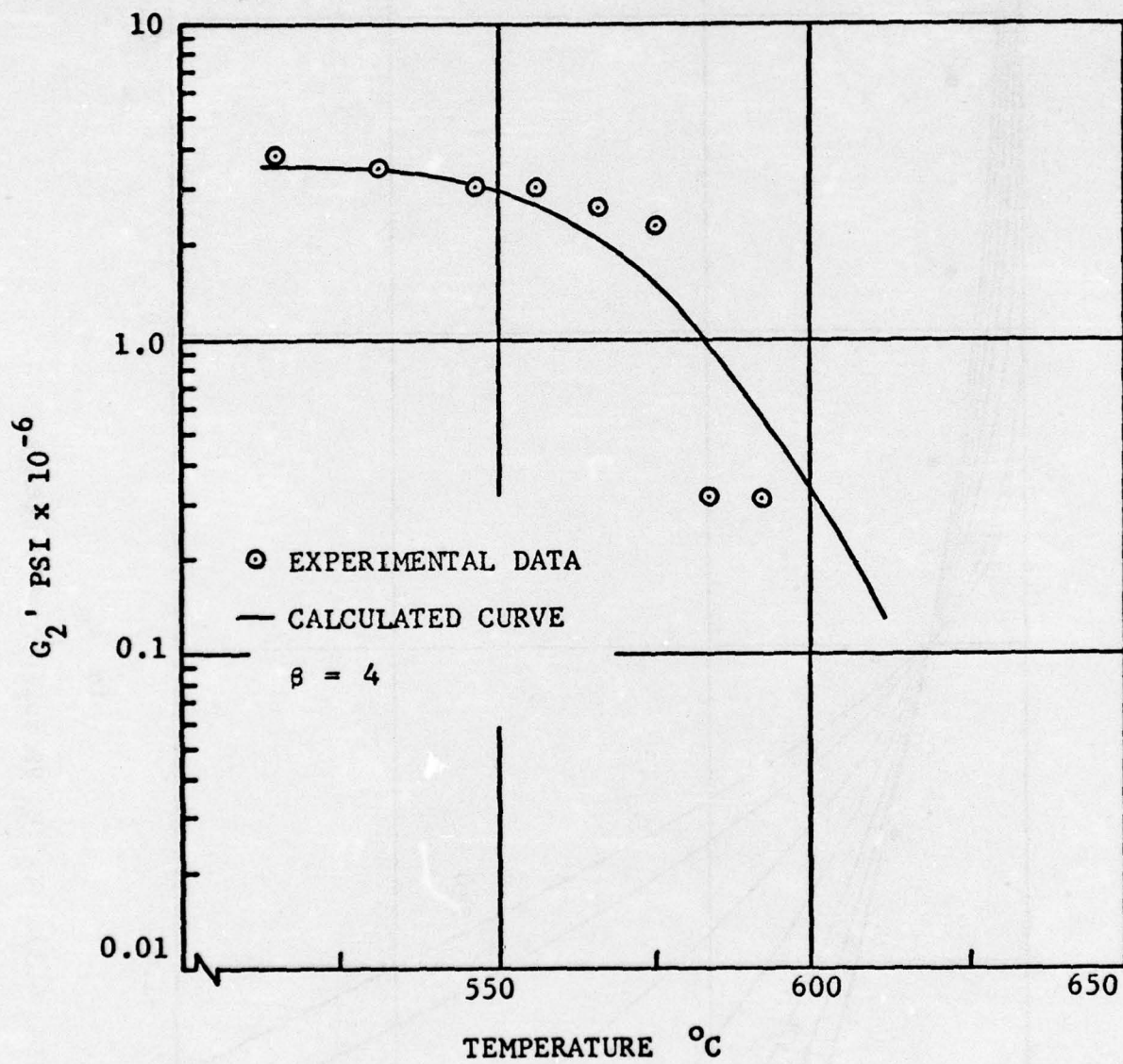


FIG. 4.38a. G_2' VS TEMPERATURE; $f = 1.2$ HZ, SP. #2, TP.

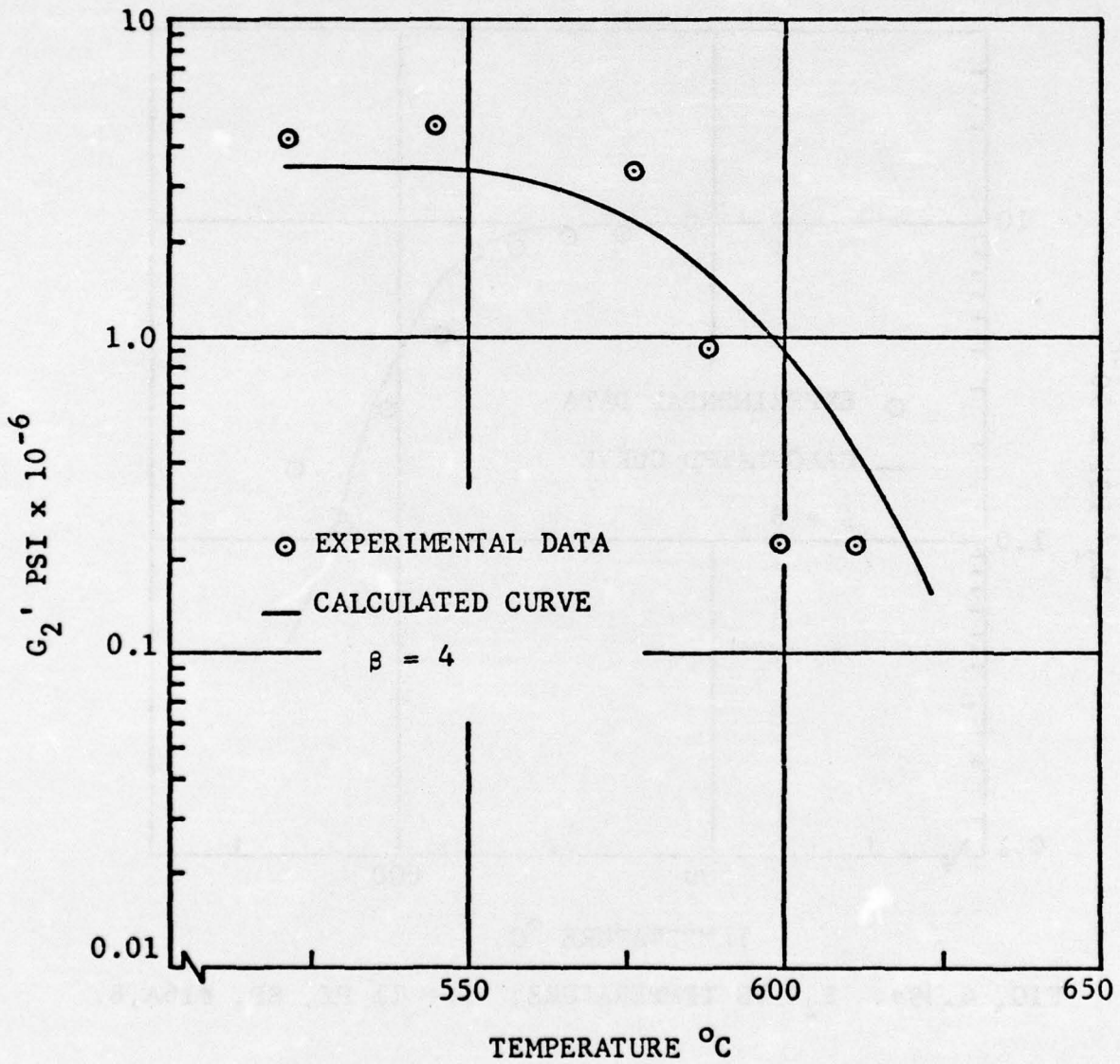


FIG. 4.38b. G_2' VS TEMPERATURE; $f = 8.4$ HZ, SP. #2, TP.

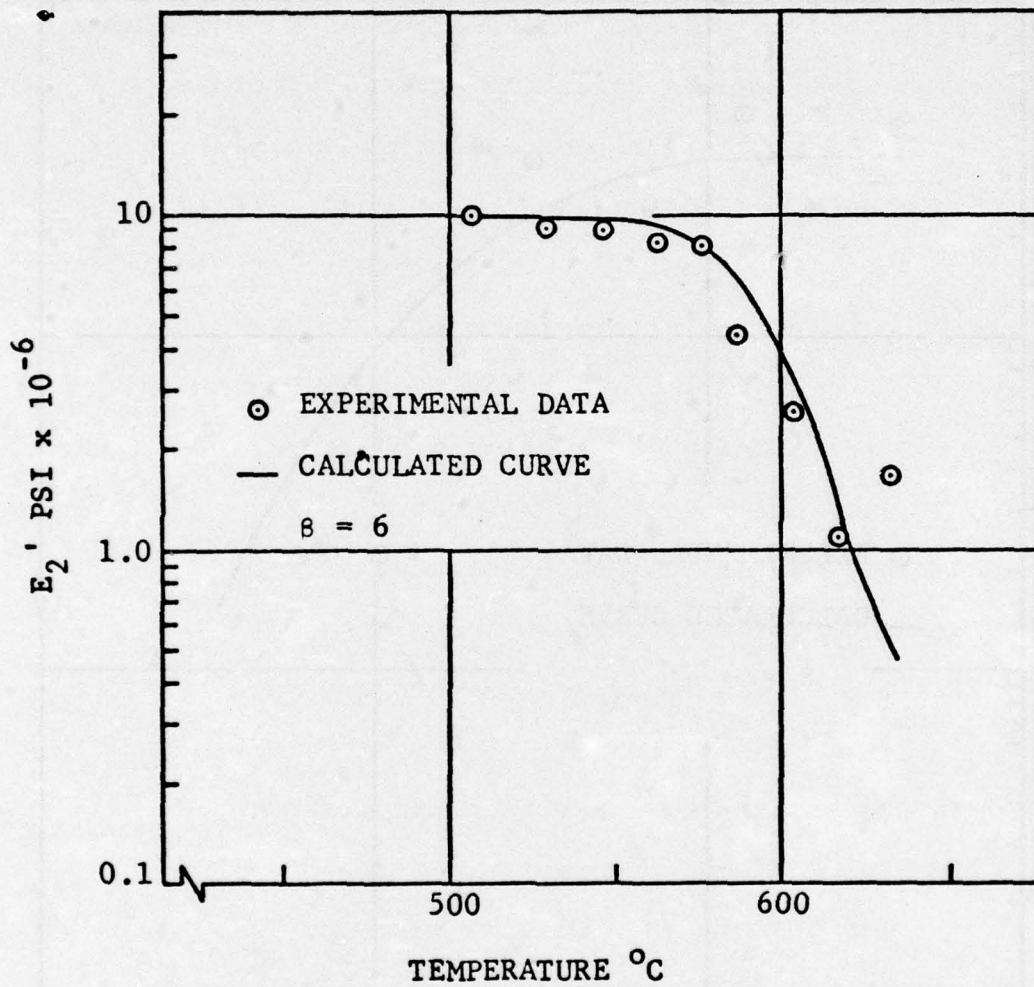


FIG. 4.39a. E_2' VS TEMPERATURE; $f = 11$ HZ, SP. #16A,B.

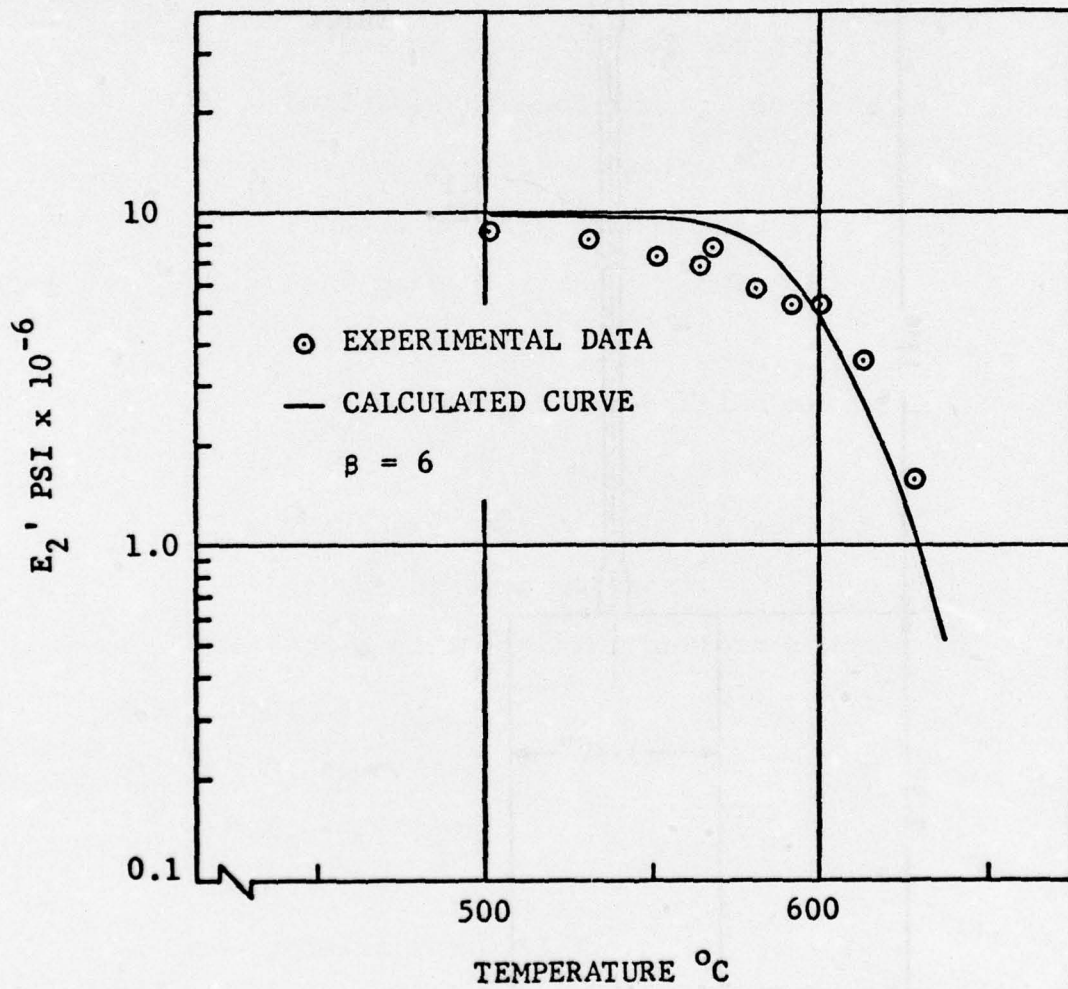


FIG. 4.39b. E_2' VS TEMPERATURE; $f = 47$ HZ, SP. #16A,B.

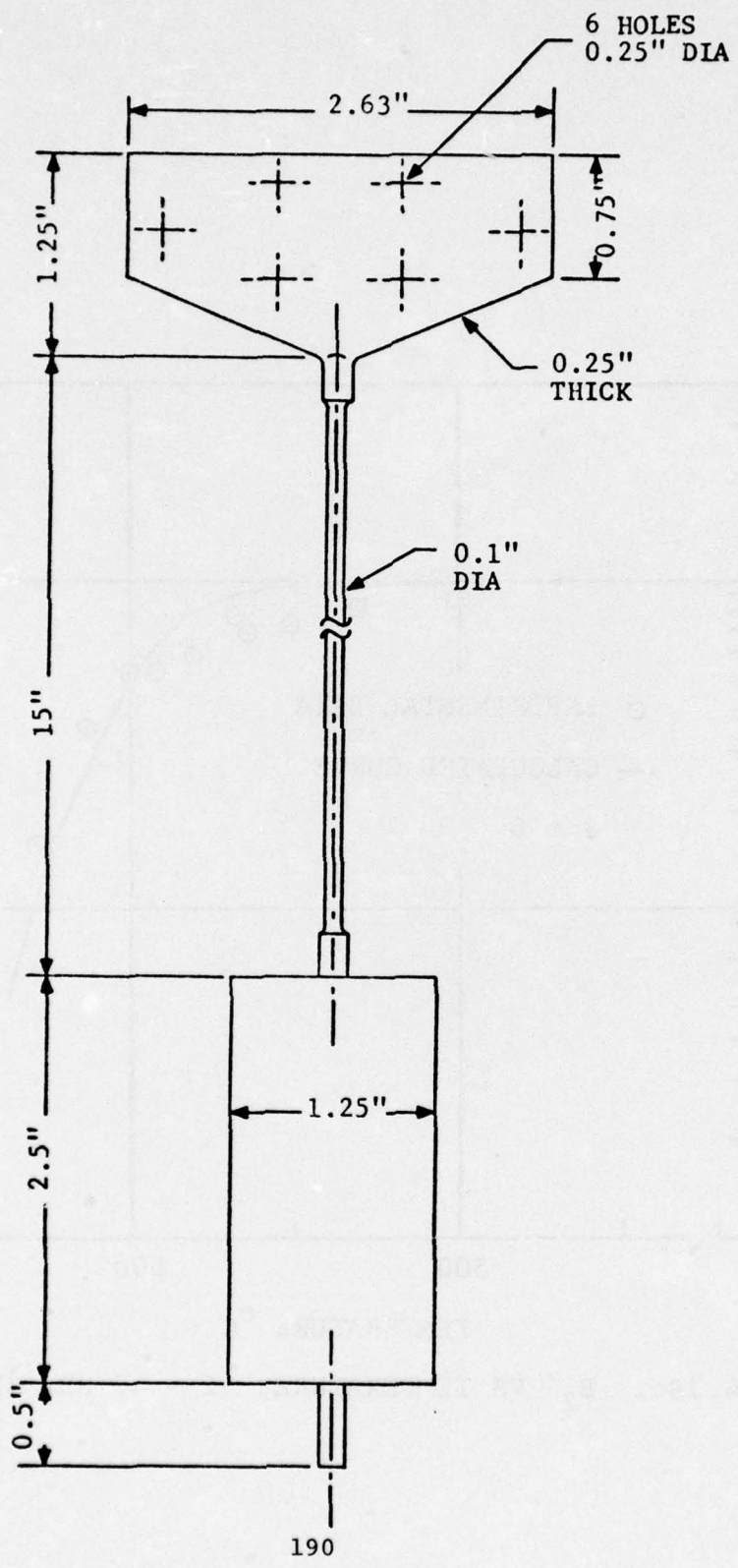


FIG. A3.1. TORSION PENDULUM SPECIMEN

- (1) SPECIMEN
- (2) FURNACE
- (3) DRIVING ARM
- (4) ADAPTER
- (5) BEARING
- (6) CAPACITANCE PLATE

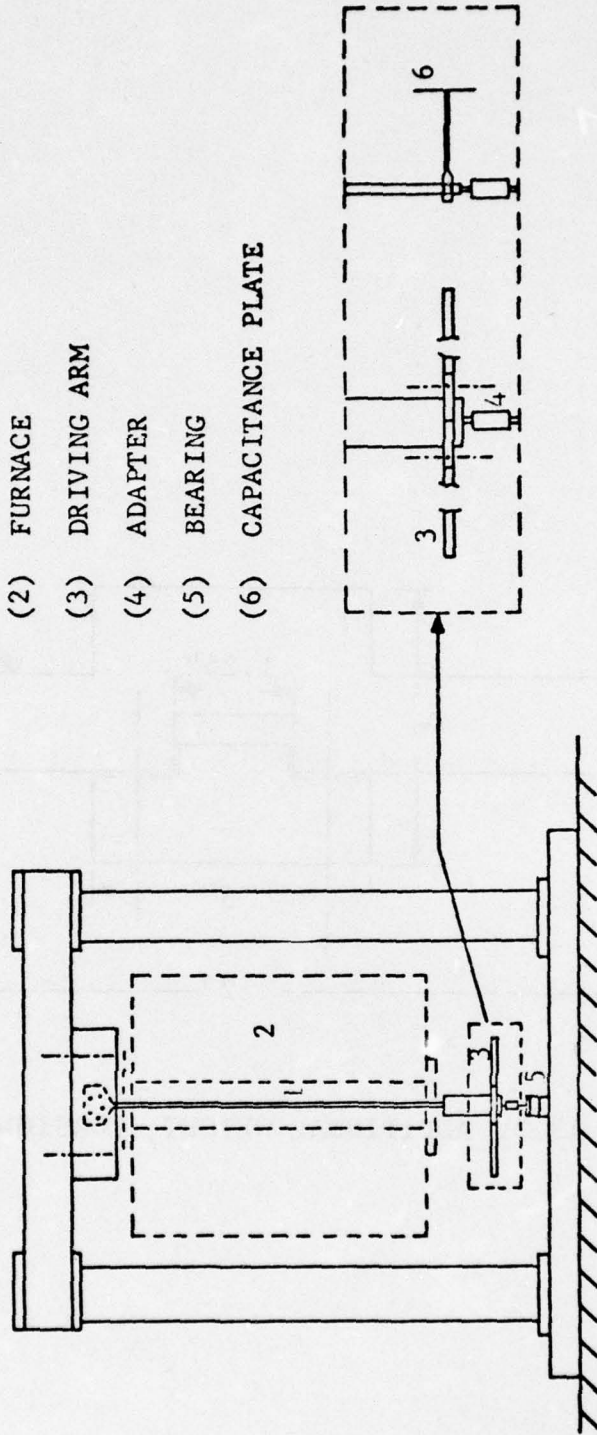


FIG. A3.2. APPARATUS FOR TORSION PENDULUM TESTS.

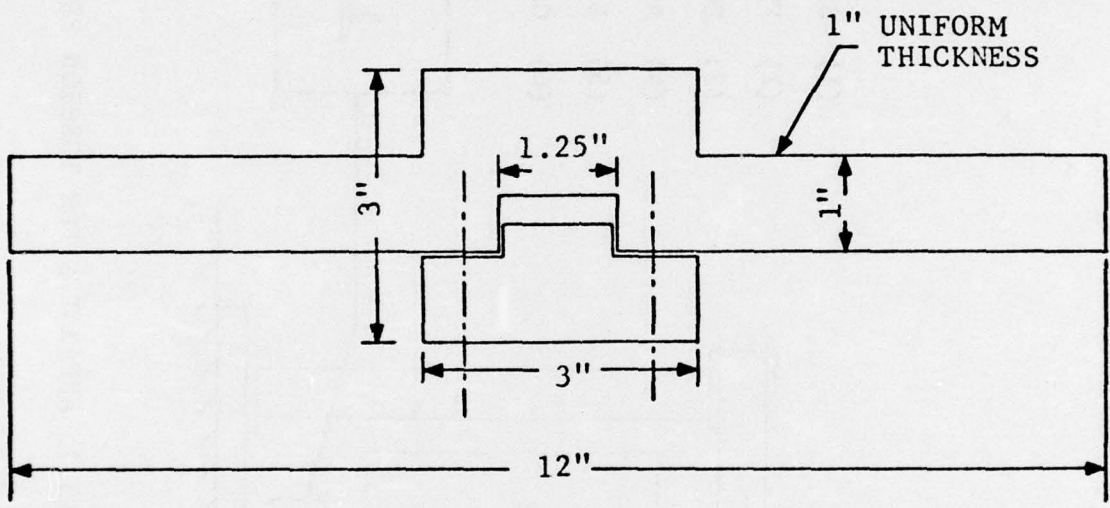


FIG. A3.3. ADDITIONAL WEIGHT; TORSION PENDULUM

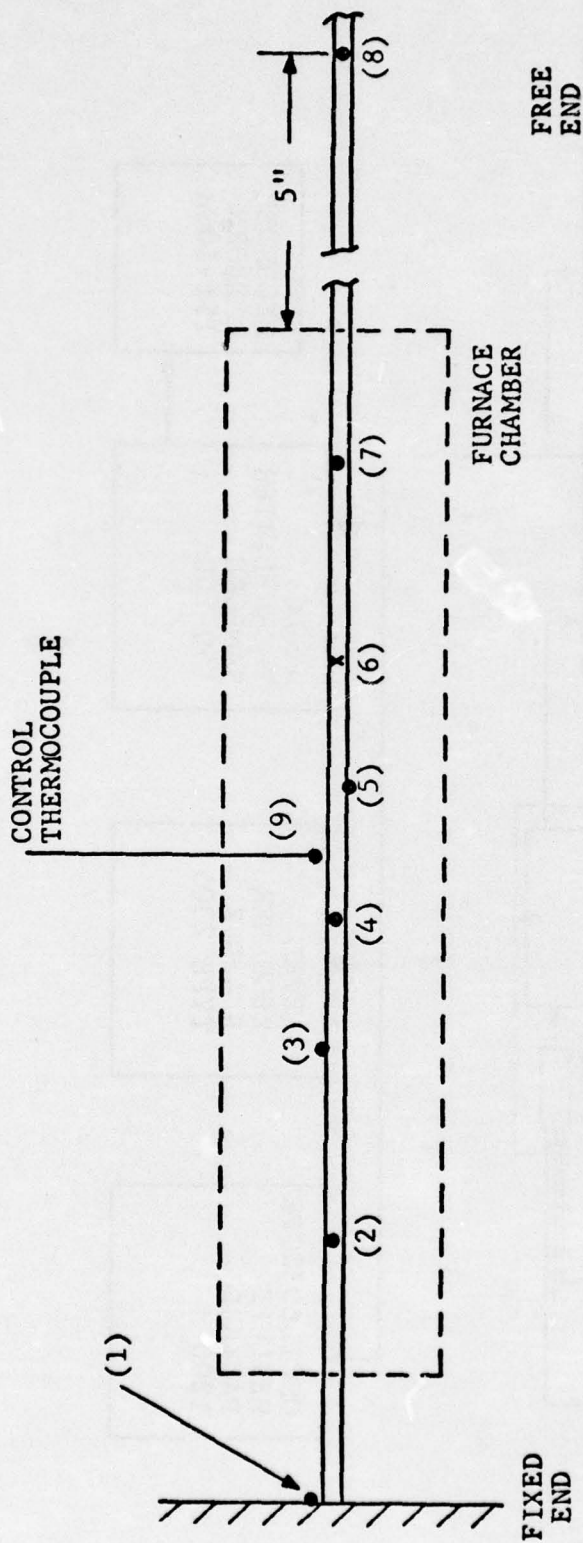


FIG. A3.4. POSITION OF THERMOCOUPLES; TORSION PENDULUM

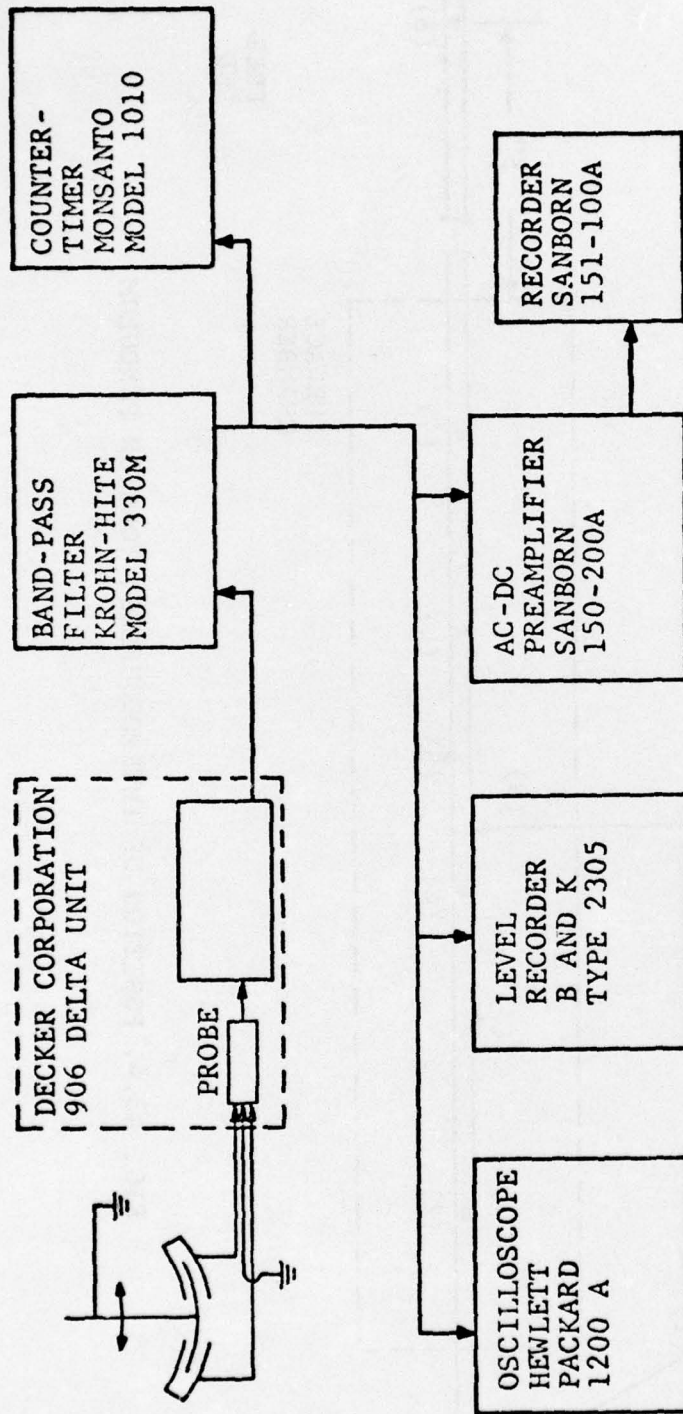


FIG. A3.5. BLOCK DIAGRAM OF EQUIPMENT; TORSION PENDULUM

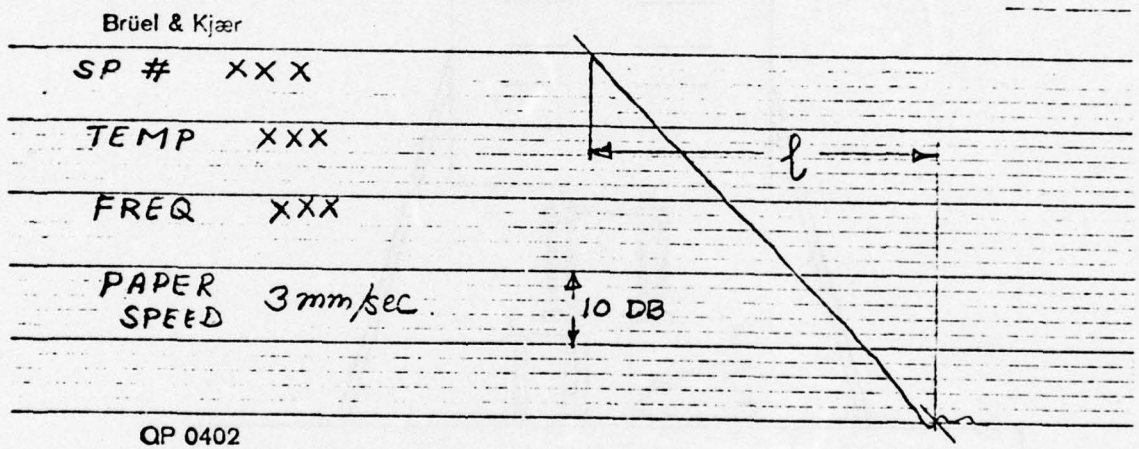


FIG. A3.6. LEVEL RECORDER PLOT

- (1) FURNACE
- (2) SPECIMEN
- (3) MICROMETER
- (4) ACCELEROMETER
- (5) STEEL PLATE

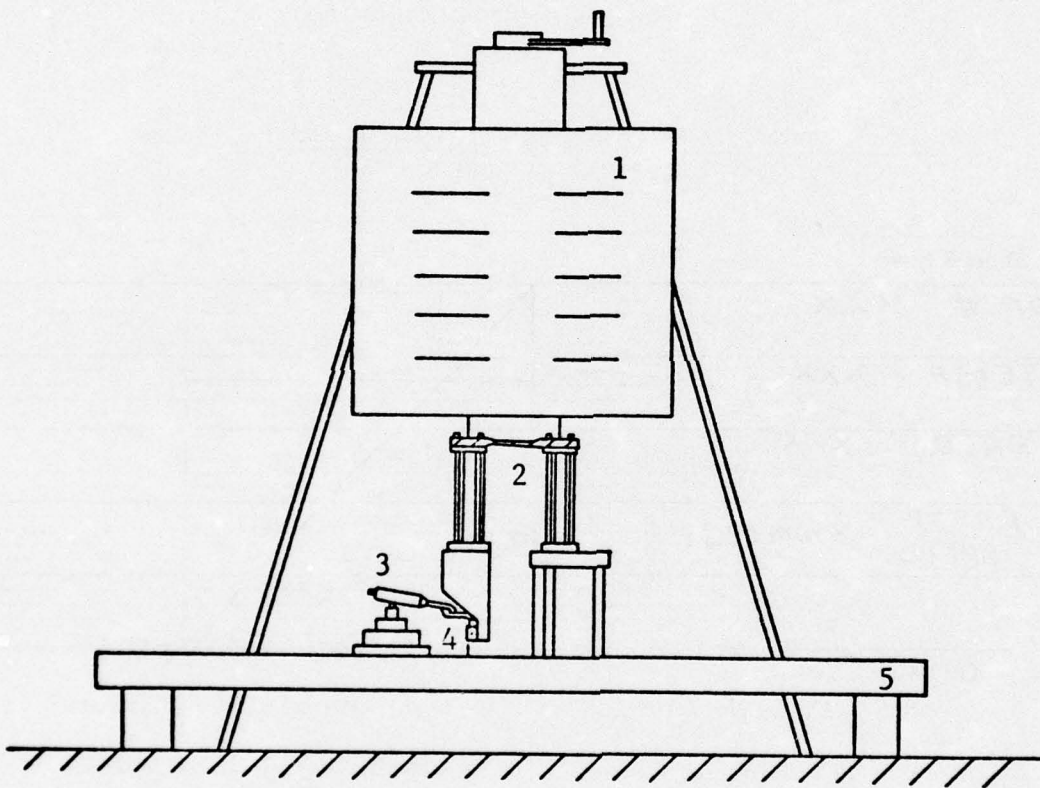


FIG. A4.1. APPARATUS FOR TESTS AT 32 HZ

- (1) SPECIMEN
- (2) ARM
- (3) ACCELEROMETER
- (4) HOOK
- (5) MICROMETER
- (6) ADDITIONAL WEIGHT
- (7) STEEL BASE

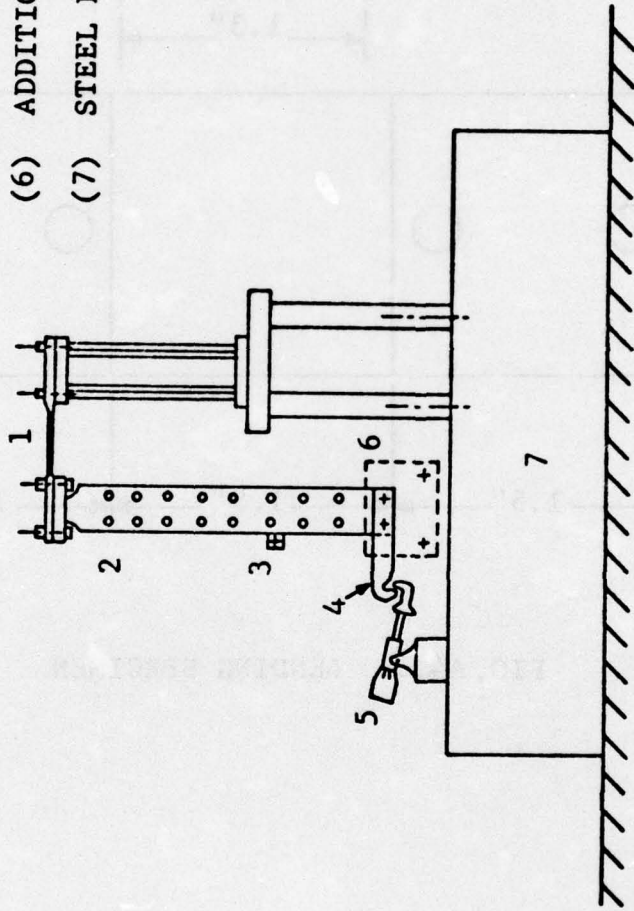


FIG. A4.2. APPARATUS FOR TESTS AT 47 AND 11 HZ.

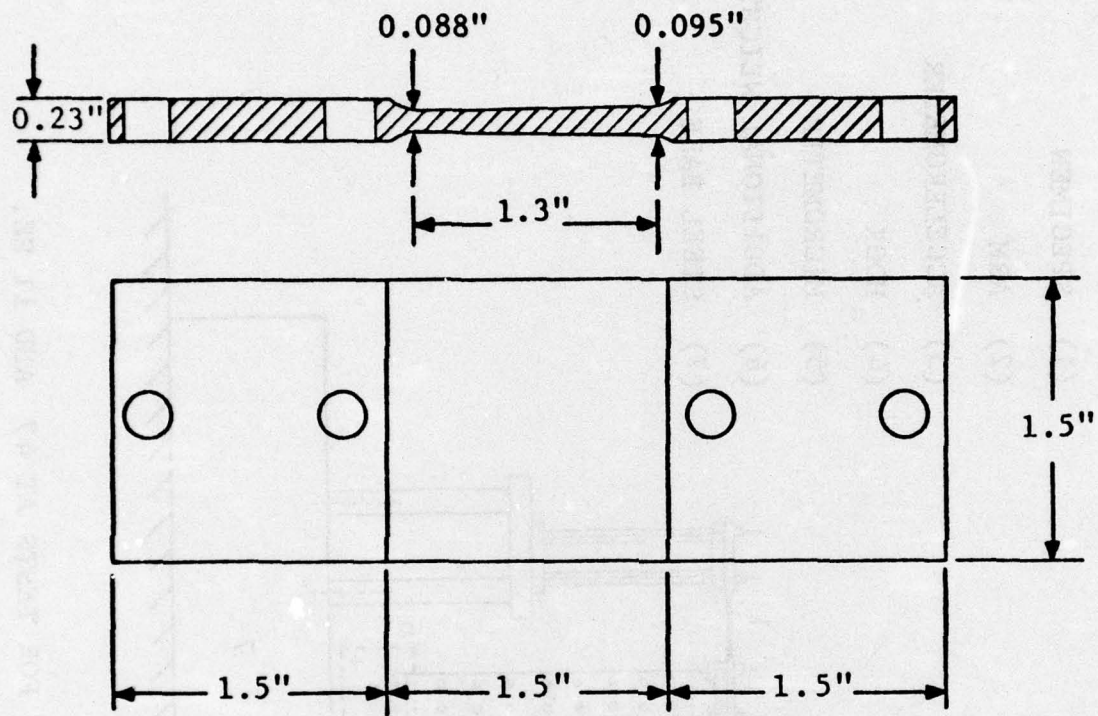


FIG. A4.3. BENDING SPECIMEN

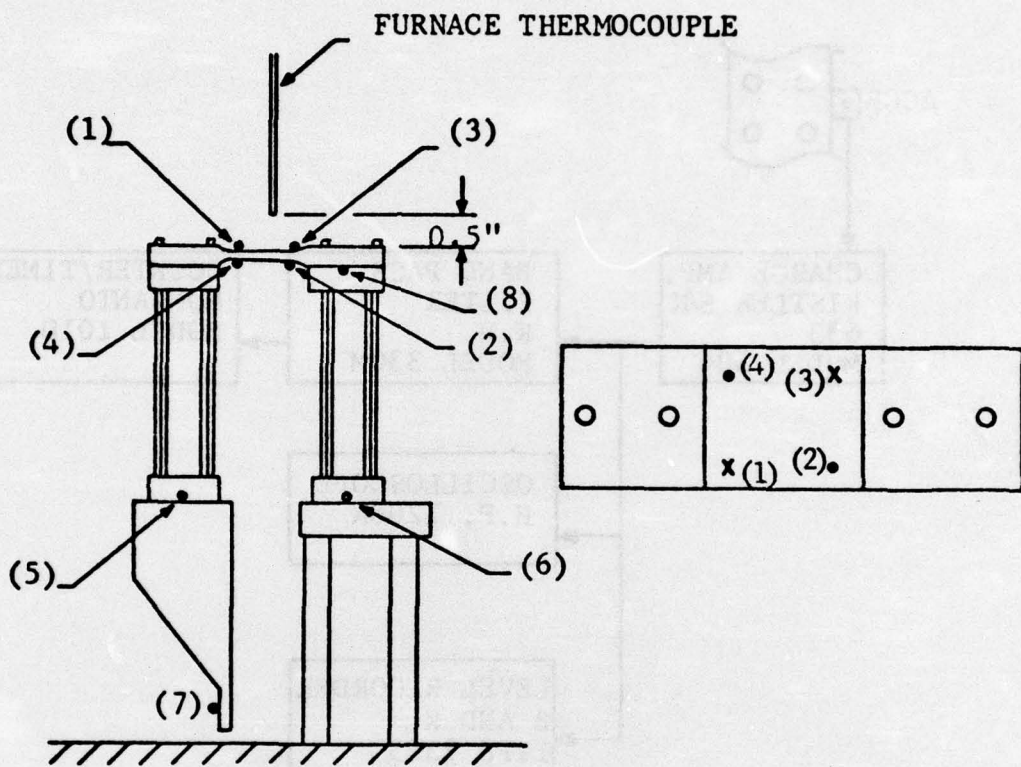


FIG. A4.4. POSITION OF THERMOCOUPLES ; BENDING

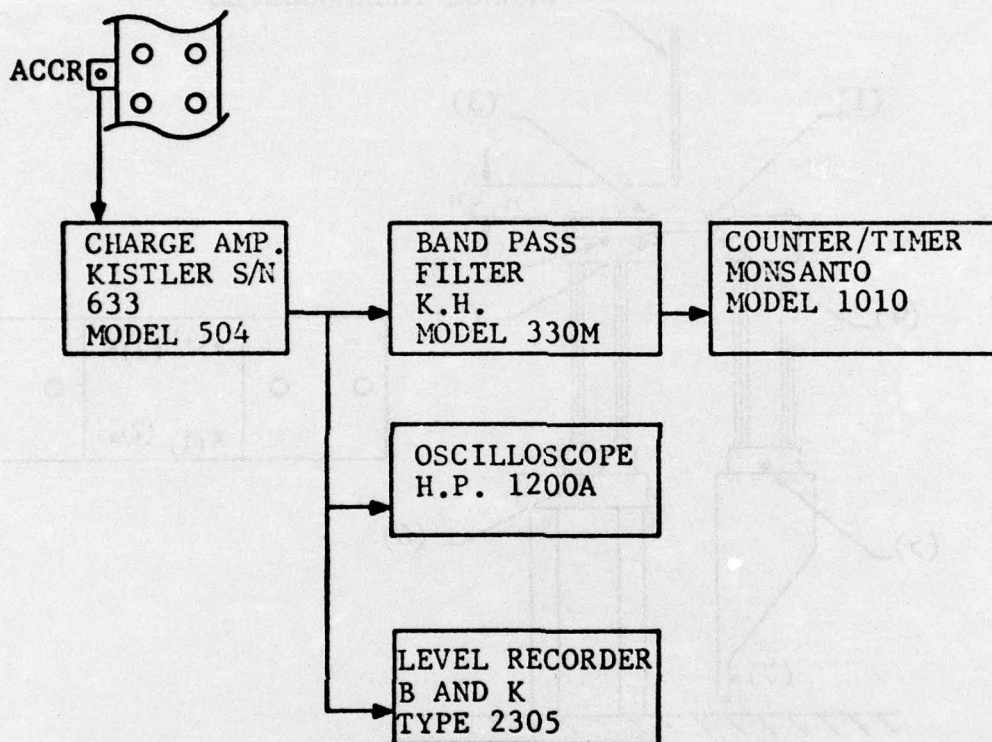


FIG. A4.5. BLOCK DIAGRAM OF EQUIPMENT; BENDING

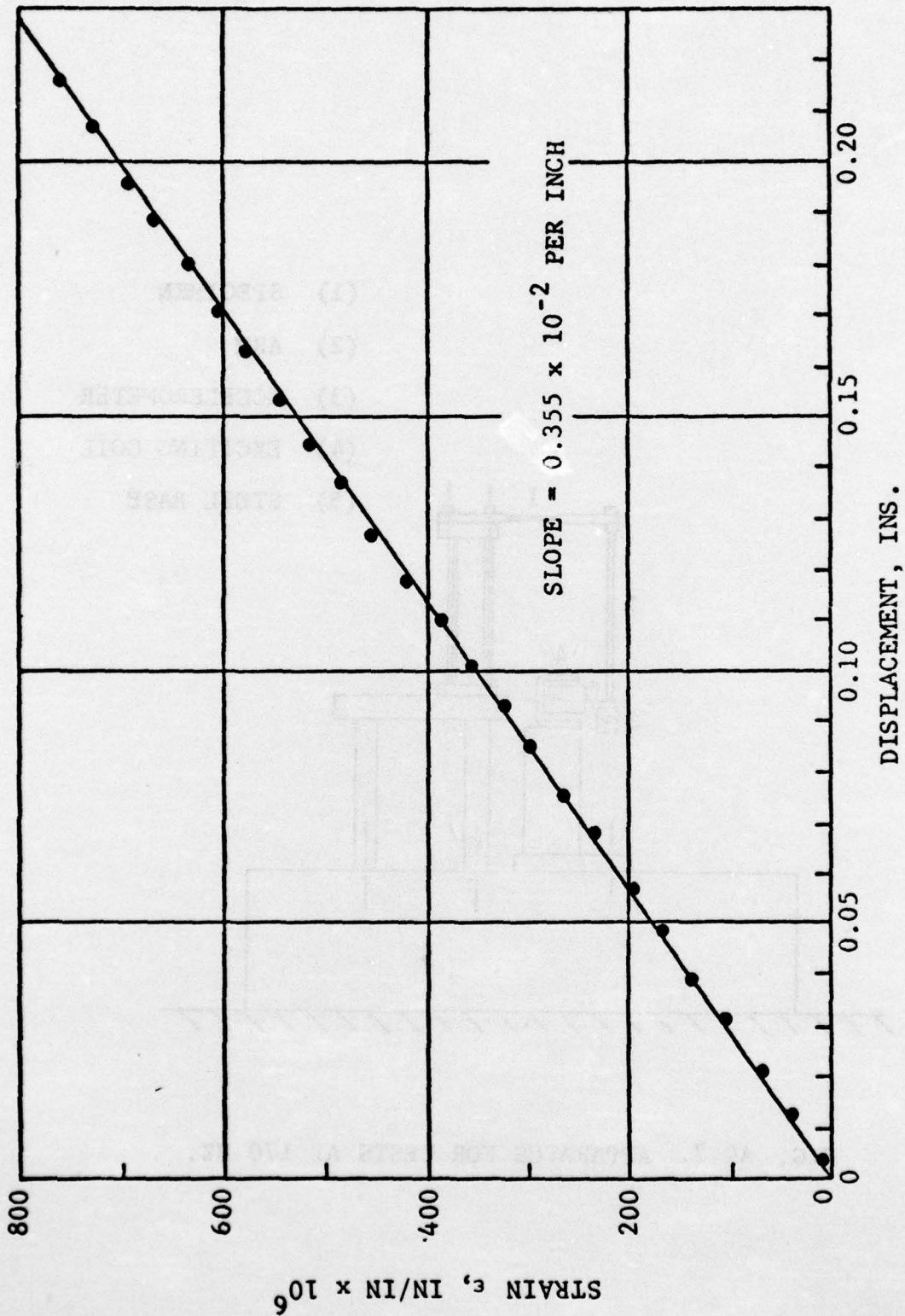


FIG. A4.6. STRAIN VS DISPLACEMENT FOR BENDING SPECIMEN

- (1) SPECIMEN
- (2) ARM
- (3) ACCELEROMETER
- (4) EXCITING COIL
- (5) STEEL BASE

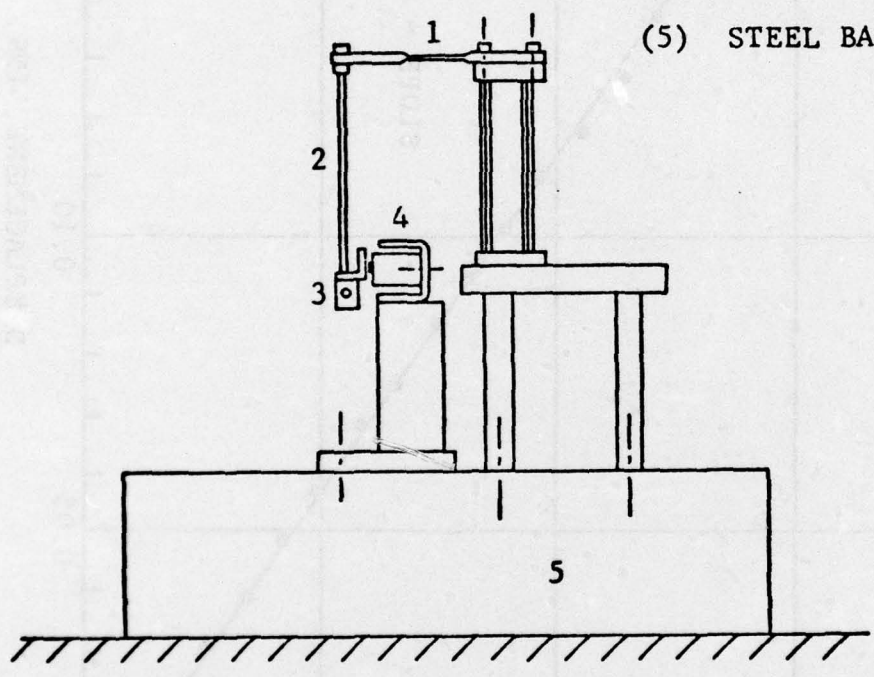


FIG. A4.7. APPARATUS FOR TESTS AT 170 HZ.

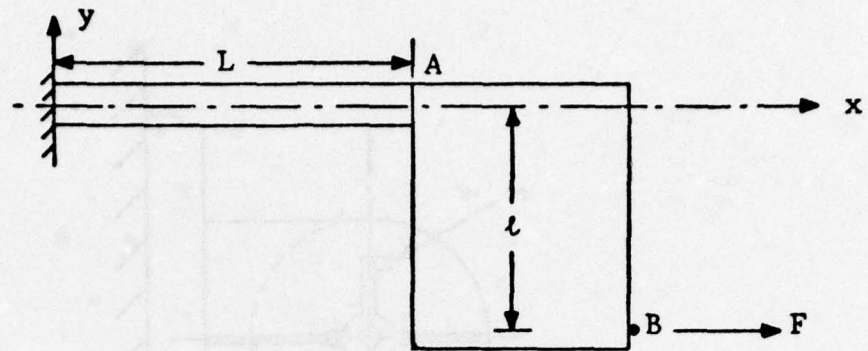


FIG. A4.8. CANTILEVER BEAM WITH EXTENDED MASS

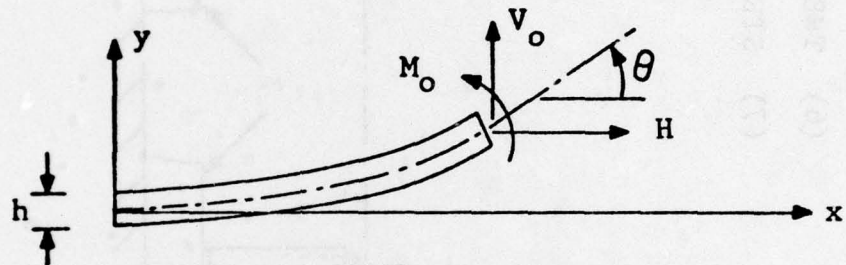


FIG. A4.9. FREE BODY DIAGRAM OF CANTILEVER BEAM

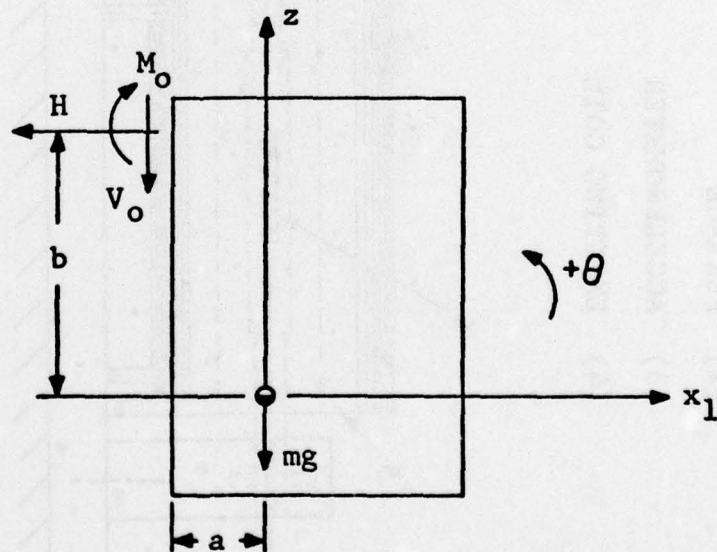


FIG. A4.10. FREE BODY DIAGRAM OF EXTENDED MASS

- (1) SPECIMEN
- (2) FURNACE
- (3) ACCELEROMETER
- (4) EXCITING COIL

- (5) INSULATING PLATES
- (6) THERMOCOUPLES
- (7) STEEL BASE

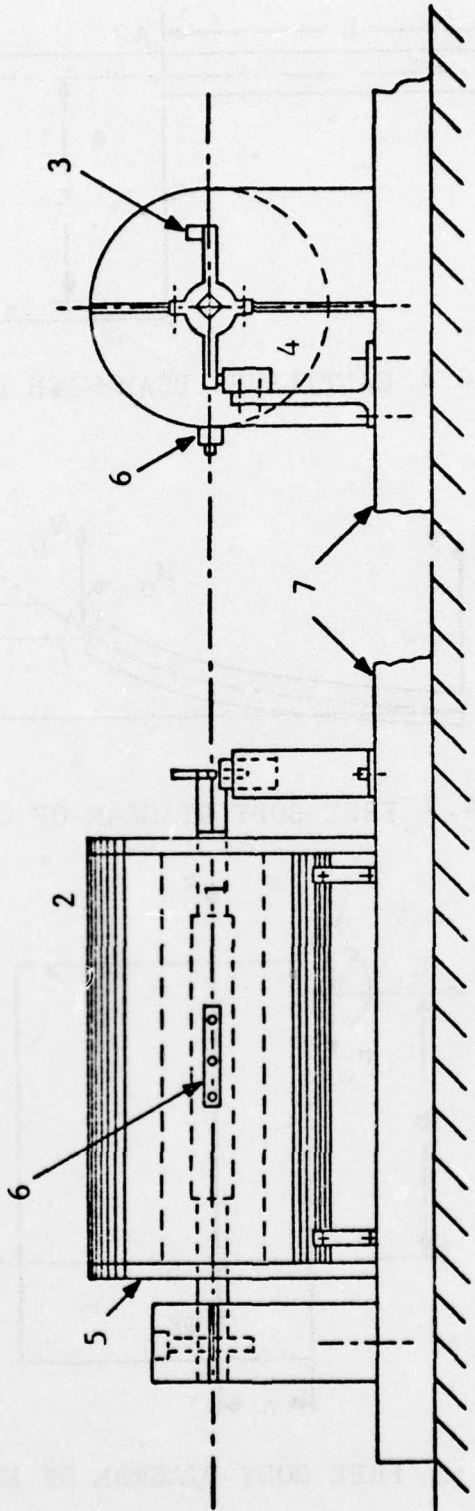


FIG. A5.1. APPARATUS FOR HIGH FREQUENCY TORSION TESTS

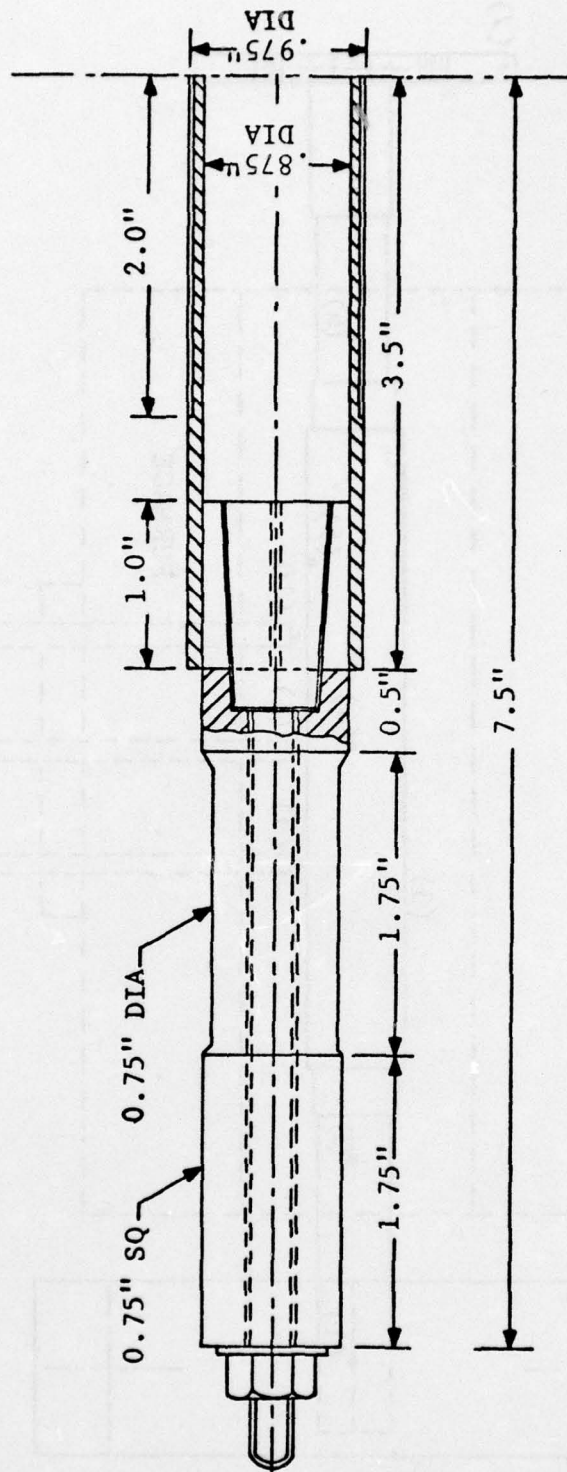


FIG. A5.2. HOLLOW TORSION CYLINDER SPECIMEN

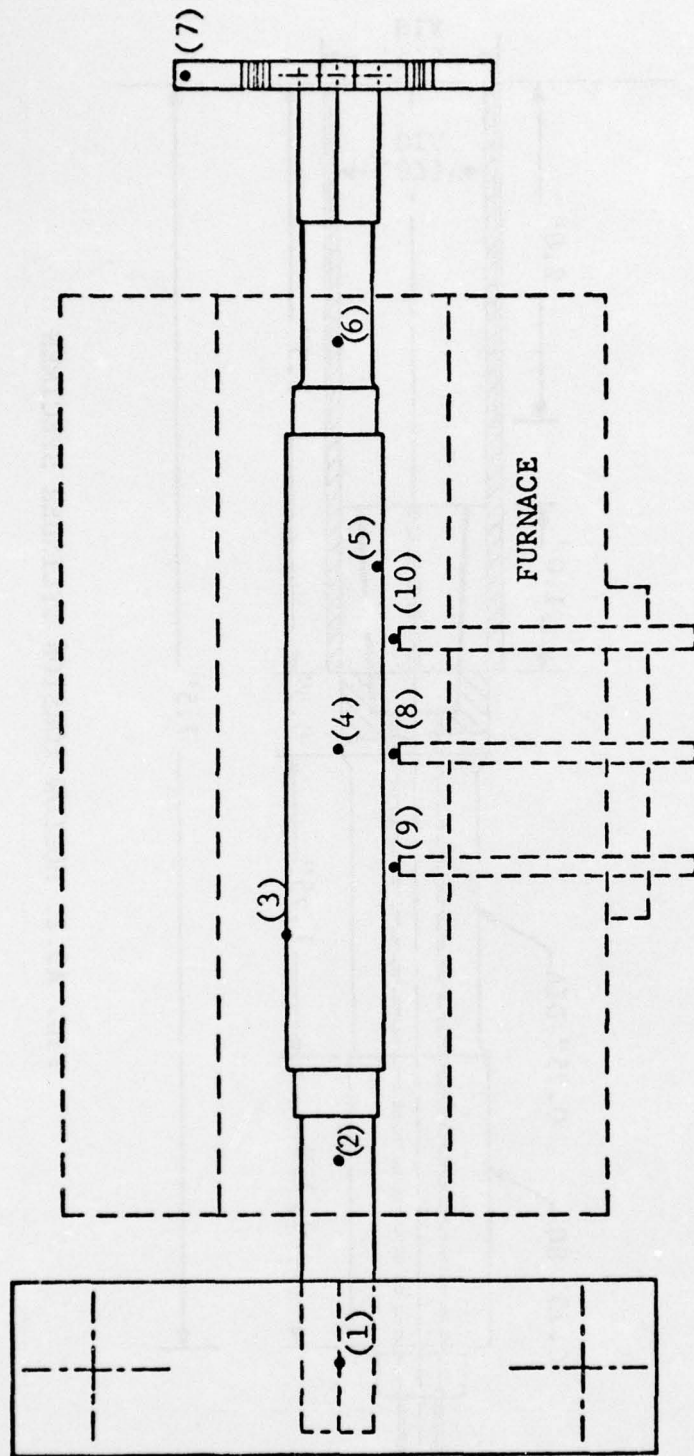


FIG. A5.3. POSITION OF THERMOCOUPLES; HIGH FREQUENCY TORSION

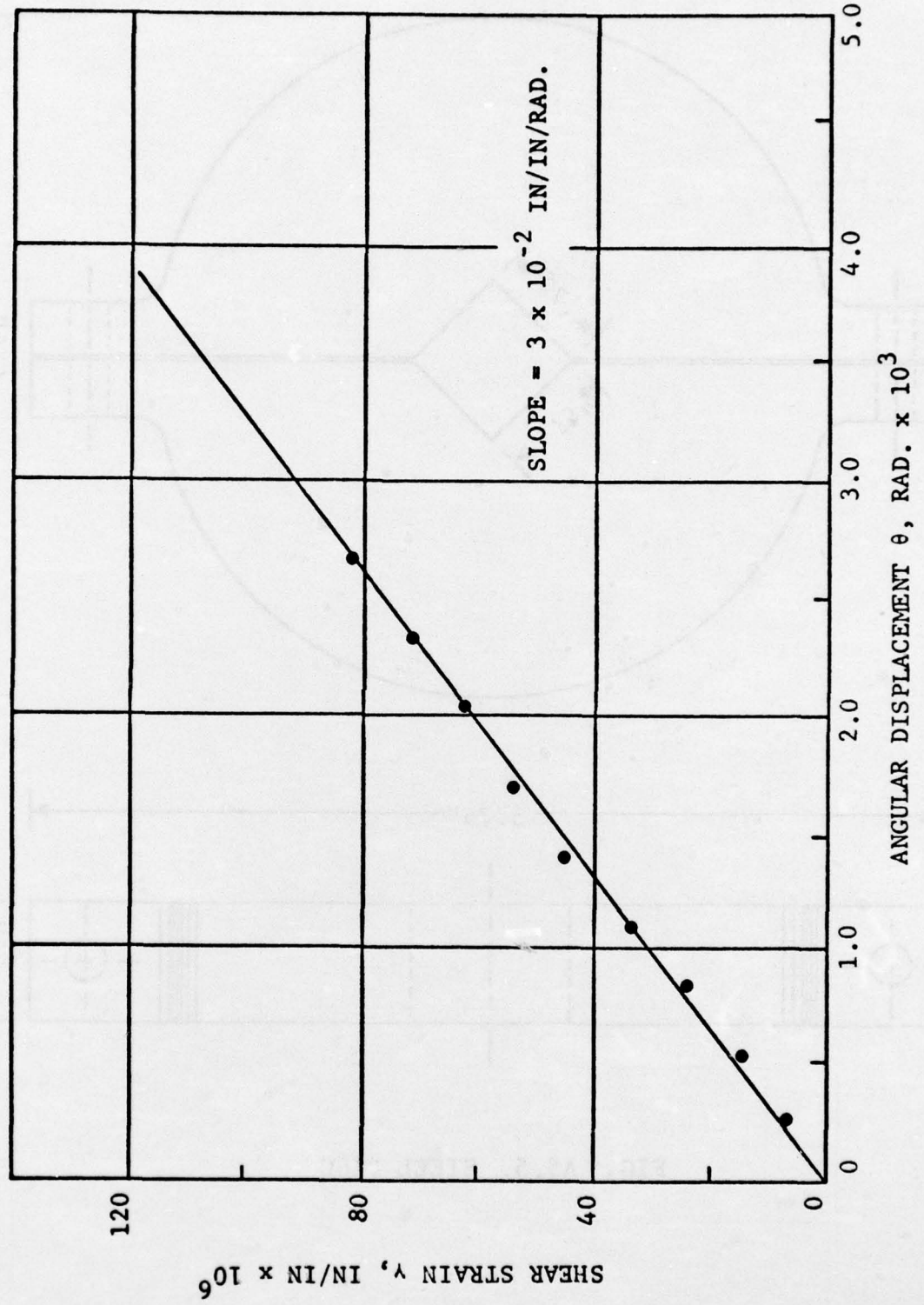


FIG. A5.4. SHEAR STRAIN VS ANGULAR DISPLACEMENT, HIGH FREQUENCY TORSION SPECIMEN

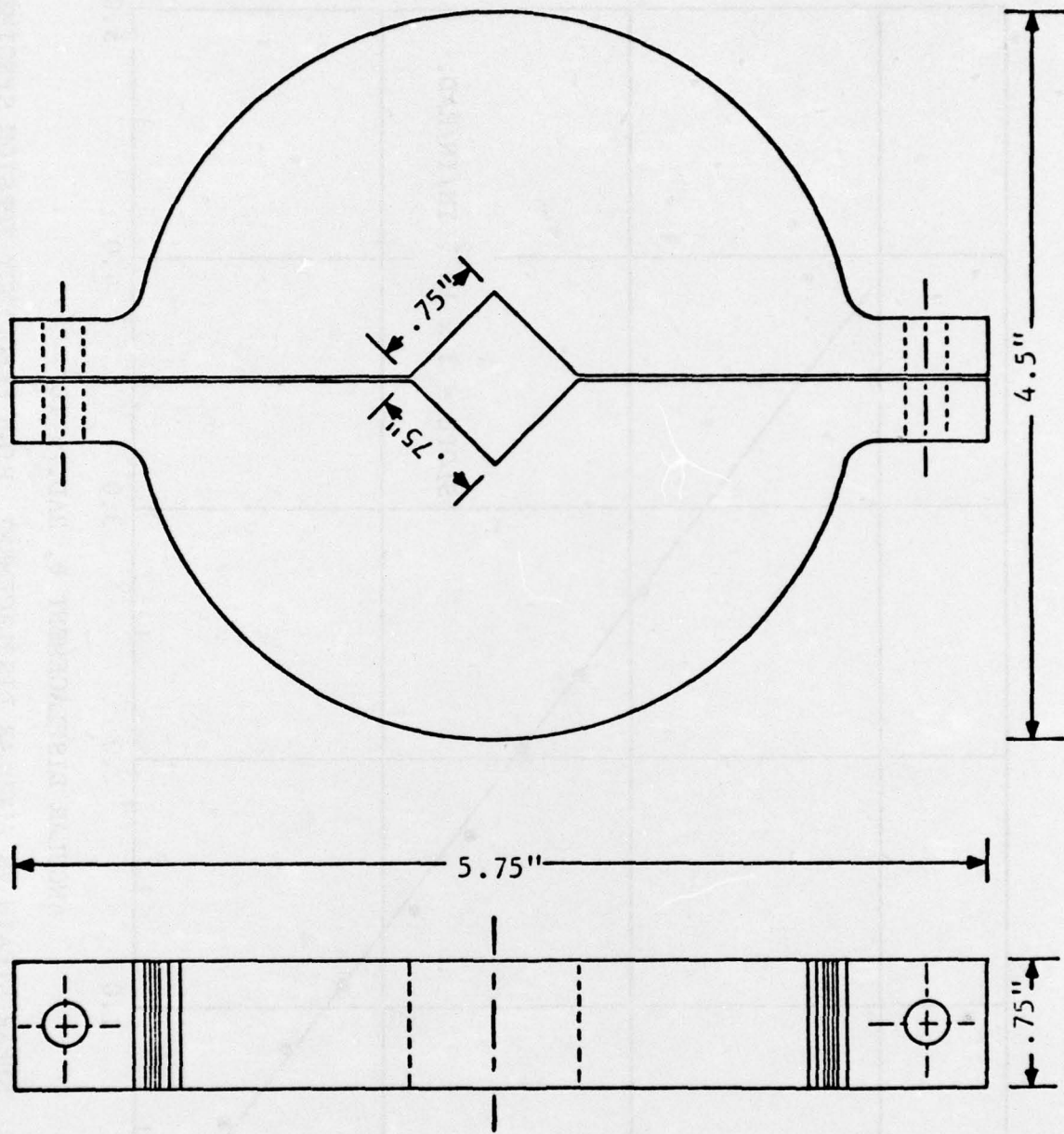


FIG. A5.5. STEEL DISC

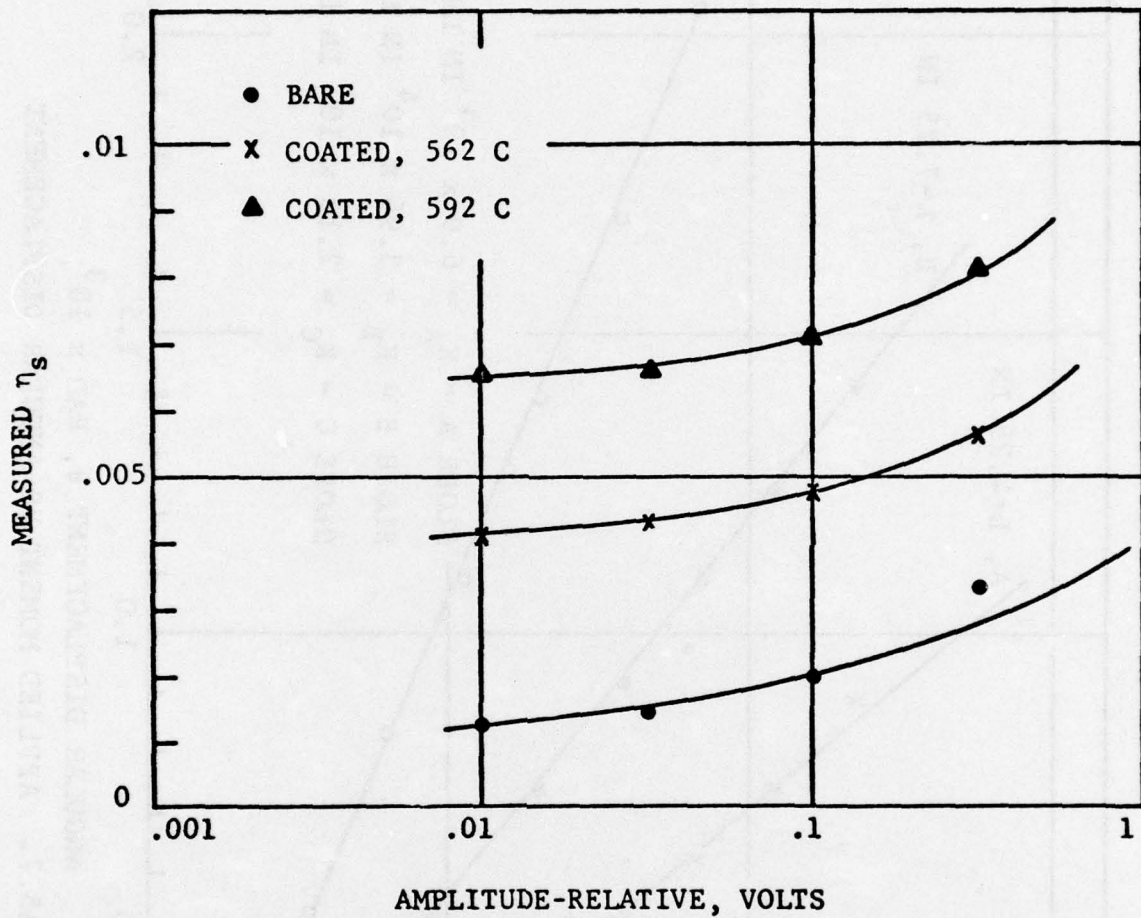


FIG. A5.6. LOSS COEFFICIENT VS AMPLITUDE;
HIGH FREQUENCY TORSION, 165 HZ

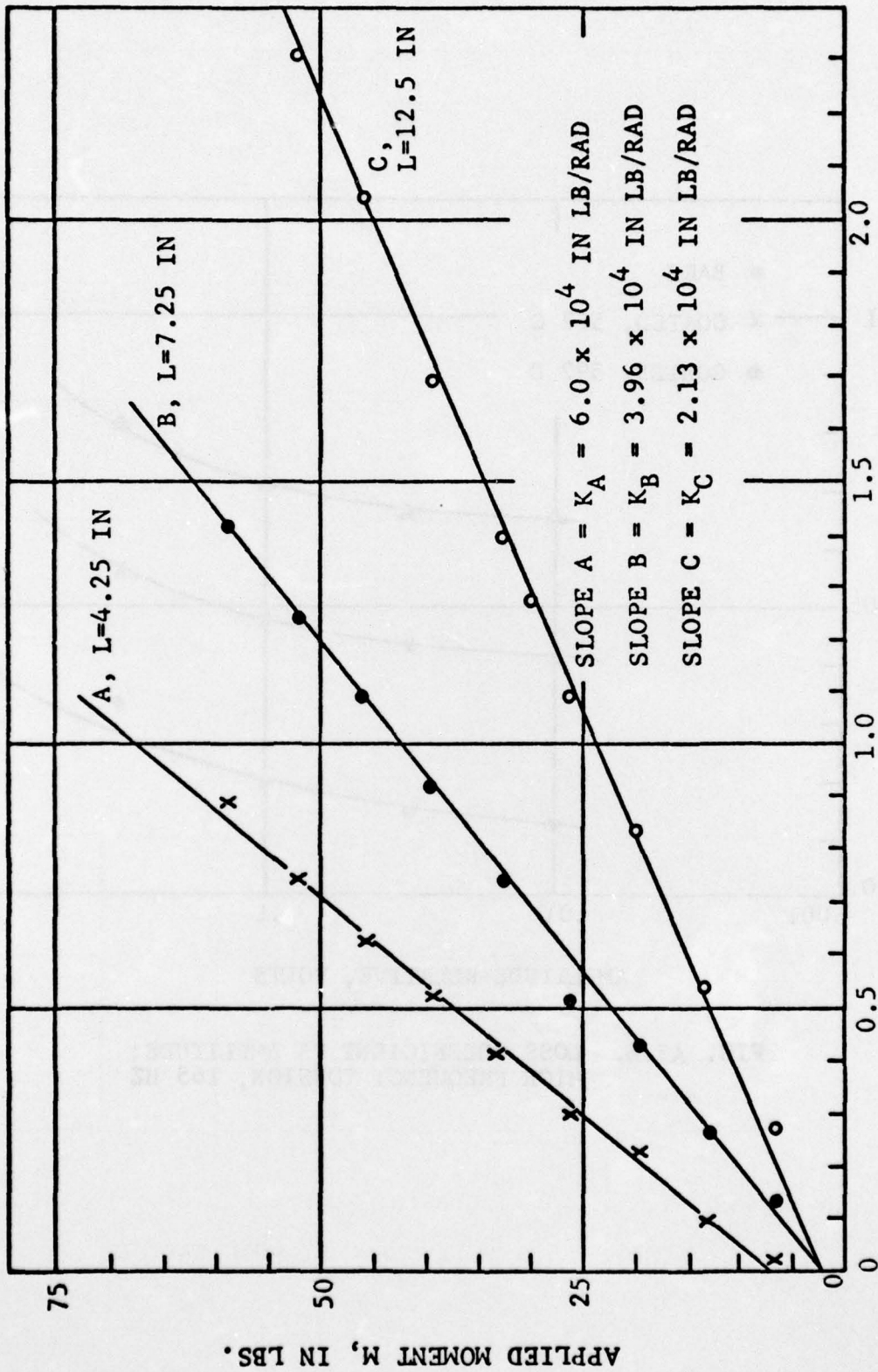


FIG. A5.7. APPLIED MOMENT VS ANGULAR DISPLACEMENT

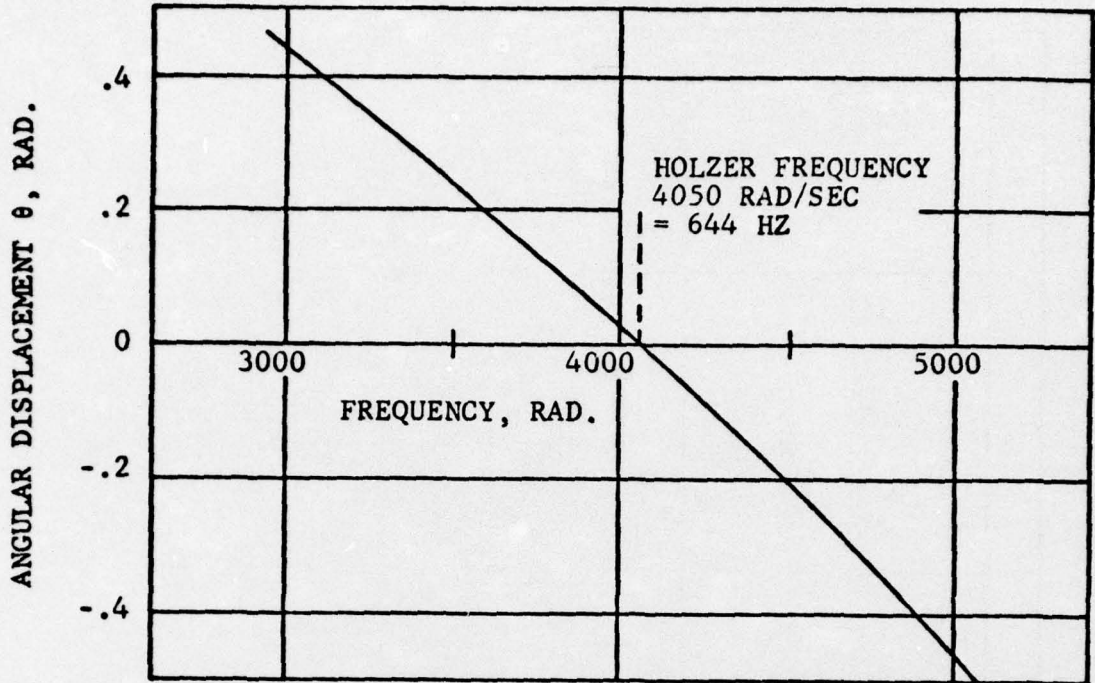


FIG. A5.8. ANGULAR DISPLACEMENT VS FREQUENCY, HOLZER

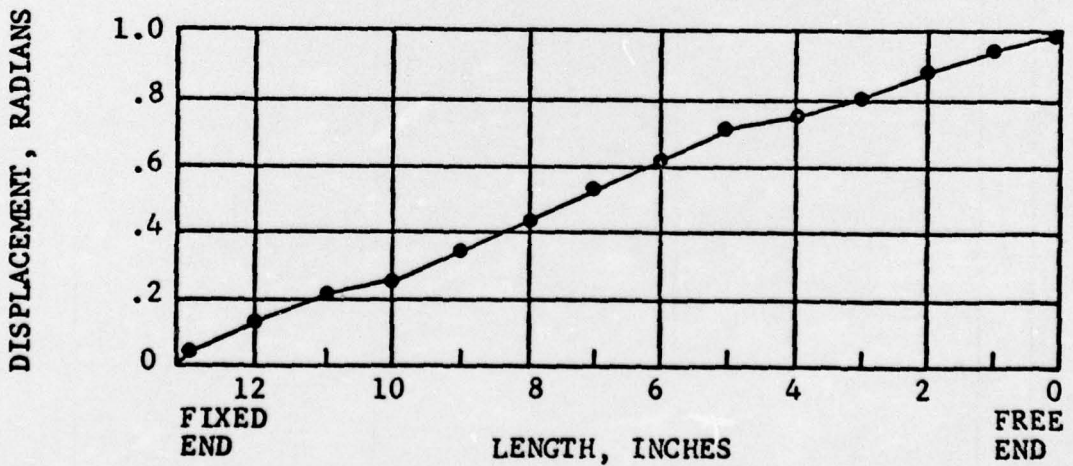


FIG. A5.9. MODE SHAPE AT 4050 RAD/SEC